THE EFFECT OF AGGREGATE POROSITY ON THE CHLORIDE PENETRABILITY OF HIGH PERFORMANCE CONCRETES

by

Kiran Lamichhane

A Dissertation Submitted in

Partial Fulfillment of the

Requirements for the Degree of

Doctor of Philosophy

in Engineering

at

The University of Wisconsin – Milwaukee

December 2005

THE EFFECT OF AGGREGATE POROSITY ON THE CHLORIDE PENETRABILITY OF HIGH PERFORMANCE CONCRETES

by

Kiran Lamichhane

A Dissertation Submitted in

Partial Fulfillment of the

Requirements for the Degree of

Doctor of Philosophy

in Engineering

at

The University of Wisconsin – Milwaukee

December 2005

Major Professor	Date
Graduate School Approval	Date

ABSTRACT

THE EFFECT OF AGGREGATE POROSITY ON THE CHLORIDE PENETRABILITY OF HIGH PERFORMANCE CONCRETES

by

Kiran Lamichhane

The University of Wisconsin – Milwaukee, 2005
Under the Supervision of Prof. Habib Tabatabai

In the present study, 12 different types of concrete mixes were prepared from 12 different coarse aggregate types (that is, a concrete type for each aggregate type) where the porosities of these aggregate types ranged from very low to relatively high values. Except for the coarse aggregate types, all other parameters remained the same in each of these concrete types. The concrete mixes thus made could easily be qualified as HP concretes due to their relatively low water-cementitious materials (w/cm) ratio and the use of supplementary cementitious materials such as silica fume and fly ash. Through a rigorous set of experiments, it was determined that aggregate porosity had an important effect on the chloride penetrability in HP concretes as indicated by Rapid Chloride Permeability Test (RCPT) results. Three aggregate/concrete types corresponding to the lowest, mid-range and highest porosities were selected for further study. A *paste-alone* mix was prepared that would represent the bulk paste regions in all representative concrete types. Chloride profiling was done on representative *paste-alone* and concrete specimens subjected to 28-, 56-, and 91-day RCPT. Additional set of experiments showed that the interfacial transition zone (ITZ) was either absent or, at least, small enough to be difficult to detect in the concretes under investigation.

An analytical model was developed to simulate the chloride migration during RCPT through a 2-dimensional (2D) concrete model. The coarse aggregate fraction was included in the model as a porous phase with its own porosity and diffusion coefficients that were different from the bulk paste porosity and diffusion coefficients. The separate effects of fine aggregates, pores and voids in the bulk paste region of the model were taken as a single *smeared-effect*. Chloride binding in the paste region was modeled as a non-linear function of free and bound chloride concentrations. A mild level of binding was assumed inside the aggregate particles as well, based on the experimental outcomes. Based on curve fitting between the analytical and experimental chloride profile values at various pre-selected penetration depths, the diffusion coefficients at the paste regions of the representative concretes were determined from simulations. According to the simulation results, the paste diffusion coefficients in mortar and concretes varied somewhat but were in the same range at any given age. A good correlation was established between the estimated paste RCPT values and the analytical paste diffusion coefficients. This correlation demonstrated that the proposed model was able to predict the bulk paste diffusion coefficient with an acceptable margin of accuracy. The short-term and long-term simulations also demonstrated that both overall average and paste chloride concentrations significantly increase with the increase in aggregate porosities.

Major Professor Date

TABLE OF CONTENTS

LIST OF FIGURES

LIST OF TABLES

LIST OF SYMBOLS

α	Initial binding rate constant
ω	Dielectric permittivity of the pore solution (Samson et al. 2003)
β	Binding capacity constant
χ	Rate of binding in an equation by Buenfeld et al. (1998)
ε	A constant used by Tang (1996) $= erfc^{-1}\left(1-\frac{2C}{C_0}\right)$
ϑ	A laboratory constant used by Tang (1996) $= 2\sqrt{\frac{RTL}{zFV}}erfc^{-1}\left(1-\frac{2C_d}{C_0}\right)$
γ	Constant used in Freundlich type of binding isotherm
φ	Constant used in Freundlich type of binding isotherm
μ	Mean
ρ	Dry bulk density
σ	Standard deviation
ξ	Constant used in Langmuir type of binding isotherm
ψ	Constant used in Langmuir type of binding isotherm
A	Area under chloride profile curve
A_{Cl}	Atomic weight of chloride (chlorine) ≈ 35.5
a_m	Constant used in Nernst-Planck equation $= \frac{zFV}{RTL}$
C	Chloride concentration (general term)
C(x,t)	Chloride concentration corresponding to x and t variables
C_b	Bound chloride concentration
C_f	Free chloride concentration
C_{fc}	Estimated free surface chloride concentration
C_i	Concentration of i^{th} ion species
C_o	Surface chloride concentration (binding not considered)
COV	Coefficient of variation
C_t	Total chloride concentration

D	Diffusion coefficient
d	Diameter of aggregate particles (Zheng 2000)
d_l	Lower diameter limit of aggregate particles (Zheng 2000)
D_{mig}	Migration coefficient used by Andrade et al. (1994)
d_u	Upper diameter limit of aggregate particles (Zheng 2000)
E	Voltage per unit length $= \frac{\partial V}{\partial x} = \frac{V}{L}$
erfc	Complementary error function
F	Faraday's constant = 96,485 Coulombs/mole
J	Chloride ion flux
k_b	Chloride binding rate constant
L	Specimen dimension along chloride penetration depth
M_{NaCl}	Molarity of NaCl solution
n	Porosity
N_1	Free surface chloride concentration divided by porosity $= \frac{C_{fs}}{n}$
P(d)	Probability associated with particle diameter d (Zheng 2000)
Q	Total charge passed through the concrete specimen during RCPT
Q_f	Charge passed through the aggregate fraction of concrete during RCPT
R	Universal gas constant = 8.314 Joules/mole-K
r^2	Correlation coefficient
t	Time variable
T	Temperature (in Kelvin)
u	Ion mobility factor $= \frac{zFD}{RT}$
V	Voltage (electrical potential difference)
V_1	Electrical potential at one end of the proposed model
V_2	Electrical potential at the other end of the proposed model
W_{OD}	Weight of oven-dry specimen
W_{SM}	Weight of water-submerged specimen
W_{SSD}	Weight of saturated surface-dry specimen
x	Space variable along x-coordinate

x_d	Penetration depth (Tang 1996)
z	Ion valence (general term)
z_i	Valence of i^{th} ion species

ACKNOWLEDGEMENTS

I would like to express my sincere gratitude to my major advisor Prof. Habib Tabatabai for his guidance and leadership during different phases of experimentation and thesis writing. It was only because of the invaluable suggestions and guidance provided by Prof. Tabatabai that the present study was able to qualify as a Ph. D. thesis. I would also like to sincerely thank Prof. Hani Titi for giving me an opportunity to work with him on a project sponsored by the Minnesota Department of Transportation (Mn/DOT project) and granting me the permission to share the project outcomes in the present study. The completion of the present study would not have been possible without the generous help and unwavering support provided by Prof. Titi. Similarly, I would like to sincerely thank Prof. Al Ghorbanpoor, Prof. Adeeb Rahman and Prof. Istvan Lauko for kindly accepting my request to sit in my thesis defense committee and providing valuable suggestions on different aspects of the study.

I owe many thanks to Mr. Mohammed Elias, a graduate student of Prof. Titi, for his help and support during different concrete mixing and testing phases. I also owe many thanks to Mr. Rahim Reshadi of Structural Lab (UWM), Mr. Mike Brown of Machine Shop (UWM) and Dr. Andrei Skliarov of Advanced Analysis Facility (UWM) for extending their help and expertise during different experimental and testing phases. I am very much indebted to Mr. Earl Blevis of pdesolutions.com for providing me trial licenses for FlexPDE software on several occasions.

At last but certainly not the least, I would like to dedicate this work to my parents, father Harihar Lamichhane and mother Bhagwati Lamichhane, for their unconditional love and support during these many years of my learning.

1.0 INTRODUCTION

1.1 Problem Statement

Concrete is a permeable material consisting of a vast network of pores ranging in sizes from nano- to micro-scales. Under favorable circumstances, various deleterious agents would be able to enter into the concrete through these pores, which in turn, could weaken the concrete system and compromise its strength and durability. Chloride penetration in concrete is one such durability-related issue. For the concrete structures exposed to the chloride environment, performance of concrete in terms of chloride penetration resistance becomes a key issue.

Hardened concrete is a heterogeneous material that has several compositional phases. On a microscopic level, concrete has pores, voids, unhydrated cement particles and hydration products. On a mesoscopic level, concrete can be regarded as a two-phase material, divided into bulk mortar paste (which includes cement paste and fine aggregate particles) and coarse aggregate particles. Depending on the type of concrete, a third important phase from chloride transport point of view, known as interfacial transition zone (ITZ), might also be present in concrete.

Coarse aggregates are an essential constituent of concrete. Traditionally, coarse aggregates are regarded as inexpensive fillers in concrete and as a result their influencing role in concrete is sometimes overlooked. In fact, coarse aggregates (referred to as aggregates hereafter) are capable of affecting several of concrete properties in both fresh and hardened states. Coarse aggregates not only influence the strength of hardened concrete but also play a vital role in several of the durability related issues as well. For example, aggregates are

considered to be contributing factors to a host of durability related issues such as freezing and thawing, abrasion resistance and alkali-silica reaction (ASR).

Generally, coarse aggregates are either crushed or naturally available particles of various rock origins. Hence, they significantly differ in physical and chemical properties, as do their parent rocks. Water absorption and porosity are two major inherent physical characteristics of rocks. Some of the strongest rock types that come from igneous and metamorphic rock origins are found to have very low porosity and low water permeability. On the other hand, the rocks of sedimentary origin such as limestone have relatively high porosity and water absorption ratios. When the aggregates from a given rock origin are used in concrete, the aggregate properties such as water absorption and porosity become an integral part of the concrete property. ACI 211R-96 (1997) indicates that the durability issues such as freezing and thawing and wetting and drying are directly related to aggregate porosity.

Since the aggregates and the paste can both be porous, it would be interesting to find the answer to a very fundamental question: is the movement of chloride ions possible through aggregate pores as well? The basic law of diffusion indicates that there should be no problem, whatsoever, for the chlorides to move through the aggregate pores provided the aggregates have sufficient porosity to facilitate the penetration process. However, aggregates are routinely treated merely as inert fillers (impervious materials with negligible porosity) when it comes to considering the chloride penetration in concrete. This assumption is more or less valid for ordinary portland cement (OPC) concretes due to the fact that the capillary porosities of OPC concretes are typically much higher than the aggregate porosities. Additionally, the possible presence of interfacial transition zone (ITZ) around the aggregates may result in chloride ions choosing the ITZ region as a preferential path and avoiding the aggregate pores all together. As a result, the proportion of the chloride penetration through

the aggregate pores may be negligible as compared to the paste or ITZ penetration. On the other hand, high performance (HP) concretes are designed to withstand harsher environments and are significantly less porous with much finer pore systems than OPC concretes. Therefore for HP concretes, the role played by aggregate porosity towards chloride penetration in concrete should not be overlooked.

Several laboratory test methods are in use to determine a concrete's ability to resist chloride penetration. The RCPT method is one of the widely popular short-duration test methods to assess the resistance of concrete to chloride penetration (Shane et al. 1997). In this test method, the movement of chloride ions in the concrete specimens is mainly driven by an electrical potential (voltage) that is applied across the test specimen. The ionic movement under the influence of an electrical voltage is typically known as migration. RCPT does not directly measure the chloride penetration in concrete but qualitatively rates concrete based on the total electrical charge passed (in coulombs) through it at the end of the 6-hour test.

A direct measurement of chloride penetration is possible by chloride profiling the test specimens subjected to RCPT and determining the actual chloride concentrations at different pre-determined specimen depths. Through this procedure, it is possible to correlate RCPT values to the diffusion coefficient values of bulk mortar pastes and aggregates (if any) with the help of analytical modeling.

1.2 Background

Many reinforced concrete structures are exposed to severe salt environments and as a result their deterioration occurs much earlier than expected. In cold climatic regions, a common form of salt, chemically known as sodium chloride (NaCl), is sprayed on the roads and bridges to lower the melting point of accumulated snow and ice. A portion of the sprayed

salt may also be transported to parking lots and other structures due to vehicular movements. On the other hand, coastal and marine structures are subjected to salt environment due to continual or occasional exposure of those structures to seawater and salty air mist. The third type of structures subjected to chloride environment is the sub-grade structures directly in contact with soils that have high chloride content. For the concrete structures subjected to various forms of chlorides, corrosion of the embedded reinforcing steel is one of the primary durability related issues in the field of concrete technology. Salt (sodium chloride) in aqueous form is dissociated into sodium (Na^+) and chloride (Cl^-) ions where chloride ions have been found to be responsible for the initiation and acceleration of corrosion in steel. Chloride ingress in concrete takes place through small pores in concrete and corrosion starts when these penetrating chloride ions come into contact with reinforcing steel and destroy its passive protection layer.

Protection of reinforcing steel is provided by concrete through the formation of a passive protective layer between concrete and the steel. This phenomenon takes place when highly alkaline plastic concrete comes into contact with reinforcing steel, and a chemical reaction takes place leading to the formation of the protective layer around the reinforcement (SCA 2002). The protective layer acts as a physical barrier between the steel and moisture (and oxygen), preventing them from coming in contact with each other. Overtime, chlorides ions are known to destroy the passive protective layer, exposing the reinforcing steel to corrosion in presence of moisture and oxygen. Even though the exact nature of interaction between chloride ions and the protective layer in not fully known, it is believed that once the chloride concentration in the vicinity of reinforcing steel reaches a threshold value, chloride ions start chemically reacting with the steel, resulting in the formation of ferrous chloride or ferrous chloride complex. This new compound replaces the protective layer (Orlova et al. 1999) and

paves the way for another set of chemical reactions between the steel and moisture (and oxygen) in which the steel readily turns into its thermodynamically more stable states such as oxides and hydroxides. This crucial stage marks the initiation of the corrosion process. The products of corrosion, mainly ferric oxide and ferric oxide complex (commonly known as rust), take up to six times the original steel volume (Thoft-Christensen 2002) and as a result, exert expansive pressure on the surrounding concerete leading to cracking and spalling. The cracking and spalling propagates as more chloride ions are able to reach to the depth of reinforcing steel through these cracks and openings, accelerating the entire cycle of corrosion, resulting in a major durability issue.

In light of this major durability related issue associated with the chloride penetration in concrete, it is desirable to conduct more research on various aspects of this problem for the purpose of developing a more durable concrete.

1.3 Objectives

- To determine the role of aggregate porosity in influencing the chloride penetrability and RCPT results for high performance concretes.
- To determine whether the RCPT or other similar migration tests can be used to determine diffusion properties for long-term assessment of durability conditions in concrete.
- To determine the role of aggregate porosity in influencing the chloride contents in the paste. Since the paste is in contact with the reinforcing steel bars, the chloride content of the paste is an important factor.
- To develop a 2-dimensional analytical model that can properly simulate the chloride migration during RCPT and other short-term tests.

1.4 Scope and Outline of the Study

The present study utilizes the experimentations and outcomes from a project sponsored by the Minnesota Department of Transportation (Mn/DOT) entitled *The Effect of Minnesota Aggregates on Rapid Chloride Permeability Tests* (Titi et al. 2004). The outcomes of this project indicated a strong correlation between the coarse aggregate porosities and the RCPT results. Therefore, additional experimental works were designed in the present study to provide further insight into the relationship between aggregate porosities and RCPT results. An analytical model and approach was also developed that included coarse aggregates as porous inclusions with their own diffusion properties. In general, the scope of the present study can be outlined as follows:

1. Results from the Mn/DOT project indicated that there was a strong correlation between the porosities of coarse aggregates and the RCPT results at all three test ages (28, 56 and 91 days) (Titi et al. 2004). Three aggregate types that resulted in the highest, midrange and the lowest RCPT results were selected for further investigation in the present study.
2. Three selected aggregate types were subjected to various tests to further analyze their respective roles in influencing RCPT results and to determine whether aggregate porosities, in fact, play an important role in determining the total charge passed during the chloride migration tests such as RCPT.
3. A 2-dimensional analytical approach and model was developed that included coarse aggregates as porous inclusions in the model allowing chlorides to migrate through them. This model could simulate the chloride migration during RCPT. The simulated results could then be compared with the experimental chloride profile results. Based on the comparative analyses between simulation and experimental results, the

diffusion coefficients of the paste regions of representative concrete specimens were determined. A good correlation was established between these diffusion coefficients and the experimental paste RCPT values.

Chapter 1 introduces the topic and outlines the objectives of the study. Chapter 2 is devoted to the extensive literature search on all necessary aspects of chloride penetration and aggregate porosity. Chapter 3 discusses the mathematical basis for the diffusion-migration mechanism. Chapter 4 includes a summary of the experimental work carried out during the Mn/DOT project (Titi et al. 2004). Similarly, Chapter 5 includes the additional set of experimental works. Chapter 6 is devoted to the analytical simulation of chloride migration and diffusion. Chapter 7 includes the experimental results and discussion. Chapter 8 includes concluding remarks and some recommendations regarding future studies.

2.0 LITERATURE REVIEW

2.1 An Overview of Existing Test Methods

As mentioned earlier, chloride ion ingress in concrete is a durability issue. Concrete is a porous medium consisting of a vast network of different types (and sizes) of pores. Chloride ions make use of these pores to penetrate into concrete whenever these pores are filled with water. But this process is relatively slow and mainly takes place through a mechanism known as diffusion. Today, several laboratory test methods are available for evaluating the concrete by measuring, either directly or indirectly, the level of chloride penetration in concrete in relatively short duration of time.

2.1.1 Existing Test Methods

On of the main long-term chloride penetration test methods has been the Salt Ponding Test (AASHTO T 259). Another long-term method known as the Bulk Diffusion Test (ASTM C 1556) has also been in use for some years. The primary drawback in these methods has been in long durations of testing. In particular, with concrete becoming more impervious with the use of different supplementary cementing materials such as silica fume, fly ash and slag, both Salt Ponding and Bulk Diffusion Test methods need several months for chloride ions to penetrate to a measurable depth in concrete and hence significantly increase the test durations. In 1981, Whiting et al. developed a short-term test method called the RCPT. This test method used the idea of applying electrical potential (voltage) across the concrete sample to force chloride ions into the concrete, where negatively charged chloride ions in the negative terminal would force themselves into the concrete, trying to reach the positive terminal on the other side of the specimen. However, this test method does not measure

chloride penetration in concrete directly, but simply records total charge passed through the concrete specimen for a given electrical potential and test duration. The RCPT qualitatively rates the concrete based on the total charge passed. Another recent development for the rapid chloride penetration measurement in concrete comes from the Nordic tests standard NT Build 492. First developed by Tang (1996) and adopted by Nordic test standard in 1999, this test method, commonly known as the Rapid Migration Test (RMT), was further modified at the University of Toronto and recommended for its use by North American test standards. AASHTO has assigned a provisional designation PT 64 to this test method. In terms of sample preparation and test procedure, this test method is very similar to RCPT. But in terms of evaluating results, it is entirely different from RCPT. RMT takes direct measurement of chloride penetration in concrete as opposed to the measurement of total charge passed in RCPT. Another test method, which lies between long-term and short-terms methods in terms of the test duration, is the Migration Test method (NT Build 355). In this test method, chloride ions penetrate the concrete specimen under electrical potential, but the test could last several hours (or days) as the chloride ions need to penetrate the entire specimen thickness and reach the downstream solution in measurable quantities. The Salt Ponding Test, the Bulk Diffusion Test, the RCPT and the RMT are briefly described below.

2.1.1.1 Salt Ponding Test

AASHTO has designated this test method as AASHTO T 259: Resistance of Concrete to Chloride Ion Penetration. This test method is a long-term test requiring 90 days of continuous ponding of NaCl solution at the top surface of the specimen. Three slabs of at least 3-in thick and 12-in square surface area are moist cured for 14 days. Then these specimens are left to dry in a 50% relative humidity environment for another 28 days.

Finally, the specimens are uninterruptedly ponded with 3% NaCl solution for the next 90 days. The test results are provided as the chloride concentration of concrete powder at specified depths, expressed as the % mass of concrete. The test duration seems sufficient for normal quality concrete, but may not be sufficient for higher quality (high performance) concretes. Chloride penetration in high performance concretes might not reach a significant level in 90 days due to reduced porosity of concrete (Stanish et al. 1997).

2.1.1.2 Bulk Diffusion Test

This long-term test method was previously used in Nordic countries under test designation NT Build 443 and was adopted by ASTM in 2003 (ASTM C 1556: Determining the Apparent Chloride Diffusion Coefficient of Cementitious Mixtures by Bulk Diffusion). In this test, the specimens are soaked in limewater until saturated, instead of leaving them to dry for 28 days as done in the Salt Ponding Test. Also, instead of coating only the sides of the specimens as in the Ponding Test, all the sides except the one exposed to a 2.8 N NaCl solution are coated. The specimens are left ponded with the NaCl solution for 35 days before making an evaluation. This test addresses some of the shortcomings of the Salt Ponding Test such as the use of a saturated specimen instead of a dry specimen. However, the evaluation of chloride penetration (the determination of apparent diffusion coefficient based on the chloride profiling) in higher quality concretes should be performed after at least 90 days, far beyond 35-day period specified for normal quality concretes.

2.1.1.3 Rapid Chloride Permeability Test

This is a short-term test method where a water saturated slice of concrete, 50 mm thick and 100 mm in diameter, is subjected to a DC voltage of 60 V for 6 hours. Its full name under

AASHTO designation is AASHTO T 277: Electrical Indication of Concrete's Ability to Resist Chloride Ion Penetration. First, the sliced sample is conditioned by water saturating the sample to completely fill its pores. Then, the conditioned sample is mounted on a test cell which sandwiches the specimen between two reservoirs. One of the reservoirs contains a 3% NaCl solution and the other contains a 0.3 N NaOH solution. The whole test assembly is watertight to the outer environment, and the solutions come in contact with the two faces of the specimen. A DC potential of 60 V is applied to the assembly in such a way that the negative terminal is connected to the NaCl solution and the positive terminal is connected to the NaOH solution. This voltage is maintained for six hours, during which period chloride ions travel through the specimen under the electrical potential and creating a current flow. The total charge passed through the specimen (in coulombs) during the test period (6 hours) is determined at the end of the test and this value is used to evaluate the specimen in terms of chloride ion penetrability. Lower coulomb values from the test indicate lower chloride penetrability and so on. Table 2.1 below provides the specimen ratings for different total charge values.

Table 2.1: Chloride ion penetrability based on charge passed (AASHTO T277 2000).

Charge Passed (Coulombs)	Chloride Ion Penetrability
> 4,000	High
2,000 - 4,000	Moderate
1,000 - 2,000	Low
100 - 1,000	Very Low
< 100	Negligible

This test was first developed by the late Dr. David Whiting in 1981 (Whiting 1981) and has now been adopted both by AASHTO and ASTM (ASTM C1202). Schematic diagram of a typical test setup is given in Figure 2.1.

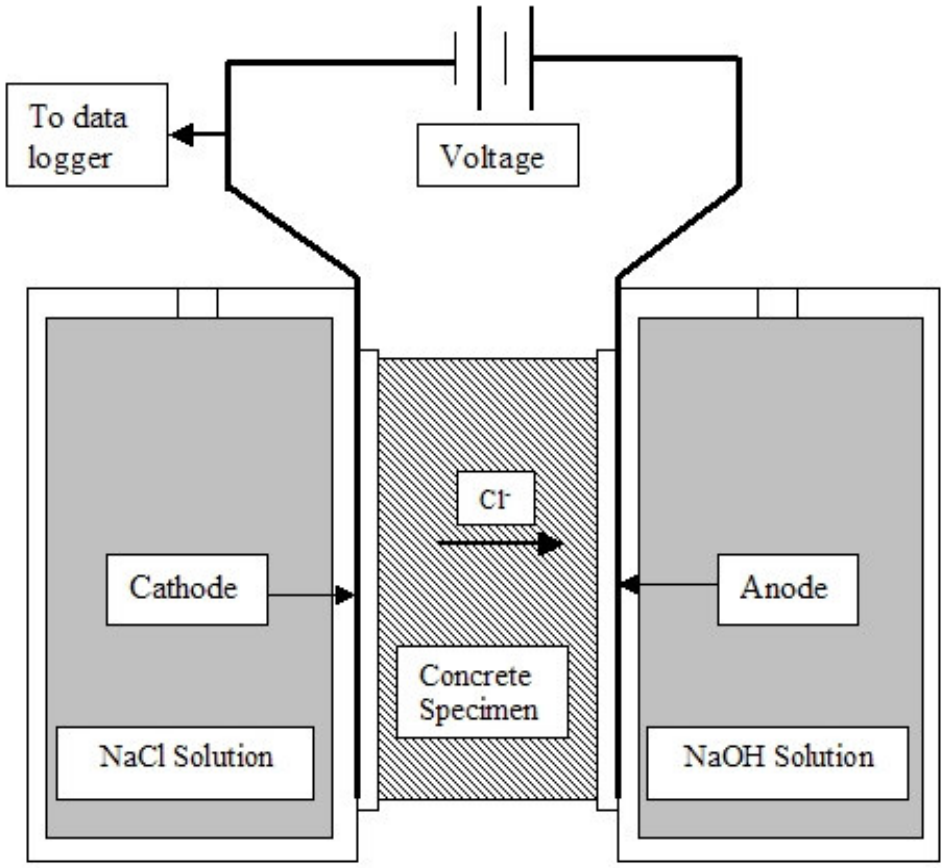

Figure 2.1: Schematic diagram of a typical RCPT setup.

During the test's development, a correlation was established between the results from RCPT and long-term chloride ponding procedure such as AASHTO T 259. Since a good correlation was found between the results from these two test procedures, the RCPT was proposed as a new test method to rapidly measure the chloride ion penetration in test specimens (Russell 2001). This method is the most common test to determine the relative

permeability of concrete despite some criticisms made regarding some aspects of this test. Some of the criticisms made about this test are: (1) the test is performed before a steady state condition for chloride migration is reached, (2) the current passed is related not just to chloride ions but all ions in the pore, and (3) the high voltage during the test increases the temperature of the specimens, especially for low-strength concretes which could provide misleading results. In short, the test cannot be conducted in a constant temperature environment.

2.1.1.4 Rapid Migration Test

This test was first proposed by Tang and Nilsson (Tang and Nilsson 1992). Since 1999, this test has been standardized as NORDTEST Standard (NT Build 492: Chloride Migration Coefficient from Non-Steady State Migration Experiments). The same test has a modified version simply known as the Rapid Migration Test, which was proposed by Hooton et al. (2001) based on their research at the University of Toronto. A schematic diagram of a typical test setup is provided in Figure 2.2.

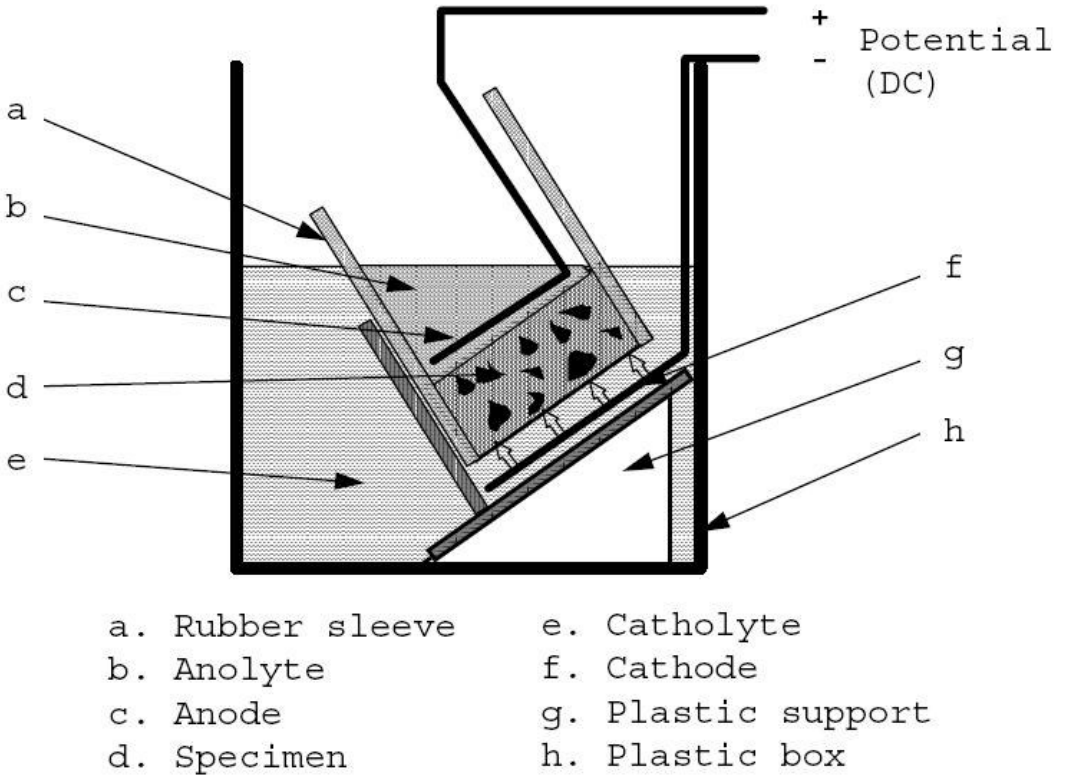

Figure 2.2: Schematic diagram of a typical RMT setup (NT Build 492 1999).

The RMT is standardized by AASHTO as provisional standard TP 64 (Stanish et al. 2005). This test is very similar to RCPT in terms of the size of test specimen, sample conditioning and the test setup. The duration of the test, however, is 6 to 96 hours with voltage ranging from 10 to 60 V in NT Build 492. In the RMT, the test duration is kept constant at 18 hours and the voltage is set at 10 V, 30 V or 60 V depending on the initial current passed thorough the specimen. The main difference between this test and the RCPT lies in the evaluation of the results. In this test method, the specimen is split open after the test and sprayed with a 0.1 N silver nitrate solution. The portion that has more than 0.15% chlorides by weight of cement will turn white and the portion with less than this amount of chlorides will turn

brown. The penetration depths are measured at 10 mm intervals across the edges and the evaluation of chloride penetration is done based on the average penetration depth. This test is capable of addressing some of the concerns raised regarding the RCPT because of direct measurement of chloride profile rather than relying on charge passed through the sample, application of a lower voltage and hence the reduced temperature rise during the test etc. Still, this test is not immune to some of the common drawbacks associated with the rapid migration techniques. Inclusion of conductive materials like steel and carbon in the concrete specimen or blending of more conductive admixtures such as calcium nitrite might alter the extent of chloride migration through the sample (Russell 2001, Stanish et al. 1997). The original (NT Build 492) version of this test allows for the determination of diffusion coefficient (known as migration coefficient), but the modified version (RMT) simply provides a table for the evaluation of the tested concretes based on the penetration depths for a specified test voltage and duration. The derived relationship used in the original version of this test for calculating diffusion coefficient and the theory behind the derivation will be analyzed in detail in Chapter 3. Table 2.2 below provides the RMT rating based on the study by Hootan et al. (2001) and an equivalent RCPT rating corresponding to each RMT level of rating (Stanish et al. 2005).

Table 2.2: RMT Ratings of Concrete and Equivalent RCPT Ratings (Hooton et al. 2001 and Stanish et al. 2005).

Rate of Penetration (mm/(V-hr))	RMT Concrete Performance Grade	Equivalent RCPT Rating (C)
$0.034 \geq x > 0.024$	1	$3000 \geq x > 2000$
$0.024 \geq x > 0.012$	2	$2000 \geq x > 800$
$0.012 \geq x$	3	$800 \geq x$

2.1.2 Summary of Test Methods

Table 2.3 below summarizes some of the important characteristics of each of the test methods discussed above.

Table 2.3: Basic Characteristics of Different Test Methods (Stanish et al. 1997).

Test Methods		Considers Chloride Ion Movement	Temperature	Effect of Conductors (steel bars etc.) in the Concrete	Approximate Duration of Test Procedure
Long Term	AASHTO T259: Salt Ponding Test	Yes	Constant	Not affected	90 day after curing and conditioning
	ASTM C1556: Bulk Diffusion Test	Yes	Constant	Not affected	40 – 120 days after curing and conditioning
Short Term	AASHTO T277: RCPT	No	Varies	Affected	6 hours
	NT Build 492 (also RMT)	Yes	Constant	Affected	18 hours

2.1.3 Relationship between Transport Theories and Test Methods

None of the above test methods are entirely based on the basic forms of transport theories such as the diffusion theory or the diffusion-migration theory (detailed discussions on both of these theories are provided in Chapter 3). Still, each of the above test methods is loosely based on one of the above two theories. The general relationship between transport theories and test methods can be established as follows:

- Salt Ponding Test: The chloride ions in this test penetrate into concrete due to diffusion (and possibly due to capillary absorption, at least initially, because the test specimens are initially dry).
- Bulk Diffusion Test: Diffusion is the major transport mechanism in this test as the specimens subjected to this test are fully saturated with limewater.
- RCPT and NT Build 492/RMT: Non-steady-state diffusion-migration is the major transport mechanism in these test methods.

2.2 Transport Related Concrete Characteristics

Studies have found that there is a significant level of resistance to the chloride movement in concrete as compared to the chloride movement in a free aqueous solution. According to Atkinson and Nickerson (1984), the level of resistance to chloride transport is several orders higher in concrete as compared to simulated pore solutions (for example, free aqueous solution). A number of microstructural and electrochemical factors are attributed to the resistance to chloride transport in concrete. Stanish (2002) has recongnized tortuosity, constrictivity and connectivity as major microstructural components. Tortuosity can be thought of as a zigzag path the ions have to assume during their transport because of the random positioning of pores in concrete. Constrictivity pertains to a pore system being constrictive. A constrictive pore system can be thought of as a pore system with intermittent narrower or tapered regions (bottle-neck effect) (Stanish 2002). Connectivity is related to a pore being isolated or connected to other pores in the neighborhood. In short, more tortuous and constrictive pores lead to reduced ion penetration whereas more connected pores lead to an increased ion penetration. Apart from microstructural factors, other researchers have listed electrochemical factors such as interaction between different ionic

species (ionic interaction) and membrane effects due to charged pore walls, as contributing factors in transport processes of chlorides (Buenfeld et al. 1998, Tang and Nilsson 1999, Tang 1999).

Microstructural factors such as tortuosity, constrictivity and connectivity are essentially related to the pore structure. Similarly, electrochemical factors such as ionic interaction and membrane effects are related to the pore solution chemistry and chloride binding, two characteristics that are unique to concrete. Structurally, concrete is a composite material consisting of pores and ITZ as well as fine and coarse aggregates. In other words, pores and ITZ make an integral part of the pore structural system in concrete. In the following sections, discussions and definitions of pore structure, porosity, ITZ, pore solution chemistry and chloride binding are presented.

2.2.1 Pore Structure

Pores can be divided into two categories: gel pores and capillary pores. Gel pores are much smaller in size (0.5 to 4 nm) as compared to capillary pores (10 nm to 10 μm) and most of the ion transport takes place through capillary pores (Yaman et al., 2000). Orlova et al. (1999) state that gel pores have negligible permeability due to their smaller size and the great affinity of water molecules to these pores. It is believed that once water molecules get adsorbed into the gel pores, they are not easily evaporable. The adsorption of water molecules makes gel pores even narrower and the ion transport is virtually impossible through these pores (Orlova et at. 1999).

Formation of pores begins with water-filled voids during the initial placement of plastic concrete. The cement paste consists of residual spaces filled with water (known as capillary pores) along with unhydrated portland cement. Unhydrated cement undergoes the hydration

process in the presence of water and moisture forming hydration products. Hydration products mainly consist of calcium silicate hydrate (C-S-H) gel, which is highly porous (porosity of about 28%), and crystals of calcium hydroxide ($Ca(OH)_2$) (Buenfeld et al. 1998). Since the hydration products formed are volumetrically more than 2 times the original unhydrated product, a portion of capillary pores formed during the initial placement of concrete disappear or get blocked with the progression of hydration, thus reducing the pore systems in concrete (Buenfeld et al. 1998, Yaman et al. 2000). As a general rule, pore structures undergo gradual refinement with age due to the hydration process. In other words, more pore spaces are filled with hydration products with the aging of concrete, leading to less porosity and reduced connectivity of pores. As a result, the rate of chloride transport is less at later ages as compared to the early ages of concrete.

Just like pores, air voids can also be divided into two categories: entrained voids and entrapped voids. Entrained voids are deliberately provided voids or bubbles in concrete by incorporating chemical admixtures such as air-entrainers in the mix as these voids have been found to be effective against the effects of freeze-thaw cycles (Yaman et al., 2000). These entrained voids are about 0.1 mm in diameter and are evenly distributed in concrete. Entrapped voids, on the other hand, are the voids that are accidentally formed in concrete because of improper or inadequate consolidation, and might be up to several times larger than entrained voids. Whenever entrained or entrapped voids are filled with air, there is no ion transport through them. But when these voids are filled with water, the transport of ions is possible through these voids provided these void are connected to pores. However, transport of ions solely through these voids is not likely as these voids are not generally interconnected.

2.2.2 Porosity

Porosity is a measure of total volume of pores present in concrete (and hence sometimes termed as total porosity) where it is expressed as the volume fraction of total pores in concrete. There are a number of ways to experimentally determine porosity. These include the determination of total porosity based on the total weight of a penetration liquid such as water or propan-2-ol (C_3H_7OH) absorbed by an oven dry concrete sample. Discussion about porosity needs a good understanding of pore size distribution because pore size distribution becomes more important than the total porosity of concrete when the chloride ingress is an issue. For example, the rate of chloride ingress might be higher in concretes with lower porosity and larger-size pores as compared to concretes with higher porosity and smaller-size pores. A common method of determining pore size distribution in concrete is the Mercury Intrusion Porosimetry (MIP). Using this technique, both total porosity and pore size distribution of concrete can be determined (Stanish 2002).

2.2.3 ITZ

In regular concrete, a thin heterogeneous region of cement paste generally exists at the interface between the cement paste and aggregates. This region needs to be treated differently because studies have found this region to be more porous than the bulk cement paste region due to higher porosity and larger-size pores (Maso 1980, Garboczi and bentz 1996a and 1996b). The formation of this region is attributed to two possible reasons: insufficient packing, and one-sided growth effect (Garboczi and Bentz 1999). Insufficient packing is a result of the so-called *wall-effect* of aggregates with respect to the cement particles. Even the smallest of the aggregate particles have much larger sizes in comparison to the cement particles and hence the aggregate surface works as a flat wall next to these cement

particles. Since the aggregate surfaces pose as walls on one side of the cement particles that are in contact with the aggregates, the packing is not as effective as in free space. The second possible reason, the one-sided growth effect, is due to insufficient cementing gel (C-S-H) being formed on the side of the aggregate surface. In such a situation, the packing (densification) during the hydration of cement takes place only on the free side of the cement particles and thus the growth of cementing gel is possible only through the free side. In any case, the lesser extent of densification in the ITZ region results in less cement and higher water/cement (w/c) ratio, which results in higher porosity with larger pore sizes. The thickness of the ITZ depends on several factors including aggregate sizes, average spacing of aggregates in the matrix, and surface conditions of aggregates such as the degree of roughness etc. (Sujata et al. 1996, Neubauer et al. 1997). These studies do not agree on a single ITZ thickness value, but most agree that it is between 10 μm to 50 μm (Jaiswal et al. 1998, Scrivener and Gartner 1988, Winslow et al. 1994). Some researchers even believe that the ITZ thickness may correspond to a median cement particle size, that is, the thickness might be equal to the median diameter of cement particles (Garboczi and Bentz 1999). But, ITZ region does not have a clear-cut boundary with the bulk cement paste. Typically, the porosity value is at its peak at the aggregate surface and gradually decreases away from the surface and drops back to the average bulk porosity. Figure 2.3 shows a typical porosity distribution in the ITZ and bulk regions as a function of distance from the aggregate surface.

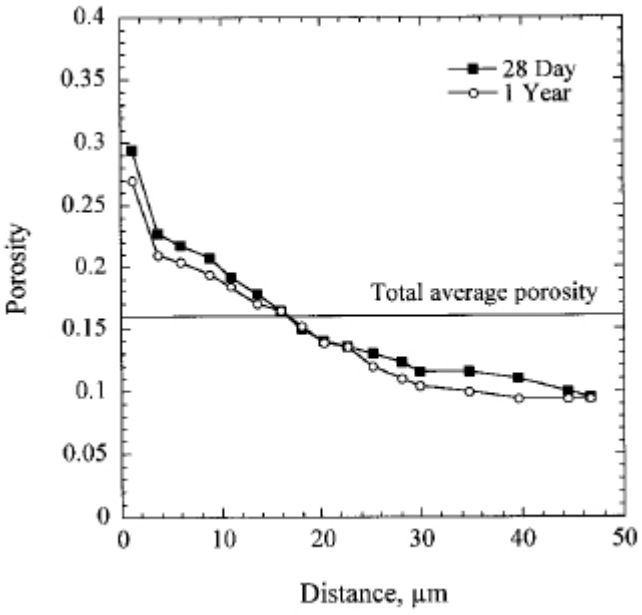

Figure 2.3: A typical distribution of porosity in the ITZ and the paste regions (Scrivener and Nemati 1996).

As it can be seen in Figure 2.3, the ITZ thickness essentially depends on the cut-off points. But the decision regarding the cut-off point entirely depends on how the porosity distribution is interpreted. For example, the cut-off point in Figure 2.3 is provided by a line pertaining to the total average porosity. But according to Shane et al. (2000), the ITZ region typically ends when the porosity drops down to within 10% of the bulk porosity, which might give a different ITZ thickness from the one found using total average porosity.

Because of the high porosity and larger pore sizes, the ITZ plays a key role in determining the overall permeability and penetrability of mortars and concretes. Just as in the ITZ thickness, there is not common agreement on how much more permeable the ITZ regions are permeable as compared to the bulk pastes. However, a study has found that the chloride diffusivity in the ITZ is 10 times higher than in bulk cement paste (Delagrave et al. 1997).

Studies have found that at aggregate volume fractions of 50% and higher, ITZ regions are interconnected, a situation commonly known as the percolation of ITZ (Garboczi and Bentz 1996a and 1996b; Xi and Bazant 1999). Figure 2.4 shows de-percolated and percolated ITZ regions with the help of simplified circular aggregates.

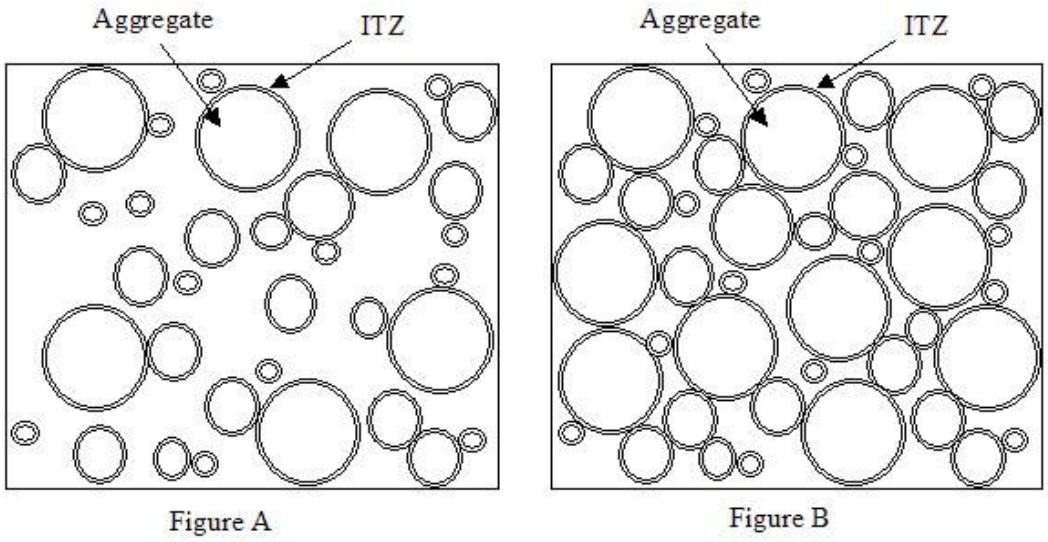

Figure 2.4: (A) De-pecolated ITZ due to low aggregate volume fraction, and (B) percolated ITZ due to high aggregate volume fraction (ITZ thicknesses are exaggerated for clarity).

Percolation of ITZ leads to a percolated ITZ path and in such a situation, most of the ion transport takes place through this path. When there is no percolation of ITZ, addition of aggregates in mortars and concretes have been found to have little effect on the permeability, because inclusion of aggregates, on one hand, introduces more tortuosity to the penetration path; but on the other hand, ITZ regions around them provide a swifter penetration path. As a result, the net effect might be minimal. But once the percolation of ITZ takes place, a continuous path with higher porosity facilitates a much faster permeation and ion transport through the system. However, it is necessary to understand that not all

concretes have the ITZ. In fact, concretes incorporating the supplementary cementitious materials such as fly ash and silica fume may not have the ITZ or, at least, they may be too small to detect in those cases.

2.2.4 Pore Solution Chemistry

Ionic interaction, or interaction between different ions, is related to the influence of ions on one another due to the charges each of these ions carry. Major ion species present in the pore solution are sodium (Na^+), potassium (K^+), and hydroxyl (OH^-). Small amounts of calcium (Ca^{2+}) and sulfate (SO_4^{2-}) may also be present in the solution (Page and Vennesland 1983). Chloride (Cl^-) is not present in any significant amount in the pore solution unless the agents having chloride ions such as calcium chloride are used initially in the mix. There is ionic interaction among different ions in the solution. The exact proportion of each of these ion species depends on the type of cement, water-cement ratio, use of supplementary cementitious materials, degree of hydration, and moisture content (Buenfeld et al. 1998). Mobility (or the moving ability) of an ion species is an important factor in determining the order of precedence it gets over other species in the solution during the transport. Atkins (1994) has provided the order in which the mobility of each of the above-mentioned species increases. In terms of mobility factors, each of these ions can be ranked in the following order (from lowest to highest): $Na^+ < Ca^{2+} < K^+ = Cl^- < SO_4^{2-} < OH^-$. According to this order, cations seem to be less mobile than anions. The overall effect of the presence of different ion species in the pore solution and the corresponding mobility factors give rise to two fundamental transport related issues: (a) restriction in charge separation, and (b) the possible difference between actual concentration and effective concentration of ion species (Buenfeld et al. 1998). Both of these issues highlight a fundamental difference between

dealing with ions as charged particles and uncharged particles. Issue (a) is related to the electroneutrality of an electrolytic solution such as NaCl where total negative charge should be equal to the total positive charge. However, during the rapid chloride transport tests such as RCPT, the electrodes at the two ends work as a sink or a source to the electrons in charged ions and as a result, cations and anions are able to move relatively independent of each other because the original electroneutrality is broken by the electrodes. Issue (b) is more relevant at higher ionic concentrations in the solution. Even though the conductivity and diffusivity of pore solutions increase at increasing concentrations, this increase in conductivity and diffusivity becomes less pronounced at higher solution concentration levels. Due to ionic interaction, the effective concentration, known as activity, becomes less than the actual concentration in the solution at higher concentration levels. The ratio of effective concentration to actual concentration is known as activity coefficient. Less activity coefficient means a reduced activity of ions in the solution, which in retrospective, means that the ions are less mobile and hence result in the reduced ion diffusion (Snyder et al. 2003).

2.2.5 Chloride Binding

A portion of chloride ions entering concrete gets bound on its way, meaning this portion is no longer able to move forward. This unique situation is termed as *chloride binding* in concrete. Chloride ions are bound in concrete in three different ways: chemically bound, physically bound, and trapped in pores. Chloride ions may be chemically bound with some of the hydration products such as tricalcium aluminate and the ferrite phase ($4CaO.Al_2O_3.FeO$) of concrete resulting in a new compound known as Friedel's salt ($3CaO.Al_2O_3.CaCl_2.10H_2O$) (Midgley and Illston 1984). Physically bound chlorides are the

adsorbed chloride ions on the C-S-H surfaces of pore wall. Physical chloride binding is attributed to a so-called membrane effect where this effect is developed as a result of pore walls being charged. It is believed that during hydration, hydration products release surface hydroxyl through the pore walls and in turn become positively charged. These positively charged walls have high affinity for anions and hence work as an anion exchange membrane (Buenfeld et al. 1998). However, the surface charge might change overtime from positive to negative and vice versa depending on the exposure solution and its alkalinity as well as on the types of binders and hydration products (Nagele 1986, Nagele 1987, Cocke and Mollah 1993). A schematic diagram showing free and bound chlorides in a simulated pore is presented in Figure 2.5. In this figure, fixed (bound) chloride is shown to be the sum of two types where Cl^- is the physically bound chloride and Cl is the chemically bound chloride.

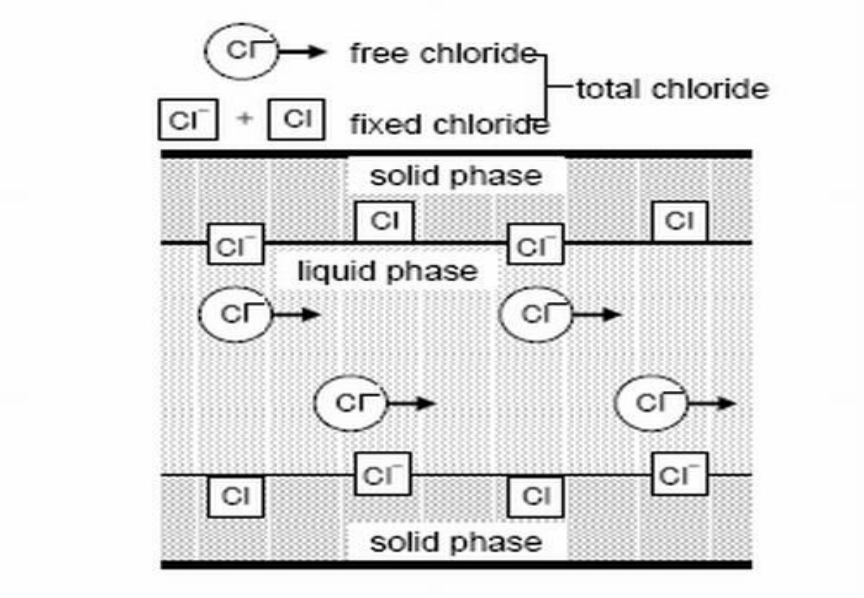

Figure 2.5: Schematic representation of free and bound chlorides in a concrete pore (Maruya et al. 2003).

A small portion of chloride ions might also be trapped in narrow pores where these ions are no longer able to move because of high constrictivity of the pores. Regardless of how the chlorides are bound, bound chlorides are *lost* chlorides from transport point of view, as these chlorides are no longer available for the transport. Chloride binding may be affected by several factors including cement type and proportion, w/c ratio, curing, addition of supplementary cementing materials etc. In case of supplementary cementing materials, binding capacity has been found to increase with the addition of alumina containing materials such as fly ash and slag, whereas this capacity has been found to decrease with the addition of materials without alumina such as silica fume (Justnes 1998).

When one discusses bound chlorides, it is necessary to talk about free chlorides as well. By definition, free chlorides are that portion of chloride ions which are not bound one way or the other, and hence are available for the transport. In other words, total chloride concentration is the sum of free and bound chloride concentrations. Mathematically, it can be expressed as:

$$C_t = C_f + C_b \quad \text{.....(2.1)}$$

where, C_t is the total chloride concentration, C_f is the free chloride concentration and C_b is the bound chloride concentration.

The amount of chloride binding is of particular interest, as this amount is responsible for the added complexity of chloride transport mechanism in concrete. Numerous studies have shown that the amount of binding is a nonlinear function of free chloride concentration in solution even though these studies differ in the appropriateness of relationships defining the amount of binding. Two types of relationships are proposed in such studies to determine the bound chloride concentration corresponding to the specified value of free chloride

concentration, known as binding isotherm. One of these relationships is known as the Langmuir isotherm, which is of the form (Stanish 2002):

$$C_b = \frac{\xi C_f}{1 + \psi C_f} \quad \text{.....(2.2)}$$

where ξ and ψ are two constants that are determined experimentally. Another type of relationship is known as the Freundlich isotherm, which is of the form (Stanish 2002):

$$C_b = \varphi C_f^{\gamma} \quad \text{.....(2.3)}$$

where φ and γ are two constants determined experimentally. According to Tang and Nilsson (1993), the Langmuir isotherm may be appropriate for lower levels of free chloride concentration (less than 0.05 mol/L) whereas the Freundlich isotherm may be appropriate for higher concentration levels (more than 0.1 mol/L),.

As can be seen in both isotherm relationships above, the bound chloride concentration depends on the free chloride concentration. Equation (2.1) above can be used to derive a mathematical expression for chloride binding rate. Differentiating both sides of Equation (2.1) with respect to C_t, we get (Oh et al. 2004):

$$\frac{dC_t}{dC_t} = \frac{dC_f}{dC_t} + \frac{dC_b}{dC_f}\frac{dC_f}{dC_t} \quad \text{.....(2.4)}$$

Rearranging the terms, we get:

$$\frac{dC_f}{dC_t} = \frac{1}{1 + \frac{dC_b}{dC_f}} \quad \text{.....(2.5)}$$

where free and bound chloride concentrations are expressed in grams per gram of concrete. Even though the binding rate in Equation 2.5 is expressed as the change in free chloride

concentration with respect to total chloride concentration $\left(\frac{dC_f}{dC_t}\right)$, the actual binding rate is controlled by the change in bound chloride concentration with respect to free chloride concentration $\left(\frac{dC_b}{dC_f}\right)$ as shown in Equation 2.5 (Oh et al. 2004).

2.3 Cementitious Materials: Uses and Effects

2.3.1 Introduction

Ever since the invention of portland cement in early 1800's, this material was used single-handedly as a binding ingredient in concrete for more than a century. But in recent years, other cementitious materials, commonly known as supplementary cementitious materials (SCM's), have been incorporated in concrete, either in addition to the cement or through the replacement of a portion of cement, to enhance the properties of concrete both in plastic and hardened states. Commonly used SCM's are silica fume, fly ash (Class C and Class F) and ground-granulated blast-furnace slag (GGBS). All of these materials are byproducts of different manufacturing processes where stringent government regulations require the industries to contain these byproducts before they are air-borne in the open air. As a result, the use of these SCM's in concrete industry fulfills a two-fold mission: proper utilization of byproducts and enhancement of concrete properties.

2.3.2 Cementitious Materials

Since silica fume and Class C fly ash were the two SCM types incorporated in the mixes in the present study, the influence of these two SCM's on the different aspects of concrete

properties is discussed in this section. But first, the basic information on portland cement, silica fume and fly ash are provided below.

2.3.2.1 Portland Cement

The manufacturing of portland cement starts with heating limestone and clay where the limestone has calcium chemically bound with carbonate and the clay is a silica-rich material. The product resulting from the heating, known as cement clinker, consists of dark nodules up to 4 – 5 cm in size. The clinker is rich in calcium and silicon oxides and includes some impurities such as aluminate, ferrite, and magnesia that are already present as impurities in limestone and clay. After extraction from the kiln, the cement clinker is mixed with gypsum (calcium sulfate dehydrate), a key compound in moderating the hydration process. Once the clinker and gypsum are ground together, the final product is a multi-size, multi-phase powder consisting of irregularly shaped particles varying in diameters from 1 μm to 100 μm with an average diameter of 15 to 20 μm (Garboczi and Bentz 1999). Cement chemistry notations are a little different from the regular chemistry notations and each of the typical mineral oxides present in cement have their own notations, such as C for CaO, S for SiO_2, F for Fe_2O_3, A for Al_2O_3, etc. Even water has its own notation, which is simply H in place of H_2O. When cement particles come in contact with water, the surface of these particles react with water and produce cementing gel known as calcium silicate hydrate (C-S-H) and $Ca(OH)_2$ as byproduct. The simplified reaction between the cement particle and water can be written as:

Cement + H_2O = C-S-H (cementing gel) + $Ca(OH)_2$

2.3.2.2 Silica fume

Silica fume is generated as a byproduct during the production of silicon metal or ferrosilicon alloys (Engineering Bullenting-1 2002). This material is made almost exclusively of amorphous silicon dioxide (SiO_2) where its content is in excess of 90% of the total mass. It is an extremely fine, spherical powder with a relatively uniform size. The average diameter of a silica fume particle is about 0.1 μm, which is about one one-hundredth the size of a cement particle (Nawy 1997). Because of its fineness, the specific surface area of silica fume is very high, about 20,000 m^2/kg, whereas this value is only about 350 m^2/kg for ordinary portland cement. For up to 2% to 3% replacement of cement by silica fume in the concrete mix, the presence of silica fume may reduce the water demand. However, at higher replacement levels, the water demand will increase substantially due to high specific surface area of the material. Chemical admixtures such as super-plasticizers may be required to maintain the plasticity of the fresh mix without having to increase the water/cementitious material (w/cm) ratio. Different studies (Hooton et al. 1997 and Abou-Zeid et al. 2003) have found 7% replacement of cement by silica fume to be the optimum replacement level. However, most research studies agree on the replacement level ranging between 5% and 10%, depending on the type of concrete properties desired.

2.3.2.3 Fly ash

Fly ash is another type of byproduct generated by electric power plants that utilize coal as their source of energy. Fine air-borne particles are formed during the combustion of coal. These particles are known as fly ash on a mass scale. As mentioned earlier, fly ash is classified as F and C. The distinction between Class F and Class C fly ash types is based on their chemical compositions. Just as in other cementitious materials, fly ash is made of

several mineral oxides. The major constituents of fly ash are silicon dioxide (SiO_2), aluminum oxide (Al_2O_3), iron oxide (Fe_2O_3) and calcium oxide (CaO). According to ASTM C 618, when the sum of the first three mineral oxides (SiO_2+Al_2O_3+Fe_2O_3) exceeds 70%, the fly ash is designated as Class F. When the sum of those three oxides is more than 50% but less than or equal to 70%, the designation is Class C. Also, Class F fly ash has a low CaO content whereas Class C has high CaO content, usually exceeding 20%. Fly ash particle are found to be smaller than cement particles, usually in the range of less than 1 μm. As a result, the specific surface area of fly ash is about 550 m^2/kg. Unlike silica fume, water demand is found to decrease even at higher replacement levels of cement with fly ash. For example, 2% to 3% reduction in water demand can be expected for every 10% of fly ash replacement of cement. At 25% replacement level, the water demand may decrease by as much as 6% to 10%. On the negative side however, fly ash reacts more slowly than portland cement. This, in turn, slows down the hydration process and the strength gain in concrete. Studies have shown that 15% to 25% replacement of cement by fly ash results in the best concrete performance (Thomas et al. 2003). However, higher replacement ratios such as 20% to 50% have been recommended for cost saving purposes (Myers 2001). Similarly, when the concrete is designed to control the expansion due to alkali-silica reaction (ASR), a replacement ratio of up to 65% is recommended (Shehata and Thomas 2000, Thomas 1996).

2.3.3 Chemical Composition of Cementitious Materials

Before understanding the different reaction phases of cement and SCM's during the hydration process, we need to assess the chemical composition of each of these materials. Chemical composition of cement and SCM's is expressed in terms of constituent mineral oxides. Chemical composition and some pertinent particle properties of interest for ordinary

portland cement (Type I), silica fume (microsilica) and fly ash (Class C) are presented in Table 2.4.

Table 2.4: Typical chemical composition and physical particle properties of ordinary portland cement (Type I), silica fume (microsilica) and fly ash (Class C).

Mineral Oxides	Notations	Cement[a] (Weight %)	Class-C Fly Ash[b] (Weight %)	Silica Fume[c] (Weight %)
SiO_2	S	21.0 – 23.0	34.3 – 40.5	92.0 – 98.0
Al_2O_3	A	4.5 – 6.5	19.8 – 22.3	0.5
Fe_2O_3	F	2.5 – 3.5	4.9 – 5.9	2.1
$SiO_2+Al_2O_3+ Fe_2O_3$	S+A+F	-	61.9 – 68.0	-
CaO	C	63.0 – 65.0	17.7 – 24.5	0.8
MgO	M	< 3.0	3.6 – 5.6	0.3
Na_2O	N	< 1.1	1.6 – 2.0	0.1
K_2O	K	-	0.6 – 0.9	1.0
Average Specific Gravity	-	3.15	2.55	2.20
Average Particle Diameter[d] (μm)	-	10	< 1.0	0.1
Specific Surface Area[d] (m^2/kg)	-	350	550	20,000

a: According to ASTM C150 (1997).
b: Typical values according to a producer's actual weekly analysis.
c: Engineering Bulletin 1 (2002) (a literature by a producer).
d: Average values from Nawy (1997).

2.3.4 Chemical Reaction Phases in SCM's

Depending upon the types of chemical reactions SCM particles undergo during the hydration process of concrete, SCM's are categorized in the following manner:

- Pozzolanic: Silica fume and Class F fly ash

- Hydraulic: GGBS, and
- Partially hydraulic and partially pozzolanic (PHPP): Class C fly ash.

In pozzolanic SCM's (pozzolans) such as silica fume and Class F fly ash, SiO_2 is the main constituent compound, which is amorphous and hence does not directly react with water; however, it does react with calcium hydroxide ($Ca(OH)_2$), a byproduct from the reaction between water and cement particles during the hydration, and produces calcium silicate hydrate (C-S-H) gel (cementing gel). Hence, the chemical reaction takes place in two stages:

Stage 1: Cement + H_2O = C-S-H (cementing gel) + $Ca(OH)_2$

Stage 2: $Ca(OH)_2$ + Pozzolan = C-S-H (additional cementing gel)

On the other hand, the constituent mineral oxides such as CaO and SiO_2 in hydraulic SCM's (such as GGBS) produce the cementing gel by directly reacting with water, the same way as the cement does. The chemical reaction of this type of SCM with water takes place side by side with the reaction between the cement and water:

Cement + H_2O = C-S-H (cementing gel) + $Ca(OH)_2$

SCM + H_2O = C-S-H (cementing gel) + $Ca(OH)_2$

Similarly, PHPP SCM's such as Class C fly ash take part in both hydraulic and pozzolanic reaction phases of the hydration process. Because of high CaO content, Class C fly ash directly reacts with water in presence of SiO_2 in the initial stage to produce C-S-H gel (cementing gel) and $Ca(OH)_2$. This reaction phase (hydraulic reaction phase) is similar to the reaction of cement particles with water. In the second stage (pozzolanic reaction stage), SiO_2 present in the fly ash reacts with $Ca(OH)_2$, a byproduct from the reaction in the initial stage, and produces additional C-S-H gel. In Class F fly ash, the hydraulic reaction phase is not possible because of the negligible CaO content. The chemical reaction during the hydration process of cement and PHPP SCM completes in two stages:

Stage 1: Cement + H_2O = C-S-H (cementing gel) + $Ca(OH)_2$

SCM + H_2O = C-S-H (cementing gel) + $Ca(OH)_2$

Stage 2: $Ca(OH)_2$ + SCM = C-S-H (additional cementing gel)

In the present study, 25% of cement mass was replaced with SCM's where 5% was replaced with silica fume and the remaining 20% was replaced with Class C fly ash. Therefore, the combination of cementitious materials used in the study was cement, PHPP SCM and a pozzolan. The set of chemical reactions representing the actual combination of different cementitious materials in the present study can be written as:

Stage 1: Cement + H_2O = C-S-H (cementing gel) + $Ca(OH)_2$

PHPP SCM + H_2O = C-S-H (cementing gel) + $Ca(OH)_2$

Stage 2: $Ca(OH)_2$ + PHPP SCM = C-S-H (additional cementing gel)

$Ca(OH)_2$ + Pozzolan = C-S-H (additional cementing gel)

2.3.5 Effect of Silica Fume on Concrete Properties

According to Bentz (2000), use of silica fume is known to enhance concrete properties at three different levels: filling the voids in the ITZ region, reducing the overall porosity of bulk paste and ITZ regions, and producing additional C-S-H gel that has significantly less diffusivity than the C-S-H gel produced by the cement hydration. The resulting concrete is a less porous and more durable product that is more resistant to harmful chemical attacks such as sulfate and chloride attacks. Using computer modeling, Bentz (2000) showed the volume fraction of cement and silica fume in the ITZ region. Figure 2.6 shows the distribution of cement and silica fume particles starting right from the surface of an aggregate particle, passing through the ITZ region and extending on to the bulk paste system. If an ITZ thickness of 15 μm is assumed, which is a reasonable assumption, cement volume fraction is

clearly smaller in the ITZ region as compared to the bulk cement paste whereas the distribution of silica fume is the opposite, that is, it is slightly more in the ITZ region as compared to the bulk paste region.

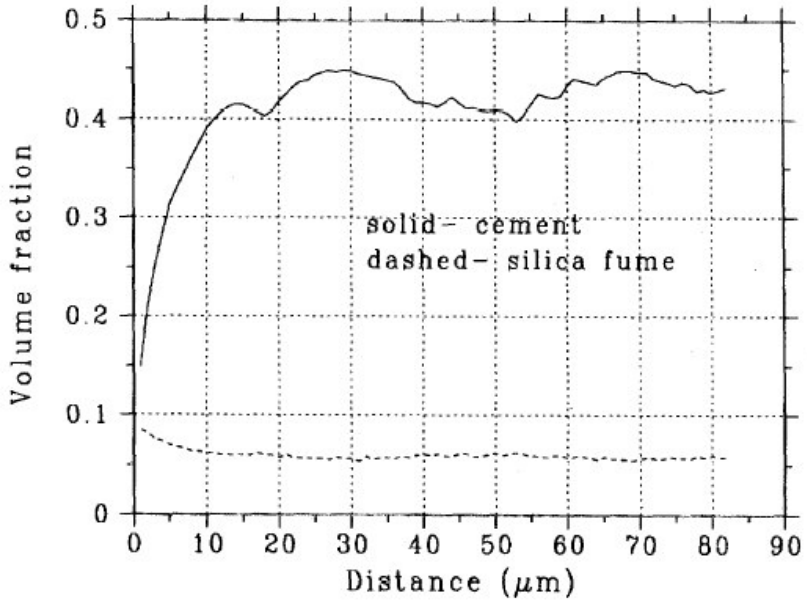

Figure 2.6: Distribution of cement and silica fume starting at the aggregate surface, passing through the ITZ and extending onto the bulk cement paste (Bentz 2000).

The filling of voids by silica fume in ITZ and bulk regions in concrete is attributed to an effect known as the *microfiller effect* of silica fume (Engineering Bulletin-1 2002). Because of the extreme fineness of silica fume, every cement particle is surrounded by more than 50,000 silica fume particles at 10% replacement level of cement by silica fume (Engineering Bulletin-1 2002) and by more than 2,000,000 particles at 15% replacement level (Cohen et al. 1990). A representative sketch of *microfiller effect* of silica fume around cement particles is shown in Figure 2.7.

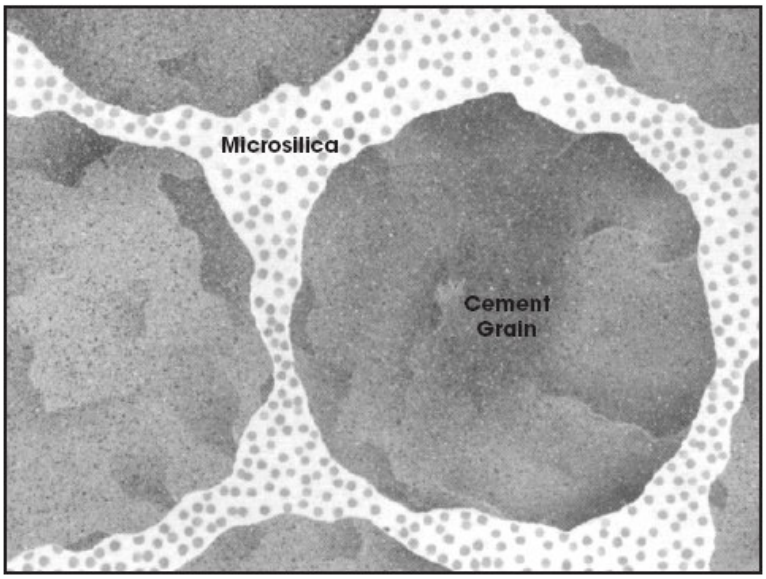

Figure 2.7: *Microfiller effect* of silica fume around cement particles (Engineering Bulletin 1 2002).

The formation of ITZ region is believed to be caused by insufficient compaction of cement particles at the interface between the aggregate surface and the binding matrix. Most studies have found an ITZ thickness of about 15 to 30 μm in the concrete made of ordinary portland cement (without any SCM's); most interestingly the median diameter of a cement particle is almost equal to the thickness of the ITZ. If an ITZ thickness is the result of the insufficient packing of the binding particles and is dependent on the diameter of the these particles, then the concrete incorporating silica fume should result in much smaller ITZ thickness due to extremely small size of silica fume particles. It is believed that the use of SCM's having finer particles such as silica fume helps reduce both pore size and the total porosity in ITZ as well as in bulk cement paste. According to Alexander et al. (1995), the ITZ may be absent or, at least, difficult to detect when low w/c ratio is maintained or the finer mineral admixtures such as silica fume are used. Similarly, with the help of back scattered electron microscopy, Scrivener et al. (1988) confirmed that the ITZ porosity in

silica fume concrete is less than in OPC concrete. Numerous other studies suggest that the better performance of high quality concretes incorporating silica fume, at least in part, is the result of the modifications in the ITZ region (Regourd 1985, Sellevolt and Nilsen 1987, Bentur et al. 1988, and Sarkar et al. 1988). With the help of a computer model, Bentz (2000) has shown the reduction in capillary porosity in ITZ and the bulk paste at different ages of concrete. Figure 2.8 shows the capillary porosity of two mixes, one with 0% silica fume and the other with 10% silica fume.

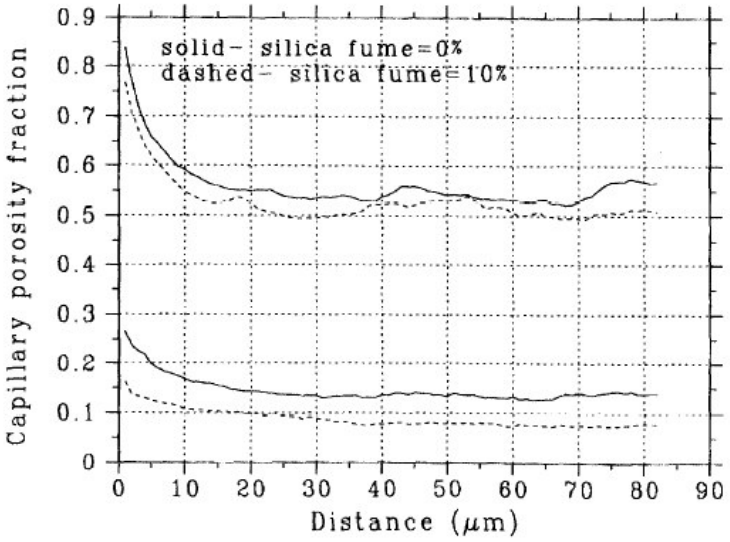

Figure 2.8: Capillary porosities in ITZ and the bulk paste for the mixes with and without silica fume (note that top two curves are at an earlier age and the bottom two are after 180 days of curing) (Bentz 2000).

In Figure 2.8, assuming an average ITZ thickness of 15 μm, total capillary porosity at both initial and hydrated stages is noticeably lower in case of silica fume concretes. Or, if a cut-off point is chosen instead of assuming a fixed ITZ thickness, it seems that the ITZ thickness

itself might be smaller for silica fume concretes. Therefore, the use of silica fume might reduce both porosity and thickness of ITZ in addition to reducing the bulk porosity.

2.3.6 Effect of Silica Fume on RCPT

In spite of the fact that silica fume undoubtedly enhances the concrete properties, the key issue lies on the role of silica fume in concrete in altering the RCPT results. Critics (Pfeifer et al. 1994, Shi 2001) argue that in concretes incorporating silica fume, total coulomb passed in RCPT is dramatically less than in similar concretes without silica fume whereas this situation is not fully supported by other test methods such as salt ponding and bulk diffusion tests. A study on the effect of silica fume incorporation in concrete in terms of chloride penetration was done by Hooton et al. (1997). Several standard and modified long-term and short-term chloride penetration tests including salt ponding test, bulk diffusion test and RCPT were carried out on concretes with 0%, 7% and 12% replacements of cement by silica fume. A graph showing relative reduction in diffusion coefficients (or, the reduction in total charge passed in case of RCPT) as supported by different chloride penetration tests at different silica replacement levels is given in Figure 2.9.

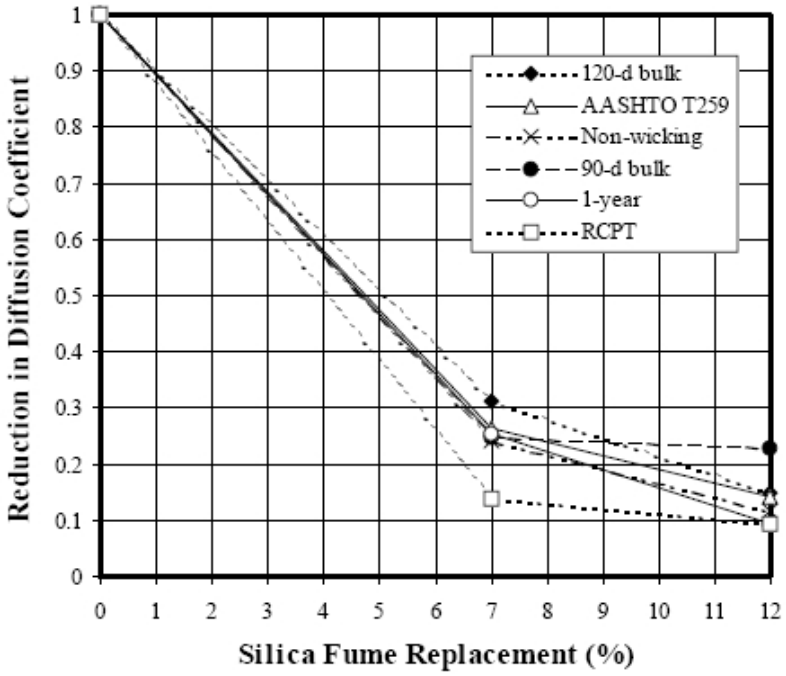

Figure 2.9: Relative reduction in test results (either diffusion coefficients or total charge passed) at different replacement levels of silica fume (Hooton et al. 1997).

It is interesting to observe the results in Figure 2.9 at 7% replacement level. For example, the relative reductions in the test results from salt ponding test (AASHTO T259), modified salt ponding test (indicated as non-wicked in the figure), 90-day bulk diffusion test and 1-year salt ponding test (indicated as 1-year in the figure) are almost the same and the reduction is about 75% for all of them as seen in Figure 2.9. The reduction from 120-day bulk diffusion test, however, is only about 68%. But the reduction in RCPT values from 0% silica fume to 7% silica fume is more than 85%. Therefore, it is apparent that despite the fact that the incorporation of silica fume does enhance the concrete properties significantly, RCPT result seems to be exaggerating this enhancement to some extent. This exaggeration is attributed to the difference in pure diffusion mechanism and diffusion-migration mechanism. For

example, migration of chloride ions in pore solution under the influence of the electrical potential depends both on microstructure of concrete (porosity and pore distribution) and pore solution chemistry whereas pure diffusion depends only on the microstructure of concrete (Shi 2001). In concretes incorporating silica fume, pore solution concentration is found to be less than in regular concretes. According to a study by Page and Vennesland (1983), the concentration of all major ions present in the pore solution are found to decrease with an increase in silica fume replacement levels. Table 2.5 provides concentration of various ions at different silica fume replacement levels for a 0.5 water/cm ratio.

Table 2.5: Analysis of pore solution chemistry at different silica fume (SF) replacement levels (Page and Vennesland 1983).

Pastes (w/c=0.5)	Age (days)	Ionic Concentration (mmole/L)					Total Ion Concentrations (mg equiv./L)	
		Na^+	K^+	Ca^{2+}	OH^-	SO_4^{2-}	Cations	Anions
Pure Cement	7	263	613	1	788	23	876	834
	28	271	629	1	834	31	900	896
	84	323	639	2	743	27	966	797
10% SF	7	161	388	1	486	20	551	526
	28	101	209	0	241	40	311	321
	84	107	192	2	228	27	303	282
20% SF	7	109	231	1	290	23	342	336
	28	59	109	1	91	33	170	157
	84	51	69	2	78	25	124	128
30% SF	7	75	143	1	152	33	220	218
	28	35	53	2	26	35	92	96
	84	30	30	7	10	32	74	74

2.3.7 Effect of Silica Fume-Fly Ash Blends on RCPT

A study conducted by the Missouri Department of Transportation (MoDOT 2003) shows that the mixes incorporating SCM's result in less RCPT values as compared to the control mix (without SCM's) at all test ages. Similarly, the mix incorporating silica fume-fly ash blend result in lower RCPT values as compared to the mixes that incorporate only silica fume. RCPT results at different ages of the mixes incorporating various combinations of SEM's are presented in Table 2.6.

Table 2.6: Average RCPT results for various combinations of cementitious materials at different ages (MoDOT 2003).

Mix Description	Approximate RCPT Values (Coulombs)		
	28-day	56-day	90-day
No fly ash and silica fume, water reducer used	2750	2400	2275
15% fly ash, no silica fume, water reducer used	2800	2175	1750
35% fly ash, no silica fume, water reducer used	2500	1375	900
6% silica fume, no fly ash, water reducer used	1375	1025	950
15% fly ash, 6% silica fume, water reducer used	1275	700	550

Similarly, in another study by Poon et al. (1999), several combinations of mixes were prepared at w/cm ratios of 0.3 and 0.5. The control mix, a mix with 5% silica fume, and a mix with 5% silica fume and 20% fly ash are selected here for comparison purposes. RCPT results on these mixes at 28, 56 and 180 days showed that the mixes using SCM's have

significantly lower RCPT values as compared to the control mix at both w/cm ratios and at all ages. On the other hand, comparison of RCPT results between the 5% silica fume mix and 5% silica fume-20% fly ash mix showed that the silica fume-fly ash blend is more resistive than silica fume alone at later ages and at higher w/cm ratios. For example, at 0.3 w/cm ratio, silica fume mix had similar results as the silica fume-fly ash mix at 28 and 90 days but the at the 180-day RCPT results indicated that the silica fume-fly ash blend is more effective. At 0.50 w/cm ratio, this trend was further pronounced, that is, silica fume-fly ash blend is more resistive to chloride migration at later ages. Table 2.7 summarizes the test results for these mixes.

Table 2.7: RCPT results for various combinations of cementitious materials at different w/cm ratios and ages (Poon et al. 1999).

w/cm Ratios	Mix Types	28-Day RCPT (Coulomb)	90-Day RCPT (Coulomb)	180-Day RCPT (Coulomb)
0.30	Control	1899	1349	1400
	5% SF	345	340	287
	5% SF, 20% FA	375	242	136
0.50	Control	3678	3093	3120
	5% SF	2162	1762	1972
	5% SF, 20% FA	1418	696	289

Yet in another study by Ozyildirim (1998), several mixes were prepared using fly ash and slag at various replacement levels of cement. One set of mixes was prepared using 5% replacement of cement by silica fume at 0.35, 0.4 and 0.45 water/cm ratios. Similarly, another set of mixes was prepared at the same three w/cm ratios by replacing 24% cement by fly ash and another 3% of cement by silica fume. The RCPT test results on these two sets

of mixes showed that at early ages, the former set of mixes resulted in lower RCPT values, but with the aging of concretes, the latter set of mixes (with silica fume-fly ash blend) showed drastically reduced RCPT results as compared to the former set of mixes (with silica fume alone). The results are summarized in Table 2.8.

Table 2.8: RCPT results on two sets of mixes at different w/cm ratios (Ozyildirim 1998).

Mixes Proportions (PC/FA/SF)	w/cm ratios	28-Day RCPT (Coulomb)	90-Day RCPT (Coulomb)	1-Year RCPT (Coulomb)	32-Month RCPT (Coulomb)
95/0/5	0.35	864	515	501	599
	0.4	1122	710	813	936
	0.45	1556	933	1021	1086
77/24/3	0.35	1454	490	225	150
	0.4	2689	842	297	216
	0.45	2219	711	274	201

PC: Portland Cement; FA: Fly Ash; SF: Silica Fume.

2.3.8 Effect of Silica Fume-Fly Ash Blends on Pore Solution Chemistry

According to a study by Shehata and Thomas (2002), the reduction in pore solution concentration due to the incorporation silica fume and fly ash is higher than the incorporation of silica fume alone. They prepared several mixes using a combination of either high alumina cement (HAPC) or low alumina cement (LAPC), silica fume (SF), and one of three fly ash types: low calcium content (FM), medium calcium content (WM) and high calcium content (OK). Pore solution expression showed that combination of SF/FA resulted in less ion concentrations in pore solutions as compared to SF alone.

2.3.9 Conclusions on SCM's and RCPT

Based on the above studies, a number of conclusions can be drawn:

1. The RCPT results in concretes incorporating silica fume, fly ash or both will be significantly lower than in the concretes made from ordinary portland cement alone. Primary reason for this reduction can be classified as:
   - Refinements in porosity and pore size distribution, and
   - Reduction in ion concentration in the pore solution.

   This is similar to the observation made by Poon et al. (1999) in their study where they concluded that the drop in RCPT results in fly ash and silica fume concretes might be the result of microstructural changes as well as reduction in the conductivity of the concrete which, obviously, is due to the drop in the ion concentration in pore solution.
2. Silica fume-fly ash blend is more effective in lowering RCPT values as compared to silica fume alone, at least, at higher concrete ages.

2.4 Effect of aggregate Porosity on Chloride Transport

Porosity in coarse aggregates is a well-known physical property. Several durability related issues in concrete such as freezing and thawing, and wetting and drying, in fact, are attributed to the porosity of incorporated aggregates in concrete (ACI 221R-96 1997). As aggregates are crushed stones or naturally available stones from wide varieties of rock origins, their physical and chemical properties including porosities vary widely as well. Stronger rock origins such as granite and gneiss are found to have very low porosity (0.5% to 1.5%) whereas weaker rock origins such as sedimentary rocks (limestone) are found to have higher porosity (5% to 20%) (Attewell and Farmer 1976).

The ingress of chloride ions in concrete is possible only because of the concrete porosity. In OPC concretes with relatively high w/c ratios, porosities in the cement paste region of concrete are found to be in the range of 30% to 40% (Monteiro 2004), which is much higher than a typical porosity range of aggregate. As a matter of fact, typical porosities in aggregates are less than 3% and they seldom exceed 10% even for the aggregates derived from the most porous rock origins (Monteiro 2004). For this reason, most of the researchers tend to neglect the effect of aggregate porosities during studies of chloride penetration in concrete. Most of the time, aggregates are treated as impervious fillers in concrete that do not take part in the process of chloride movement in concrete. The idea behind marginalizing the role of aggregate porosity in chloride penetration might have come from the notion that the aggregate porosities do not significantly contribute to the bulk chloride penetration and hence do not deserve additional consideration. This notion is aided by the presence of an ITZ around the aggregates in OPC concretes that can be up to 10 times more porous than the cement paste (Delagrave et al. 1997), making a significant contribution to the bulk chloride penetration. Because of the highly porous ITZ regions around significantly less porous aggregate particles, chloride ions may choose ITZ as a preferential path and avoid the aggregate particles altogether. Under this assumption, it seems reasonable not to take aggregate porosity into account in an OPC concrete during chloride penetration.

But recent innovations in concrete technology have given rise to the types of concretes that are significantly less porous (with smaller-size pores) than OPC concretes. Typically designed to work under severe environments, these types of concretes are highly resistant against the penetration of deleterious elements into them and hence are known as high performance (HP) concretes. According to some studies, the ITZ regions may be absent or, at least, difficult to detect in HP concretes (Alexander et al. 1995, Scrivener et al. 1988). In this

respect, aggregate porosity may become an important parameter for the determination of chloride penetration in concrete. Because of the use of supplementary cementitious materials such as silica fume and fly ash, low water-to-cementitious material (w/cm) ratio, and the use of water reducing and air entraining agent, the concretes prepared in the present study qualify as HP concretes. These concretes show significantly lower RCPT values as compared to the OPC concretes from some other studies with similar w/cm ratios. For example, the concrete mixes without SEM's are reported to have their 28-day RCPT coulomb values in the order of 2000 to 4000 (Abou-Zeid et al. 2003, Hootan et al. 1997) for a typical w/c ratio of 0.40. But at the same w/cm ratio, the concretes prepared in the present study resulted in much lower 28-day RCPT values (on the order of 1500 to 2500 coulombs as will be seen in Chapter 4) (Titi et al. 2004). In general, the bulk porosity values in HP concretes may be low to such an extent that the aggregate porosities, at least for the so-called highly porous aggregate types, cannot be overlooked. In other words, the contribution made by aggregate porosities of relatively porous aggregates towards the total chloride penetration in an HP concrete may not be negligible. Therefore, the proper understanding of the effects of aggregate porosity and ITZ during chloride penetration in HP concretes is of paramount importance.

Several studies in the field of chloride transport have attempted to analyze different penetration mechanisms using computer simulation methods. They include the extensive research studies carried out by the National Institute of Standards and Technology (NIST) in both OPC and HP concretes. According to published reports, aggregates in these studies have always been treated as impervious inclusions (Bentz et al. 1997; Bentz et al. 1998; Garboczi and Bentz 1996a, 1996b and 1999; Schwartz et al. 1995). Among the studies done outside of NIST, Jaiswal et al. (1998) and Takewaka et al. (2003) have included aggregates as

impervious particles in their respective analytical models. On the other hand, ITZ regions in all of these models are included as highly porous membranes surrounding the aggregate particles.

The author is not aware of any chloride transport studies that account for the contribution made by aggregate porosity towards the bulk chloride penetration in concrete. On the other hand, a strong correlation between the aggregate porosities and the RCPT results for HP concretes is found in the present study, which will be discussed in detail in Chapter 4. Therefore, it is believed that the study of the effect of aggregate porosity on the chloride penetration in HP concretes is an important topic.

3.0 CHLORIDE TRANSPORT THEORIES

3.1 Introduction

Chloride ions penetrate concrete structures in the field by means of diffusion, capillary absorption, and hydraulic pressure. Diffusion is the most common transport mechanism that takes place under a concentration gradient. For the diffusion to take place, there must exist an uninterrupted liquid phase in concrete as well as a chloride ion concentration gradient (Stanish et al. 1997). The second means of penetration, capillary absorption, is a phenomenon where the contaminant solution enters concrete pores down to some shallow depth through capillary suction. This process takes place when the concrete surface is dry and is driven by moisture gradients. This means that the capillary absorption itself is not capable of transporting chloride ions all the way down to the level of reinforcing steel. Its role, however, lies in transporting the ions to some depth in concrete and reducing the total distance to be traveled by chloride ions before they reach the steel (Thomas et al. 1995). The third mechanism, hydraulic pressure, occurs through permeation driven by pressure gradients.

In the following section, the theory of diffusion is discussed briefly not only because it is the predominant chloride transport mechanism but also because several of the researchers working in the area of diffusion-migration transport mechanism in concrete have attempted to modify the diffusion theory itself to address the diffusion-migration situation. Next, the diffusion-migration theory is discussed in its basic form. Then, the literature on the analytical treatment of chloride migration in concrete is reviewed. Finally, a number of conclusions are made based on the literature review.

3.2 Diffusion Theory

Fick's First Law for a one-dimensional problem is given as follows:

$$J = -D\frac{\partial C}{\partial x} \quad \text{.....(3.1)}$$

where J is the flux, D is the diffusion coefficient, C is the concentration, and x is the position variable. The above equation is applicable only to steady-state conditions. However, the same equation can be used to derive a relevant non-steady state equation as well. According to the law of conservation of mass, the relationship between the chloride concentration and flux can be expressed as:

$$\frac{\partial C}{\partial t} = -\frac{\partial J}{\partial x} \quad \text{.....(3.2)}$$

where, t is the time variable. Substituting the value of J from Equation 3.1 into 3.2, we obtain the following equation which is a diffusion equation often referred to as the Fick's second law:

$$\frac{\partial C}{\partial t} = D\frac{\partial^2 C}{\partial x^2} \quad \text{.....(3.3)}$$

Equation 3.3 takes the change in concentration with time into consideration. Assuming a semi-infinite media, Equation 3.3 is solved by applying the following initial and boundary conditions:

$C\ (x > 0, t > 0) = C\ (x, t)$

$C\ (x = 0, t > 0) = C_0$

$C\ (x > 0, t = 0) = 0$

$C\ (x = \infty, t > 0) = 0$

where x and t are the space and time variables respectively. The closed-form solution of Equation 3.3 for the above initial and boundary conditions is:

$$\frac{C(x,t)}{C_0} = erfc\left(\frac{x}{2\sqrt{Dt}}\right) \quad \text{.....(3.4)}$$

where, C(x,t) is the chloride concentration corresponding to x and t variables, and *erfc* is the complementary error function.

3.3 Diffusion-Migration Theory

When an electrical potential is applied to accelerate the ion transport, the problem becomes a diffusion-migration problem. The diffusion-migration mechanism for the steady-state condition is represented by a relationship, commonly known as the Nernst-Planck equation, given as:

$$J = -D\frac{\partial C}{\partial x} + \frac{zFV}{RTL}DC \quad \text{.....(3.5)}$$

where, z is the valence of transport ions, F is the Faraday's constant (96485 C/mol), V is the electrical potential difference (voltage), R is the gas constant (8.314 J/mol-^{o}K), T is the temperature in Kelvin, L is the specimen length in the direction of voltage application, and the rest are as defined above. Let's introduce a migration term (a_m), where:

$$a_m = \frac{zFV}{RTL} \quad \text{.....(3.6)}$$

According to the law of conservation of mass, we have:

$$\frac{\partial C}{\partial t} = -\frac{\partial J}{\partial x} \quad \text{.....(3.7)}$$

Substituting the value of a_m from Equation 3.6 in 3.5 and then substituting the vale of J from Equation 3.5 in 3.7, we obtain the non-steady state Nernst-Planck equation, given as:

$$\frac{\partial C}{\partial t} = D\frac{\partial^2 C}{\partial x^2} - a_m D\frac{\partial C}{\partial x} \quad \text{.....(3.8)}$$

Assuming a semi-infinite transport media, the following initial and boundary conditions can be applied to the above equation:

C (x > 0, t > 0) = C

C (x = 0, t > 0) = C_0

C (x > 0, t = 0) = 0

C (x = ∞, t > 0) = 0.

The closed-form solution of Equation 3.8 is,

$$\frac{C}{C_0} = \frac{1}{2}\left[e^{a_m x} erfc\left(\frac{x + a_m Dt}{2\sqrt{Dt}} \right) + erfc\left(\frac{x - a_m Dt}{2\sqrt{Dt}} \right) \right] \text{.....(3.9)}$$

where, C_0 is the chloride ion concentration of upstream solution, C is the chloride ion concentration at depth x, and *erfc* is as defined above. Sometimes, Equation 3.5 is given in terms of the mobility factor (u) of an ion species. In this case, the equation is expressed as:

$$J = -D\frac{\partial C}{\partial x} + uC\frac{\partial V}{\partial x} \text{.....(3.10)}$$

where, $u = \frac{zFD}{RT}$ .....(3.11)

and, electrical potential difference per unit distance across the specimen length,

$$\frac{\partial V}{\partial x} = E = \frac{V}{L} \text{.....(3.12)}$$

Subsequently, Equation (3.8) becomes:

$$\frac{\partial C}{\partial t} = D\frac{\partial^2 C}{\partial x^2} - u\frac{\partial}{\partial x}\left(C\frac{\partial V}{\partial x} \right) \text{.....(3.13)}$$

As will be seen in the subsequent sections, several inherent physical and chemical characteristics of concrete make it necessary to modify both diffusion and diffusion-migration theories before they can be explicitly applied to chloride transport in concrete.

However, the importance of understanding each of these theories in their basic forms lies in the fact that these theories work as backbones in several studies related to the diffusion-migration of chloride ions in concrete. The proper understanding of the basic theories is also essential when considering the possibility of applying any concrete-specific modifications.

3.4 Analytical Treatment of Transport Theories: Literature Review

3.4.1 Study by Andrade et al. (1994)

Andrade (1993) and Andrade et al. (1994) modified the basic diffusion equation (Equation 3.3 above) to represent the diffusion-migration condition. The diffusion coefficient (D) in the equation is changed to the migration coefficient (D_{mig}) and Equation 3.3 is modified as (Andrade et al. 1994):

$$\frac{\partial C}{\partial t} = D_{mig}\frac{\partial^2 C}{\partial x^2} \quad \text{.....(3.14)}$$

D_{mig} is defined as:

$$D_{mig} = a_m D \quad \text{.....(3.15)}$$

where, a_m is as defined in Equation 3.8 above.

As a result, Equation 3.4 becomes:

$$\frac{C(x,t)}{C_0} = erfc\left(\frac{x}{2\sqrt{a_m Dt}}\right) \quad \text{.....(3.16)}$$

By observing Equations 3.15 and 3.16, it seems the migration coefficient is thought to increase several folds due to the application of electrical potential in the test. For a typical RCPT test case, 60 V of potential difference applied across a specimen (50-mm thick) at 25°C (298°K), the multiplier (a_m) used above produces an approximate value of 47 mm^{-1}.

Stanish (2002) compared the experimental data from Hooton et al. (2001) to the prediction curve provided by Equation 3.16 and found a good correlation as shown in Figure 3.1.

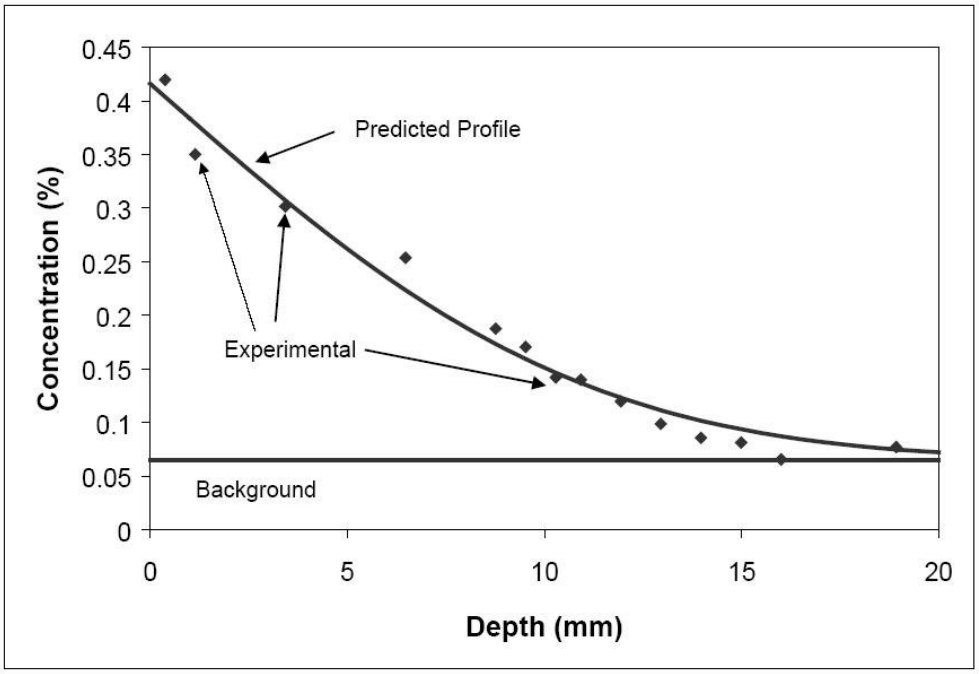

Figure 3.1: Comparison between the experimental data from Hooton et al. (2001) and the calculated profile using Equation 3.16 proposed by Andrade et al. (1994) (Stanish 2002).

However, the modification of diffusion relationship to a migration relationship as proposed by Andrade et al. (1994) is not a proper interpretation of the underlying theories because the diffusion is driven by concentration gradient whereas migration is driven by an electrical potential gradient (Stanish 2002). Another fundamental problem with this modification is that the area under the diffusion curve (concentration versus depth) (A) is not a linear function of the diffusion coefficient (D); rather the square of area (A^2) is linearly dependent on D. On the other hand, the area under the migration curve (using Equation 3.9 above) is linearly dependent on diffusion coefficient. This indicates that it is not theoretically

appropriate to modify a diffusion equation to become a migration equation simply by introducing a constant such as a_m. Even if Equation 3.16 seems to be working properly at a given diffusion coefficient value, that should be regarded as a mere coincidence. For a 2-fold increase in the diffusion coefficient (D), for instance, the chloride profile area will increase approximately by 1.41 times by using the diffusion equation (Equation 3.4) and 2 times by using the diffusion-migration equation (Equation 3.9). Therefore, the diffusion equation as modified by Andrade et al. (1994) cannot properly represent a migration situation.

3.4.2 Study by Tang (1996)

Tang (1996) proposed a relationship to determine the chloride diffusion coefficient based on the chloride penetration depth of a concrete sample subjected to a rapid chloride penetration test. For this purpose, a number of simplifications to the analytical solution of diffusion-migration relationship (Equation 3.9 above) were made. This same work was later adopted as a standard test procedure (NT Build 492), known as the RMT, by the Nordic testing agency (Stanish 2002). According to Tang (1996), when the electrical potential difference is sufficient, that is, 12 V or more, the chloride ions will be able to penetrate into a sufficient depth in the specimen. In such cases, the first term on the right side of Equation 3.9 becomes negligible, that is:

$$e^{a_m x}\,erfc\left(\frac{x+a_m Dt}{2\sqrt{Dt}}\right)\to 0 \qquad (3.17)$$

Thus, Equation 3.9 becomes (Tang 1996):

$$\frac{C(x,t)}{C_0}=\frac{1}{2}erfc\left(\frac{x-a_m Dt}{2\sqrt{Dt}}\right) \qquad (3.18)$$

Rearranging the terms, we get:

$$\frac{x - a_m Dt}{2\sqrt{Dt}} = erfc^{-1}\left(\frac{2C(x,t)}{C_0}\right) \quad \text{(3.19)}$$

Letting $\varepsilon = erfc^{-1}\left(\frac{2C(x,t)}{C_0}\right)$ and solving for D (Tang 1996):

$$D = \frac{1}{a_m t}\left(\frac{2\varepsilon^2}{a_m} + x - \frac{2\varepsilon}{\sqrt{a_m}}\sqrt{\frac{\varepsilon^2}{a_m} + x}\right) \quad \text{(3.20)}$$

Tang (1996) has proposed a colorimetric technique for the determination of chloride penetration during RMT where a 0.1 N silver nitrate ($AgNO_3$) solution is sprayed on a split-open concrete specimen subjected to RMT. Chloride reacts with AgNO3 and forms a white precipitate of AgCl. This color change boundary has been estimated by Tang (1996) to be around 0.07 N in pore solution, assuming 0.3 mL of pore solution per gram of cement. Similarly, the upstream solution in RMT is 10% (by weight) NaCl solution, which is approximately equal to 2.0 N NaCl. Now, neglecting ε^2 as this term is much smaller than a_m under normal conditions, and using corresponding boundary conditions, Equation 3.20 can be rewritten as (Tang 1996):

$$D = \frac{RTL}{zFV}\frac{x_d - \vartheta\sqrt{x_d}}{t} \quad \text{(3.21)}$$

where, ϑ is a laboratory constant and is equal to:

$$\vartheta = 2\sqrt{\frac{RTL}{zFV}}erfc^{-1}\left(\frac{2C(x,t)}{C_0}\right) \quad \text{(3.22)}$$

The parameters used in Equations 3.21 and 3.22 can be redefined specifically for RMT in the following manner (NTBuild 492 1999):

C_0 = Surface chloride concentration (2.0 N)

C(x,t) = Chloride concentration at color change boundary (= 0.07 N)

D = Diffusion coefficient ($\times 10^{-12}$ m^2/s)

V = Potential difference

T = Test temperature (^oC)

L = Specimen thickness (mm)

x_d = Depth of penetration (color change boundary) (mm)

t = Test duration (hour)

Substituting the respective values of notations and ϑ, Equation 3.21 can be written as (NTBuild 492 1999):

$$D = \frac{0.0239(273+T)L}{(V-2)t}\left(x_d - 0.0238\sqrt{\frac{(273+T)Lx_d}{(V-2)}}\right) \quad \text{.....(3.23)}$$

An estimated 2 V is subtracted from the applied voltage to account for the potential drop at both electrode-solution interfaces (McGrath and Hooton 1996).

One major shortcoming of this model is that it does not take chloride binding into consideration (Stanish 2002). Another issue associated with this model is its inability to properly predict experimental chloride profiles found in RMT tested specimens. Stanish (2002) showed that the actual chloride profile curves do not match the shapes of the calculated chloride profile using Equation 3.23 above. Typical experimental and calculated chloride profile curves are shown in Figure 3.2.

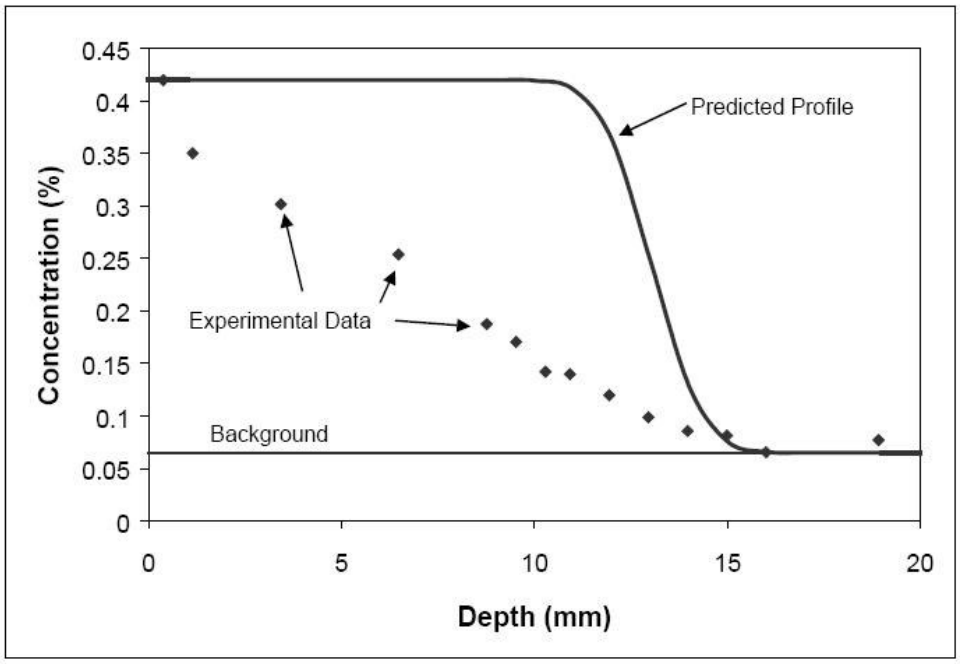

Figure 3.2: Comparison between the calculated chloride profile using Equation 3.18 and the experimental chloride profile (Stanish 2002).

Unfortunately, this comparison is not appropriate. As Equation 3.18 does not take binding into account, the chloride concentration determined according to Equation 3.23 is, in fact, the free chloride concentration (C_f). But the experimental chloride concentration according to Stanish (2002) is the total chloride concentration (C_t), which is the sum of free and bound chloride concentrations. The experimental results are obtained through powder sampling and chemical testing, which reflects both types of chlorides (total of free and bound chlorides). Therefore, an appropriate comparison between the analytical chloride profile according to Equation 3.18 and the experimental chloride profile would be as shown in Figure 3.3.

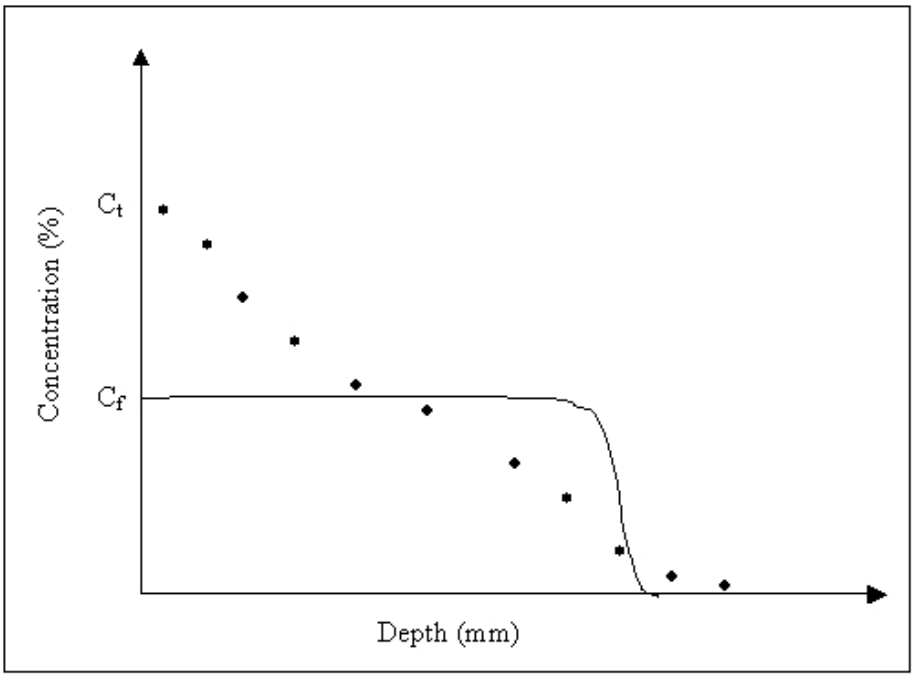

Figure 3.3: A sketch showing an appropriate comparison between the analytical chloride profile according to Equation 3.18 and the experimental chloride profile data.

In spite of the discrepancy between the chloride profile by Tang's proposed equation (Equation 3.18) and the typical experimental chloride profiles curves, Stanish (2002) indicates that the diffusion coefficients calculated using Equation 3.23 for the 28-day concrete specimens subjected to RMT and the diffusion coefficients from 90-day bulk diffusion test showed a reasonable correlation. Using the data by Hooton et al. (2001), Stanish (2002) found that the calculated relative diffusion coefficient (ratio of analytical diffusion coefficient to experimental diffusion coefficient from the bulk diffusion test) was 0.99 on average. Figure 3.4 shows the relative diffusion coefficients using Equation 3.23 against the values obtained from the bulk diffusion test.

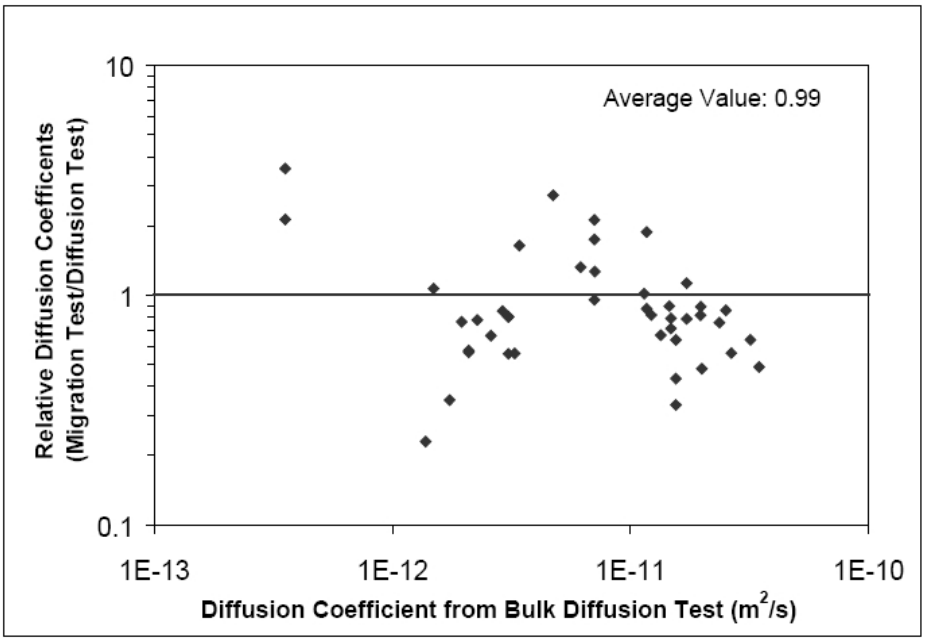

Figure 3.4: Relative diffusion coefficient versus the diffusion coefficient from the bulk diffusion test (Stanish 2002).

The first issue with the comparison made in Figure 3.4 is the data scatter. Even though the average relative diffusion coefficient is very close to 1, the data points are very widely scattered. There is a second issue originally raised by Stanish (2002). The diffusion coefficients from 90-day bulk diffusion test are, in fact, not the diffusion coefficients exactly at 28 days, but an average value over a period starting at 28 days and ending 90 days later (because the test starts at 28 days and ends 90 days later). Hence, the diffusion coefficient values are actually at an average age of 73 days. On the other hand, the calculated diffusion coefficient values using Equation 3.23 were based on 28-day RMT results. This means that the diffusion coefficient values using Equation 3.23 should be higher than the diffusion coefficient values from bulk diffusion test and this situation should give us average relative diffusion coefficient values (migration test/diffusion test) greater than 1.0. The third issue,

which is the most important among all, is that Equation 3.23 does not take chloride binding into account but the bulk diffusion test includes binding. Because of binding, a significant portion of the solution chloride concentration is *lost* into binding and as a result the actual diffusion is noticeably slower that if there were no binding. In this context, the calculated migration coefficients (Equation 3.23) were supposed to be significantly higher than the bulk diffusion coefficients which, in turn, would give the average relative diffusion coefficient much higher than 1. Therefore, even though the comparison between the migration diffusion coefficients (using Equation 3.23) and from bulk diffusion test seem to show a good correlation at first, this comparison misses a number of points as discussed above and hence does not provide meaningful information regarding the ability of Equation 3.23 in accurately estimating diffusion coefficients based on RMT results.

3.4.3 Study by Buenfeld et al. (1998)

In a study by Buenfeld et al. (1998), an additional binding term is included in the Nernst-Planck equation (Equation 3.8 above) to take chloride binding into account. Once the chloride concentration is distinguished between free (C_f) and bound (C_b) chloride concentrations and the binding term is introduced, the equation becomes:

$$\frac{\partial C_f}{\partial t} = D\frac{\partial^2 C_f}{\partial x^2} - uE\frac{\partial C_f}{\partial x} + \chi \quad \text{.....(3.24)}$$

where, χ is the binding rate of concrete. The rate of binding can be defined as:

$$\chi = \frac{\partial C_b}{\partial t} \quad \text{.....(3.25)}$$

Now, Equation 3.24 can be written as (Buenfeld et al. 1998):

$$\frac{\partial C_f}{\partial t} = D\frac{\partial^2 C_f}{\partial x^2} - uE\frac{\partial C_f}{\partial x} + \frac{\partial C_b}{\partial t} \quad \text{.....(3.26)}$$

Buenfeld et al. (1998) defined the rate of binding as a simple first-order chemical reaction, given as:

$$\chi = \frac{\partial C_b}{\partial t} = k_b C_f \quad \text{.....(3.27)}$$

where, k_b is the binding rate-constant (Xu and Chandra 1994; Zhang 1997). The problem of using a rate-constant such as k_b was realized during the execution of trial models in the present study. When our models were run with all necessary parameter values, the binding rates remained constant no matter how long the test duration were set. In other words, at a given location of the model (depth of concrete), the bound chloride kept on adding up at a constant rate regardless of the duration. In fact this situation is not possible in the real world. Even binding isotherms determined in different studies suggest a limit as to how much binding is possible in a given concrete. Since the porosity is finite, the pore-wall surface area is finite as well; and therefore, the binding capacity should be finite. A typical binding isotherm is presented in Figure 3.5.

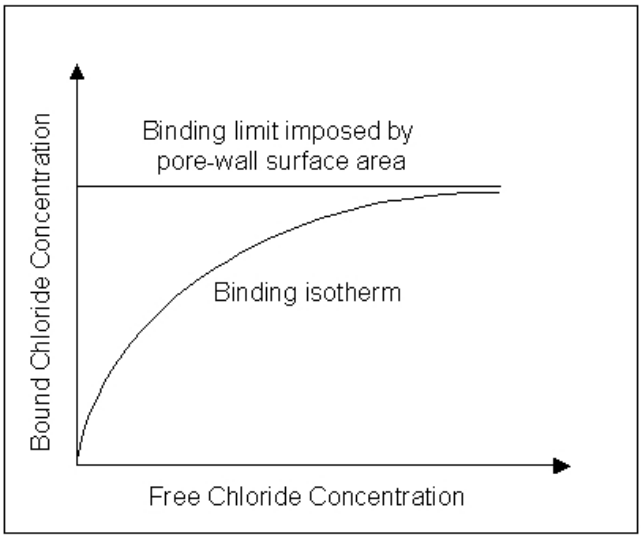

Figure 3.5: A typical binding isotherm and a binding limit boundary line (Stanish 2002).

An additional horizontal line in Figure 3.5, to which the binding isotherm is asymptotical, suggests that there will be an upper limit to the binding capacity for a given porosity. As the free chloride concentration increases, the bound chloride concentration increases sharply at first as shown in Figure 3.5. But once the bound chloride concentration approaches its limit, there is no appreciable increase in bound chloride concentration even at increasing free chloride concentration levels. Therefore, a linear binding mechanism assumed by Buenfeld et al. (1998) needs a revision to appropriately address the real-life binding situation.

3.4.4 Additional Studies

Several other studies have used the Nernst-Planck equation either in its basic form or with some modifications during the analytical simulation of chloride migration. In a study by Tang and Nilsson (1992), the Nernst-Planck equation in its basic form (Equation 3.8) is used to simulate the chloride migration in non-steady state migration test procedures. Similarly, in a study by Halamickova et al. (1995), the closed-form equation of the basic Nernst-Planck equation (Equation 3.9) is used to simulate the chloride migration during a modified RCPT on mortar specimens. In another study, Samson et al. (2003) proposed an alternative approach to simulate chloride migration during migration tests where the Nernst-Planck equation is coupled with the Poisson's equation to derive the Nernst-Planck-Poisson equation.

3.5 Conclusions on Chloride Transport Theories

Based on the above literature review, a number of conclusions are drawn as provided below:

- The Nernst-Planck equation is the most common relationship used by researchers for the numerical treatment of chloride migration during laboratory migration tests such as RCPT or RMT.
- Some studies take the effect of chloride binding during migration into account while others don't. When chloride binding is taken into account, a linear binding function of free chloride is used. However, it should be noted that chloride binding is not a linear function of free chlorides as discussed above.

4.0 PHASE I: MN/DOT PROJECT

4.1 Background

The concept of investigating the effect of aggregate porosity on the RCPT results for the present study was first formulated while working, along with Mr. Mohammed Elias, on a project sponsored by the Minnesota Department of Transportation. The project was titled *The Effect of Minnesota Aggregates on Rapid Chloride Permeability Tests*, in which the final report was published by Mn/DOT (Titi et al. 2004). This project analyzed the effects of 12 different aggregates types (obtained from 12 different sources in Minnesota) on RCPT results by subjecting concrete specimens made from each of these aggregates to RCPT at specified concrete ages of 28, 56 and 91 days. The RCPT results showed a direct correlation between the aggregate porosity and the RCPT result at all test ages. This result was very interesting and encouraging, as well, from further research point of view. As aggregate type was the only variable among the 12 different concrete types, the variations in the RCPT results were determined to be due to the use of different aggregate types in those concretes. Different aggregate types were the sole contributors to the differences in RCPT values. Therefore, we decided to further analyze the role of aggregates in influencing the RCPT results in these concretes. Therefore, the focus had to be, on one hand, on the microstructure of aggregate particles, and on the other hand, on the ITZ regions around these particles. A set of additional experiments was carried out to fulfill this mission. Finally, an analytical model was developed to analyze and verify the role of aggregates in influencing diffusion and migration of chlorides. To properly organize the contents of the experimental and analytical works in the present study, these works are divided in three different phases:

- Phase I: Mn/DOT Project
- Phase II: Additional Experimental Works
- Phase III: Analytical Simulations

This chapter includes a summary of Phase I experimental works and outcomes (Titi et al. 2004). The Phase II and Phase III works are discussed in Chapters 5 and 6, respectively.

4.2 Mn/DOT Project Overview

4.2.1 Introduction

Mn/DOT personnel provided sufficient quantities of 12 different types of coarse aggregates from 12 different aggregate sources from different parts of Minnesota (Titi et al. 2004). Similarly, they provided sufficient quantities of fine aggregates (sand and grit) to be used in the mixes. The coarse aggregate types represent a wide range of aggregate sources and types typically used in highway construction in Minnesota (Titi et al. 2004). Morphological analysis of each of the 12 aggregate types, sand and grit is provided in Table 4.1.

Table 4.1: Morphological analysis of aggregates, sand and grit used in Mn/DOT project (Titi et al. 2004).

Designated Aggregate Names	Names in Mn/DOT Project	General Description
Coarse Aggregates:		
GRNT-A	Barton	Mixture of basaltic and granitic particles, mixture of smooth round particles and rough angular particles
GNSS-A	Brillmeir	Crushed gneiss particles of angular shape and dark color
GRNT-B	Fischer	Mixture of basaltic and granitic particles, mixture of smooth round particles and rough angular particles
LMST-A	Goldberg	Crushed limestone particles of angular shape, rough surface and light color
LMST-B	Kraemer	Crushed limestone particles of angular shape, rough surface and light color
GRNT-C	Lanthier	Mixture of basaltic and granitic particles, mixture of smooth round particles and rough angular particles
LMST-C	Larson	Crushed limestone particles of angular shape, rough surface and light color
GRNT-D	Marietta	Crushed granite particles of angular shape and dark color
GRNT-E	Mark	Mixture of basaltic and granite particles, mixture of smooth round and rough angular surfaces
LMST-D	Michigan	Crushed limestone particles of angular shape, rough surface and light color
QRTZ-A	New Ulm	Crushed quartzite particles of angular shape and dark color
LMST-E	Ulland	Crushed dolomitic limestone particles of angular shape, rough surface and dark color
Fine Aggregates:		
Grit	Grit	Fine particles of igneous rock origin
Sand	Sand	Fine particles of igneous rock origin

4.2.2 Basic Aggregate Properties

Material properties of sand, grit and aggregates such as specific gravity and absorption were experimentally determined. Specific gravity and absorption of coarse aggregates were determined according to ASTM C127 and those of fine aggregates were determined according to ASTM C128. Using the data obtained during these tests, one additional property, that is, total porosity was calculated for both coarse and fine aggregates. Total porosity is calculated as follows:

$$n = \frac{W_{SSD} - W_{OD}}{W_{SSD} - W_{SM}} \times 100\% \quad \text{.....(4.1)}$$

where, W_{SSD} is the saturated surface dry (SSD) weight, W_{OD} is the oven-dry weight and W_{SM} is the submerged weight of the specimen. Table 4.2 provides the calculated values of specific gravity, absorption and porosity for both coarse and fine aggregates.

From Table 4.2, it is observed that even for the aggregate types of the similar geological characteristics, the total porosity values are not close to each other. For example, even though LMST-A, LMST-B, LMST-C, LMST-D AND LMST-E are all crushed limestone (Titi et al. 2004), their porosity values are widely dispersed. LMST-C, LMST-A and LMST-B have relatively high porosity, but LMST-E has relatively low porosity and LMST-D has the lowest porosity. However, GNSS-A (crushed gneiss particles, the least permeable among the rock origins) has the lowest porosity and LMST-C (crushed limestone, the most permeable among the rock origins) has the highest porosity.

Table 4.2: Specific gravity, absorption and porosity values of coarse and fine aggregates (Titi et al. 2004).

Aggregate Types	Dry Bulk Specific Gravity	SSD Bulk Specific Gravity	Apparent Specific Gravity	Water Absorption (%)	Total Porosity (%)
Coarse Aggregates:					
GRNT-A	2.664	2.696	2.752	1.201	3.20
GNSS-A	2.688	2.696	2.710	0.300	0.81
GRNT-B	2.681	2.710	2.762	1.100	2.95
LMST-A	2.657	2.702	2.783	1.702	4.52
LMST-B	2.633	2.689	2.788	2.104	5.54
GRNT-C	2.727	2.751	2.796	0.902	2.46
LMST-C	2.636	2.694	2.798	2.202	5.81
GRNT-D	2.707	2.721	2.745	0.501	1.36
GRNT-E	2.660	2.689	2.740	1.100	2.93
LMST-D	2.762	2.779	2.809	0.600	1.66
QRTZ-A	2.615	2.634	2.664	0.701	1.83
LMST-E	2.693	2.722	2.775	1.101	2.97
Fine Aggregates:					
Grit	2.647	2.684	2.748	1.379	3.65
Sand	2.569	2.618	2.701	1.895	4.87

SSD: Saturated Surface-Dry

4.2.3 Ambient Chloride Content of Aggregates

Ambient acid-soluble chloride content in each of coarse and fine aggregates was determined according to a test method known as the Rapid Chloride Test (RCT). In this test method, 1.5 g of powdered sample is added into 10 ml of extraction liquid (10% acetic acid) in a vial, the vial is secured with a lid and shaken vigorously for 5 minutes. The reading can be taken

immediately in which case the chloride extraction is estimated to be about 90% of the total chloride content in the sample. Alternatively, the vial is left overnight and the reading is taken the next day in which case the chloride extraction is regarded to be 100% of the chloride content in the sample. The reading is done with the help of an electrode connected to an electronic meter where the electrode is dipped into the solution in the vial and the response is read in the meter. At first, the reading is recorded in mV (mili-Volt) and it is then converted into the chloride content (chloride percent by weight of the sample) with the help of a calibration chart. Calibration chart is prepared right before the RCT by recording the response of the electrode (in mV) to four reference chloride solutions of known concentrations (0.005%, 0.02%, 0.05% and 0.5% by weight). RCT along with RCTW (a similar method to determine the water-soluble chloride content in the samples) is discussed in detail in Appendix A. In the present study, representative aggregate samples were selected and washed thoroughly. Once dried out, these samples were properly ground to obtain a fine powder. These powder samples were then subjected to RCT to determine the ambient acid-soluble chloride content. Table 4.3 provides 5-minute (90% extraction) and 1-day (100% extraction) chloride contents of each of the coarse and fine aggregates. According to the 1-day RCT results, ambient chloride content values widely differ from one another. For example, for GRNT-D (crushed granite), the chloride content is as low as 0.003% whereas for LMST-D (crushed limestone) this value is as high as 0.124% (Titi et al. 2004).

Table 4.3: 5-minute and 1-day acid soluble chloride contents on powdered aggregate samples (Titi et al. 2004).

Aggregate Types	5-Minute Chloride Content (% by weight of sample)	1-Day Chloride Content (% by weight of sample)
Coarse Aggregates:		
GRNT-A	0.009	0.023
GNSS-A	0.003	0.004
GRNT-B	0.006	0.010
LMST-A	0.022	0.029
LMST-B	0.037	0.044
GRNT-C	0.002	0.004
LMST-C	0.044	0.050
GRNT-D	0.002	0.003
GRNT-E	0.010	0.020
LMST-D	0.105	0.124
QRTZ-A	0.004	0.006
LMST-E	0.010	0.010
Fine Aggregates:		
Grit	0.006	0.013
Sand	0.006	0.012

4.2.4 Mixing, Casting and Curing

The concrete mix design was according to the criteria set forth by the Mn/DOT specifications 3Y43MS. Sieve analysis done on coarse aggregates according to ASTM C136 revealed that none of the 12 aggregate types as shipped to UWM had the required particle size distribution according to 3Y43MS. Hence, each aggregate type was sieved and broken down into individual particle size range. Later on, the actual quantities of these particle sizes

as required by the 3Y43MS specification were used in the mix. Table 4.4 below presents the Mn/DOT mix design specification (3Y43MS).

Table 4.4: Mn/DOT Mix Design Specification (3Y43MS) (Titi et al. 2004).

Constituent Materials and Parameters	Material and Parameter Values	Comments
Constituent Materials:		
Cement	289.8 kg/m^3	75% by weight
Fly Ash	77.2 kg/m^3	20% by weight
Microsilica	19.6 kg/m^3	5% by weight
Water	154.4 kg/m^3	Includes admixture quantities
Coarse Aggregate (45% by weight of total aggregate):		
19.0 mm – 25.4 mm	1%	Added to 12.7 mm – 19.0 mm when this size not available
12.7 mm – 19.0 mm	16%	
9.5 mm – 12.7 mm	12%	
4.75 mm – 9.5 mm	16%	
Fine Aggregate (55% by weight of total aggregate):		
Sand	22%	
Grit	33%	
Parameters:		
w/cm ratio	0.4	Fixed
Air Content	6.5%	5% to 8%
Slump	≤ 12.7 cm	Varied up to 12.7 cm
Total Aggregate Fraction	About 65% of concrete volume (As calculated)	Cement, fly ash, silica fume, water, admixtures and air void constitute remaining 35% of the volume

Portland Cement Type I, Class C fly ash, microsilica (silica fume), a mid-range plasticizer and an air-entraining agent (all as approved by the Mn/DOT personnel) were used in the mixes (Titi et al. 2004). Trial mix calculations were made based on the absolute volume method. Summary of the trial mix calculations are presented in Tables 4.5 and 4.6.

Table 4.5: Weight of constituent materials required for 0.028 m^3 of fresh concrete as calculated using absolute volume method (Titi et al. 2004).

Materials	Weights (kg)	Volume (ml)
Cement	8.21	N/A
Fly Ash	2.19	N/A
Microsilica	0.55	N/A
Water	4.32	N/A
Air-entrainer	0.01	10.0
Plastisizer	0.04	40.0

Sufficient quantities of aggregates in each particle size of a given coarse aggregate type were left for soaking overnight and the next day, they were brought into saturated surface dry (SSD) condition right before the mixing by drying them with towels and weighing them in SSD condition. In the case of fine aggregates (grit and sand), they were used in the mix in room-dry condition and the necessary water quantity that would be absorbed by them to reach SSD condition was added in the mixing water based on the trial mix calculations. Three trial batches were made for each aggregate type except for the LMST-D aggregate type in which case two trial batches were made due to limited aggregate quantity. Approximately 0.03 m^3 of fresh concrete was prepared in each trial batch and five to seven 100-mm-diameter by 200-mm-long cylinders were cast.

Table 4.6: Weights of different aggregate types in various particle sizes ranges, weights of dry sand and dry grit, and the total weight of water (including additional water that would be absorbed by sand and grit) required to prepare 0.028 m^3 of fresh concrete (Titi et al. 2004).

Aggregate Types	Weight of 19 mm – 25.4 mm aggregate* (kg)	Weight of 12.7 mm – 19.0 mm aggregate (kg)	Weight of 9.5 mm – 12.7 mm aggregate (kg)	Weight of 4.75 mm – 9.5 mm aggregate (kg)	Weight of dry sand (kg)	Weight of dry grit (kg)	Total weight of water (kg)
GRNT-A	0.49	7.87	5.91	7.87	10.63	16.02	4.74
GNSS-A	0.49	7.87	5.91	7.87	10.63	16.02	4.74
GRNT-B	0.49	7.89	5.92	7.89	10.65	16.06	4.75
LMST-A	0.49	7.88	5.91	7.88	10.64	16.04	4.74
LMST-B	0.49	7.87	5.90	7.87	10.61	16.00	4.74
GRNT-C	0.50	7.95	5.96	7.95	10.72	16.17	4.75
LMST-C	0.49	7.87	5.90	7.87	10.62	16.01	4.74
GRNT-D	0.49	7.91	5.93	7.91	10.67	16.09	4.75
GRNT-E	0.49	7.87	5.90	7.87	10.61	16.00	4.74
LMST-D	0.50	7.98	5.99	7.98	10.77	16.24	4.75
QRTZ-A	0.49	7.79	5.84	7.79	10.51	15.85	4.74
LMST-E	0.49	7.91	5.93	7.91	10.67	16.09	4.75

*: Add this quantity to 12.7 mm – 19 mm range when this size range is not available.

Fresh concrete properties such as slump, unit weight and air content were measured using the remaining quantity of the fresh concrete to make sure these parameters fell within Mn/DOT specification limits. Slump test and air content test were done according to ASTM C 143 and ASTM C231 (pressure method) test methods respectively. Casting and curing of cylinders was done according to AASHTO T126. An electric power operated vibrating table

was used to compact the fresh concrete into the cylinder molds. After 24 hours, cylinders were demolded and transferred to the moist curing room, which had water sprinklers to keep cylinders wet uninterruptedly. Cylinders were provided with a continuous moist environment and were not removed from the curing room until the day of testing. At a concrete age of 28 days, the compressive strength test was done on a representative cylinder from each batch of each concrete type according to ASTM C39. Properties of fresh concretes and compressive strength test results are presented in Tables D.1 and D.2, respectively, in Appendix D.

4.2.5 RCPT on Concrete Specimens

The first set of Rapid Chloride Permeability test (RCPT) on the concrete specimens was done at the age of 28 days. The second and third sets of RCPT were done at the ages of 56 days and 91 days, respectively. RCPT was performed on the prepared specimens as part of the Mn/DOT project where RCPT was conducted according to AASHTO T277 (2000). A 50±3 mm thick disc specimen was cut from the top of the cylinder a day before the test. The specimen was measured to make sure its thickness fell within the required limit and a rapid-setting epoxy coating was applied on the sides (not on the ends). Once the epoxy dried out, the specimen was put inside a vacuum desiccator and subjected to three hours of continuous vacuuming under a pressure less than 1 mm Hg. With the vacuum pressure still maintained, the specimen was completely submerged under de-aerated water for an additional one hour. The vacuum pressure was released and the specimen was left submerged in water inside the desiccator for another 18±2 hours. After this period, the specimen was taken out of desiccator and mounted on the RCPT device between two exposure solution chambers in such a way that the top finished face of the specimen would face the upstream solution

(NaCl solution). Once the device was secured tight and checked for the water tightness, the upstream chamber was filled with a 3.0% NaCl solution and the downstream chamber was filled with a 0.3 N NaOH solution. The device was connected to the electronic data acquisition system and a DC voltage of 60 V was applied across the specimen with the help of appropriate wiring. The test was run for 6 hours under a constant voltage of 60 V. At the end of the test, the total charge passed (measured in coulombs) was recorded as the final result. The detail test procedure and other relevant information are provided in AASHTO T277 (or in ASTM C1202). Table 4.7 shows the RCPT results on all aggregate types at different specimen ages.

Some of the tests were done a few days later than the scheduled date due to the unavailability of the research team. Such results are indicated in the table, marked with superscripts with the exact age of concrete at which the tests were carried out (Titi et al. 2004). Later on, those values were adjusted to the standard scheduled ages by linearly extrapolating between the two nearest data points. For example, a test done on the 62^{nd} day was adjusted to the 56-day result by linearly extrapolating the 62-day and 91-day test results and so on. In Tables 4.8, 4.9 and 4.10, the adjusted RCPT results at standard 28, 56 and 91 days of concrete, respectively, are used to calculate the mean, standard deviation and coefficient of variation (COV) of the results.

Table 4.7: RCPT results of all twelve concrete types at different concrete ages (Titi et al. 2004).

Concrete Types	Batch No.	Total Charge Passed (Coulombs)		
		28-Day RCPT	56-Day RCPT	91-Day RCPT
GRNT-A	1	1918	944	662
	2	2151	1044(62)*	822
	3	2004	1125(62)*	802
GNSS-A	1	1550(33)*	1116	677
	2	1341(30)*	872	691
	3	1465(29)*	989	655
GRNT-B	1	2081	1044(58)*	959
	2	1925	1032(57)*	916
	3	1835	798(57)*	637
LMST-A	1	2432	1074(61)*	984
	2	2065	1104(60)*	899
	3	2140	1096(60)*	896
LMST-B	1	2648	1463	1195
	2	2713	1695	1269
	3	2457	1460	1194
GRNT-C	1	1549	867	661
	2	1533	809	749
	3	1451	904	686
LMST-C	1	2598	1668	1206
	2	2332	1163	1110
	3	2666	1757	1393
GRNT-D	1	1589	912	644
	2	1769	933	647
	3	1559	984	588
GRNT-E	1	1717	1402	903
	2	1788	1138	883
	3	2124**	1234	958
LMST-D	1	1878	1122	732
	3	1519	829	584
QRTZ-A	1	1782	925	701
	2	1351	740	514
	3	1565	949	587
LMST-E	1	2096	1175	974
	2	1941	1174	827
	3	2004	1113	814

* Indicates the age of the specimen at the time of testing.
** Indicates faulty data. Discarded.

Table 4.8: 28-day RCPT values and basic statistical analysis (Titi et al. 2004).

Concrete Types	Total charge passed in 28-Day RCPT (Coulombs)				Standard Deviation (σ)	COV (%)
	Batch No. 1	Batch No. 2	Batch No. 3	Mean (μ)		
GRNT-A	1918	2151	2004	2024	118	6
GNSS-A	1644	1377	1483	1501	134	9
GRNT-B	2081	1925	1835	1947	124	6
LMST-A	2432	2065	2140	2212	194	9
LMST-B	2648	2713	2457	2606	133	5
GRNT-C	1549	1533	1451	1511	53	3
LMST-C	2598	2332	2666	2532	177	7
GRNT-D	1589	1769	1559	1639	114	7
GRNT-E	1717	1788	2124*	1753	50	3
LMST-D	1878	-	1519	1699	254	15
QRTZ-A	1782	1351	1565	1566	216	14
LMST-E	2096	1941	2004	2014	78	4

* Indicates faulty data. Discarded.

Table 4.9: 56-day RCPT values and basic statistical analysis (Titi et al. 2004).

Concrete Types	Total Charge Passed in 56-Day RCPT (Coulombs)				Standard Deviation (σ)	COV (%)
	Batch No. 1	Batch No. 2	Batch No. 3	Mean (μ)		
GRNT-A	944	1090	1192	1075	125	12
GNSS-A	1116	872	989	992	122	12
GRNT-B	1049	1035	803	962	138	14
LMST-A	1089	1130	1122	1114	22	2
LMST-B	1463	1695	1460	1539	135	9
GRNT-C	867	809	904	860	48	6
LMST-C	1668	1163	1757	1529	320	21
GRNT-D	912	933	984	943	37	4
GRNT-E	1402	1138	1234	1258	134	11
LMST-D	1122	-	829	976	207	21
QRTZ-A	925	740	949	871	114	13
LMST-E	1175	1174	1113	1154	36	3

Table 4.10: 91-day RCPT values and basic statistical analysis (Titi et al. 2004).

Concrete Types	Total Charge Passed in 91- Day RCPT (Coulombs)				Standard Deviation (σ)	COV (%)
	Batch No. 1	Batch No. 2	Batch No. 3	Mean (μ)		
GRNT-A	662	822	802	762	87	11
GNSS-A	677	691	655	674	18	3
GRNT-B	959	916	637	837	175	21
LMST-A	984	899	896	926	50	5
LMST-B	1195	1269	1194	1219	43	4
GRNT-C	661	749	686	699	45	6
LMST-C	1206	1110	1393	1236	144	12
GRNT-D	644	647	588	626	33	5
GRNT-E	903	883	958	915	39	4
LMST-D	732	-	584	658	105	16
QRTZ-A	701	514	587	601	94	16
LMST-E	974	827	814	872	89	10

4.3 Correlation between Aggregate Porosity and RCPT Results

Initial analysis of the RCPT results at various concrete ages suggested that there was a marked effect of aggregates types on RCPT results (Titi et al. 2004). Since coarse aggregate type was the only variable among all the concrete mixes made, the variations in RCPT results were the result of different aggregate types in the mixes. Interestingly, the aggregate types with lower RCPT results at early concrete ages such as 28 days continued with the same trend of lower RCPT results at 56 and 91 days as well. Similarly, the aggregate types with higher RCPT results at 28 days continued to result in higher RCPT values at 56 and 91 days as well. In other words, the effect of aggregate types in concretes as shown by RCPT results was distinct and this effect was of a permanent nature. After careful observation of the RCPT results in relation to the various physical properties of the aggregates, a strong

correlation between the total aggregate porosity and the RCPT results was found (Titi et al. 2004). Table 4.11 provides the total porosity and the mean RCPT values at all three test ages.

Table 4.11: Total porosity and the mean RCPT values at different concrete ages (Titi et al. 2004).

Concrete Types	Aggregate Porosity (%)	28-Day Mean RCPT Values (Coulombs)	56-Day Mean RCPT Values (Coulombs)	91-Day Mean RCPT Values (Coulombs)
GRNT-A	3.200	2024	1075	762
GNSS-A	0.806	1501	992	674
GRNT-B	2.949	1947	962	837
LMST-A	4.521	2212	1114	926
LMST-B	5.541	2606	1539	1219
GRNT-C	2.459	1511	860	699
LMST-C	5.805	2532	1529	1236
GRNT-D	1.355	1639	943	626
GRNT-E	2.926	1753	1258	915
LMST-D	1.657	1699	976	658
QRTZ-A	1.832	1566	871	601
LMST-E	2.965	2014	1154	872

The values in Table 4.11 are used to plot the aggregate porosity versus RCPT values as shown in Figure 4.1. This figure indicates a clear trend of higher porosity values resulting in higher RCPT values and vice versa at all three test ages. Although this trend seems to be failing in some cases when the RCPT values between two adjacent aggregate types in terms of porosity values are compared (for example, between LMST-D and QRTZ-A where QRTZ-A has higher porosity but lower RCPT results), the overall trend is very pronounced and consistent.

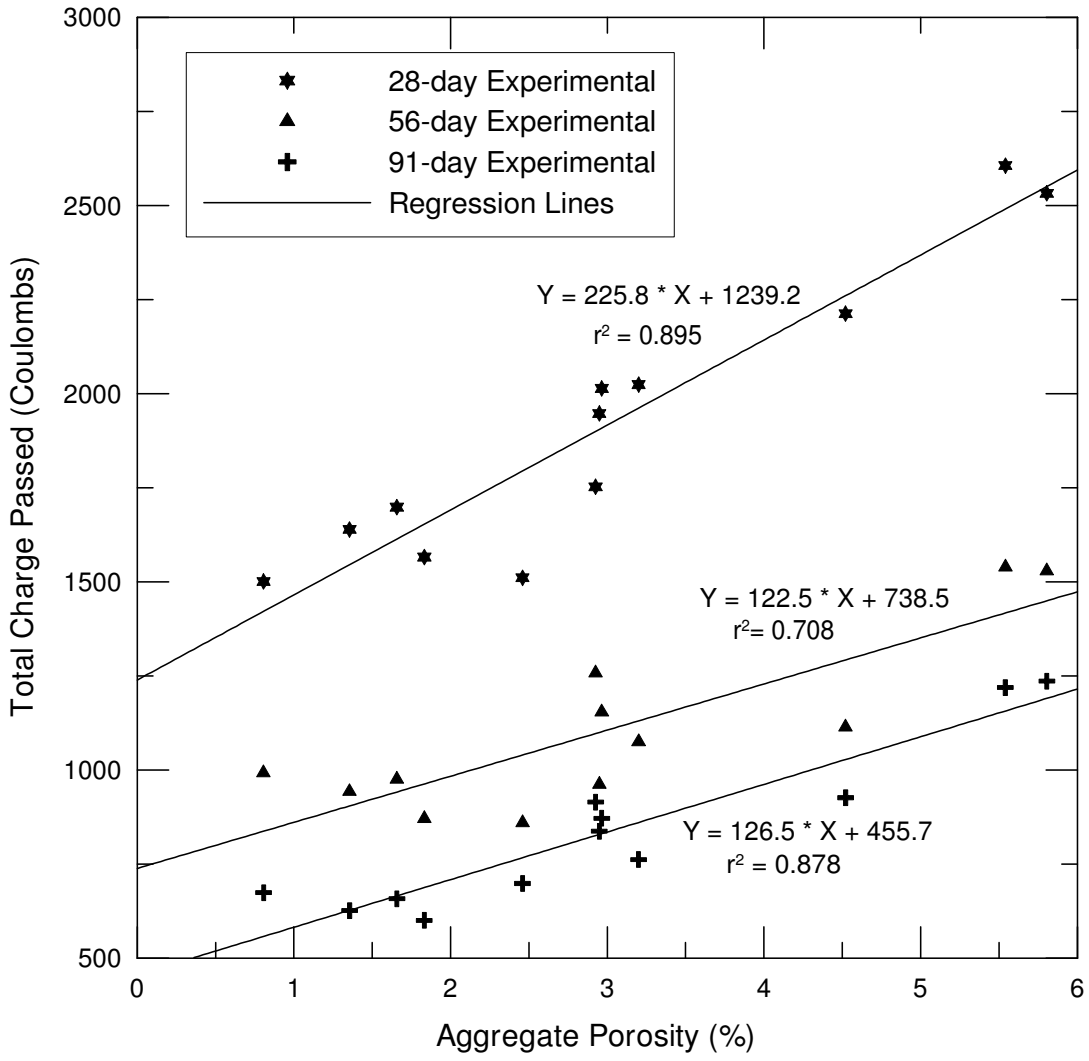

Figure 4.1: Correlation between the aggregate porosity and the total charge passed in RCPT at all three test ages.

4.4 Conclusions on Mn/DOT Outcomes

A number of conclusions can be drawn based on the outcomes of the Mn/DOT sponsored project:

- There was a direct correlation between the aggregate porosity and the RCPT results in the tested concretes. Higher porosities led to higher RCPT values and lower porosities led to lower RCPT values at all test ages.
- Since all parameters in the concretes (including aggregate gradations) were kept constant except for the type of coarse aggregates, the variations in the RCPT results were related to the aggregate types (aggregate porosities and/or ITZ regions).

5.0 PHASE II: ADDITIONAL EXPERIMENTAL WORK

5.1 Overview

Because of a large number of aggregate types used in the Mn/DOT project, it was not possible to carry out further studies on all of these aggregate types. Therefore, GNSS-A, LMST-E and LMST-C aggregate types were selected from the Mn/DOT project for further studies. These represent the aggregate types with the lowest, mid-range and highest porosity and RCPT values (see Chapter 4; Titi et al. 2004). Similarly, other relevant tests were designed and carried out to obtain the necessary data and/or information. The objective of each of the additional tests is indicated at the beginning of each related section. In broader terms, however, the additional experimental effort was designed with a two-fold mission:

- Examine the role of aggregate porosity and the ITZ in modifying the chloride transport in concrete during RCPT.
- Obtain the necessary data and information that can be utilized during the analytical simulation of the chloride migration in concrete during RCPT.

The additional experimental effort and the findings are discussed in the following sections.

5.2 Preparation of *Paste-Alone* Mix

5.2.1 Introduction

A *paste-alone* mix was prepared to further analyze the characteristics of the paste portion of the concretes (which excludes coarse aggregates) with respect to chloride migration during RCPT. Even though it is essentially a mortar mix, it's called a *paste-alone* mix to highlight its objective. The proportions of fine and coarse aggregates only marginally differed from one another in all 12 Mn/DOT concrete mixes (see Table 4.6 in Chapter 4). For this reason, a

single *paste-alone* mix was prepared that was representative of the bulk paste portion in all 3 concrete types selected for further study (that is, GNSS-A, LMST-E and LMST-C). To fulfill this mission, we averaged the proportions of sand and grit from all 12 concrete types and used the averaged quantities in the *paste-alone* mix. Similarly the quantity of mixing water was averaged as well. Obviously, coarse aggregates were not included in the mix and all other constituent materials and chemical admixtures were used in the same proportions as in the Mn/DOT concrete mixes (see Table 4.5). A schematic diagram showing the proportions of the cement paste, fine aggregates (sand and grit) and coarse aggregate in Mn/DOT concretes and the proportions of the cement paste and fine aggregates in *paste-alone* mix is presented in Figure 5.1.

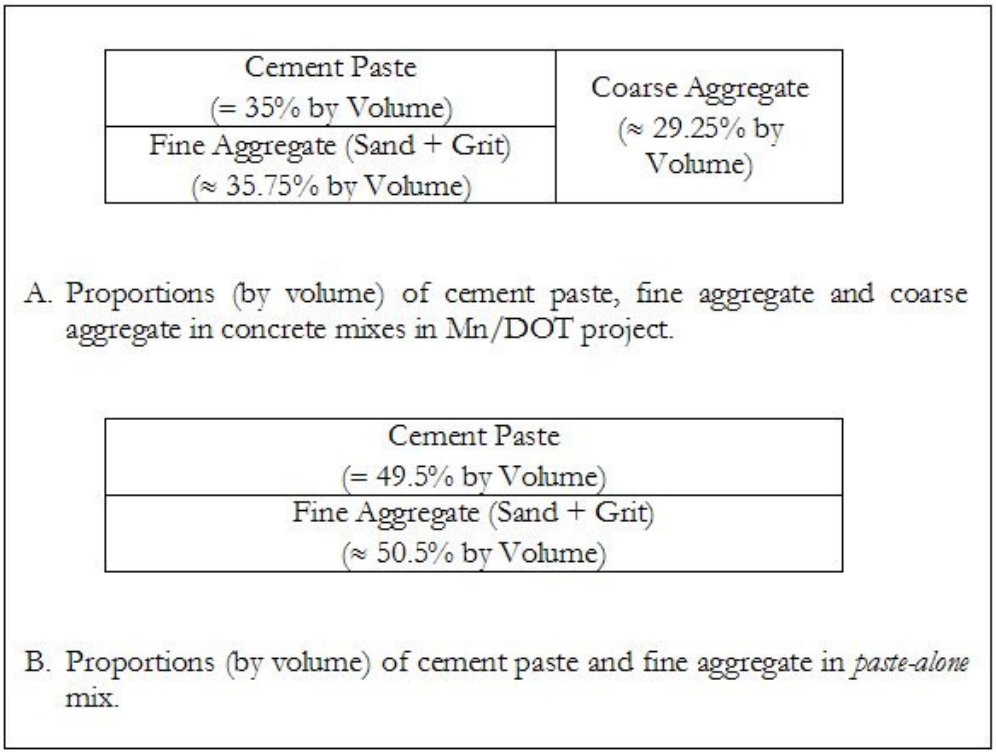

Figure 5.1: Proportions of cement paste and aggregates in (A) Mn/DOT mix and (B) *paste-alone* mix.

5.2.2 Mixing, Casting and Curing

Two trial batches (Mortar-1 and Mortar-2) were prepared. Only Mortar-1 was subjected to the air content test in accordance with ASTM C231. Air content for Mortar-1 mix was 9.25%. Other parameters such as slump and unit weights of fresh concrete were not determined in either of the batches. Four cylinders were cast from each batch where the casting and curing of cylinders was done according to AASHTO T126. An electric vibrating table was used to compact the fresh concrete into the cylinder molds. After 24 hours, cylinders were demolded and transferred to the moist curing room. Cylinders were provided with a continuous wet environment and were removed from the curing room only before testing.

5.2.3 RCPT on Mortar Specimens

Representative cylinder specimens from each batch of paste-alone mix were subjected to RCPT at the ages of 28, 56 and 91 days. The RCPT was done according to AASHTO T277. Table 5.1 provides the total charge passed during RCPT at different mortar ages.

Table 5.1: RCPT results and basic statistical analysis on both batches of *paste-alone* mix at different mortar ages.

Mortar Types	Total Charge Passed (Coulombs)		
	28-Day RCPT	56-Day RCPT	91-Day RCPT
Mortar-1	2693	1749	1148
Mortar-2	2614	1545	1164
Average	2654	1647	1156

5.2.4 Determination of Total Porosity of Mortar Specimens

Total porosity in mortar specimens was determined according to a procedure proposed by Stanish (2002) except for a modification in the specimen saturation procedures. A disc, about 50-mm thick, was cut from the leftover cylinder (after cutting a 50-mm thick specimen from the top to be used for the RCPT). Porosity test procedure, normally, takes several days. Therefore, it is desirable to explain one specific example of how porosity was calculated at a given mortar age. For example, a 28-day porosity test was carried out in the following manner:

- On 26th day (2 days before the test age), the disc specimen was placed in an oven at 105^{o}C.
- On 30th day (after 96 hours), the specimen was taken out of the oven because the specimen weight did not change noticeably from 72 hours to 96 hours. The oven-dry weight of the specimen was measured and then the specimen was subjected to the water saturation of its pores. To accelerate the penetration of water in the pores, a procedure similar to the conditioning of specimens before RCPT was followed. For this purpose, the specimen was first placed in a desiccator under a vacuum pressure less than 1 mm Hg for 3 hours. Then the deaerated water was supplied into the desiccator with vacuum pressure still working, and the specimen was allowed to completely submerge in water. The specimen was left in this condition (submerged and pressure-applied) for an additional hour. Then the pressure was released and the specimen was left in the submerged condition for another 18+-2 hours.
- On 31st day, the specimen was taken out of the desiccator, dried with a towel to get a SSD condition and SSD weight of the specimen was measured. Immediately, the specimen was placed in a wire basket, then the basket (with the specimen) was

submerged in water and the submerged saturated weight of the specimen was measured.

Similar test procedures were followed for remaining 56-day (where the test began on 54th day and ended on 59th day) and 91-day (where the test began on 89th day and ended on 94th day) mortar specimens as well. Dry bulk specific gravity and water absorption were calculated according to ASTM C 127. Similarly, the total porosity was calculated according to Equation 4.1 (Chapter 4). Table 5.2 provides the calculated total porosity values of mortar samples at 28, 56 and 91 days. Calculated dry bulk specific gravity and water absorption values also are presented in the table.

Table 5.2: Dry bulk specific gravity, water absorption and total porosity values of mortar specimens at different ages.

Mortar Types	Mortar Ages	Dry Bulk Specific Gravity	Water Absorption (%)	Total Porosity (%)
Mortar-1	28 days	1.99	10.14	20.16
Mortar-2		1.97	10.46	20.63
Mortar-1	56 days	1.99	10.19	20.31
Mortar -2		1.99	10.16	20.17
Mortar-1	91 days	1.99	10.03	19.99
Mortar-2		1.99	10.04	19.97

5.3 Chloride Profiling on Mortar and Concrete Specimens

5.3.1 Introduction

Specimens from both batches of mortar (*paste-alone* mix) and first two batches of GNSS-A, LMST-E and LMST-C concretes that were subjected to 28-, 56- and 91-day RCPT were selected for chloride profiling. The main objective of this profiling was to determine the chloride concentrations at different depths of specimens due to RCPT. Chloride profiling in each specimen was done by drilling five to seven 12.5-mm diameter holes from the top cross-section of the specimen (that is, from the surface exposed to NaCl solution during RCPT) as shown in Figure 5.2. It was believed that the number of holes drilled for sample collection was sufficient to average out the local effects.

Figure 5.2: A typical chloride-profiled specimen with the drilled-up holes.

Several 12.5-mm diameter end mills (not regular drill bits) were used for drilling holes because the end mills have flat cutting edges as opposed to the angular cutting edges in regular bits. During profiling, the powder sample from the first 2-mm depth of the specimen was discarded. This was because the region close to the surface might have gained or lost chlorides due to leaching and/or contamination. Starting at the 2-mm depth, the powder samples were collected at six to seven different average depths as shown in Table 5.3. A regular drilling machine was used for the drilling. The starting and ending depths of drilling were controlled using the standard built-in calibration ruler in the machine.

Table 5.3: Different depths of powder sample collection during chloride profiling.

Starting Depth	Ending Depth	Average Depth	Remarks
0 mm	2.0 mm	1 mm	Sample Discarded
2.0 mm	4.0 mm	3.0 mm	Sample collected
4.0 mm	6.0 mm	5.0 mm	Sample collected
6.0 mm	9.0 mm	7.5 mm	Sample collected
9.0 mm	12.0 mm	10.5 mm	Sample collected
12.0 mm	16.0 mm	14.0 mm	Sample collected
16.0 mm	20.0 mm	18.0 mm	Sample collected
20.0 mm	24.0 mm	22.0 mm	Sample collected

5.3.2 Chloride Profile Results

Chloride concentration for each of the collected powder samples was determined according to the RCT method (explained in Appendix A). The chloride concentration thus determined is, in fact, the total concentration (the sum of free and bound chloride concentrations). Moreover, this total concentration is the gross total concentration because it includes the background chloride concentration as well. Therefore, the background chloride

concentration should be deducted from the gross total chloride concentration to obtain the net total chloride concentration. To determine the background chloride concentrations, the representative specimens from each aggregate type that were not subjected to RCPT were drilled to obtain powder samples and the chloride concentrations of these samples were determined according to the RCT. An average concentration value was calculated using two to three representative samples and this value was used as the background concentration value for all three test ages. Tables 5.4 to 5.15 provide the net total chloride concentration values of individual batches and the average of two batches of mortar and all three concrete types at 28, 56 and 91 days of concrete.

5.3.2.1 Chloride Profile Data on Mortar Specimens

Table 5.4: Net total acid-soluble chloride concentrations of mortar specimens subjected to 28-day RCPT.

Depth (mm)	Chloride Concentration (% by sample weight)		Correlation Coefficient (r^2)	Average Chloride Concentration (% by sample weight)
	Mortar-1	Mortar-2		
3.0	0.345	0.367	0.996	0.356
5.0	0.315	0.303		0.309
7.5	0.268	0.268		0.268
10.5	0.179	0.154		0.167
14.0	0.035	0.031		0.033
18.0	0.008	0.011		0.009
22.0	0.000	0.001		0.001

Table 5.5: Net total acid-soluble chloride concentrations of mortar specimens subjected to 56-day RCPT.

Depth (mm)	Chloride Concentration (% by sample weight)		Correlation Coefficient (r^2)	Average Chloride Concentration (% by sample weight)
	Mortar-1	Mortar-2		
3.0	0.282	0.235	0.994	0.259
5.0	0.164	0.155		0.159
7.5	0.035	0.052		0.044
10.5	0.000	0.000		0.000
14.0	0.000	0.000		0.000
18.0	0.000	0.000		0.000
22.0	0.000	0.000		0.000

Table 5.6: Net total acid-soluble chloride concentration values of mortar specimens subjected to 91-day RCPT.

Depth (mm)	Chloride Concentration (% by sample weight)		Correlation Coefficient (r^2)	Average Chloride Concentration (% by sample weight)
	Mortar-1	Mortar-2		
3.0	0.299	0.231	1.000	0.265
5.0	0.117	0.084		0.100
7.5	0.000	0.000		0.000
10.5	0.000	0.000		0.000
14.0	0.000	0.000		0.000
18.0	0.000	0.000		0.000
22.0	0.000	0.000		0.000

5.3.2.2 Chloride Profile Data GNSS-A Specimens

Table 5.7: Net total acid-soluble chloride concentration values of GNSS-A specimens subjected to 28-day RCPT.

Depth (mm)	Chloride Concentration (% by sample weight)		Correlation Coefficient (r^2)	Average Chloride Concentration (% by sample weight)
	GNSS-A-1	GNSS-A-2		
3.0	0.167	0.236	0.985	0.202
5.0	0.109	0.125		0.117
7.5	0.076	0.076		0.076
10.5	0.030	0.014		0.022
14.0	0.000	0.000		0.000
18.0	0.000	0.000		0.000
22.0	0.000	0.000		0.000

Table 5.8: Net total acid-soluble chloride concentration values of GNSS-A specimens subjected to 56-day RCPT.

Depth (mm)	Chloride Concentration (% by sample weight)		Correlation Coefficient (r^2)	Average Chloride Concentration (% by sample weight)
	GNSS-A-1	GNSS-A-2		
3.0	0.172	0.265	0.999	0.219
5.0	0.092	0.128		0.110
7.5	0.024	0.035		0.030
10.5	0.003	0.007		0.005
14.0	0.000	0.000		0.000
18.0	0.000	0.000		0.000
22.0	0.000	0.000		0.000

Table 5.9: Net total acid-soluble chloride concentration values of GNSS-A specimens subjected to 91-day RCPT.

Depth (mm)	Chloride Concentration (% by sample weight)		Correlation Coefficient (r^2)	Average Chloride Concentration (% by sample weight)
	GNSS-A-1	GNSS-A-2		
3.0	0.083	0.069	0.983	0.076
5.0	0.016	0.000		0.008
7.5	0.000	0.000		0.000
10.5	0.000	0.000		0.000
14.0	0.000	0.000		0.000
18.0	0.000	0.000		0.000
22.0	0.000	0.000		0.000

5.3.2.3 Chloride Profile Data on LMST-E Specimens

Table 5.10: Net total acid-soluble chloride concentration values of LMST-E specimens subjected to 28-day RCPT.

Depth (mm)	Chloride Concentration (% by sample weight)		Correlation Coefficient (r^2)	Average Chloride Concentration (% by sample weight)
	LMST-E-1	LMST-E-2		
3.0	0.277	0.250	0.980	0.263
5.0	0.180	0.179		0.179
7.5	0.136	0.089		0.112
10.5	0.080	0.033		0.056
14.0	0.019	0.000		0.010
18.0	0.000	0.000		0.000
22.0	0.000	0.000		0.000

Table 5.11: Net total acid-soluble chloride concentration values of LMST-E specimens subjected to 56-day RCPT.

Depth (mm)	Chloride Concentration (% by sample weight)		Correlation Coefficient (r^2)	Average Chloride Concentration (% by sample weight)
	LMST-E-1	LMST-E-2		
3.0	0.119	0.154	0.973	0.136
5.0	0.114	0.125		0.119
7.5	0.071	0.076		0.074
10.5	0.010	0.042		0.026
14.0	0.000	0.001		0.000
18.0	0.001	0.000		0.000
22.0	0.000	0.000		0.000

Table 5.12: Net total acid-soluble chloride concentration values of LMST-E specimens subjected to 91-day RCPT.

Depth (mm)	Chloride Concentration (% by sample weight)		Correlation Coefficient (r^2)	Average Chloride Concentration (% by sample weight)
	LMST-E-1	LMST-E-2		
3.0	0.155	0.109	0.947	0.132
5.0	0.066	0.012		0.039
7.5	0.002	0.000		0.001
10.5	0.000	0.000		0.000
14.0	0.000	0.000		0.000
18.0	0.000	0.000		0.000
22.0	0.000	0.000		0.000

5.3.2.4 Chloride Profile Data on LMST-C Specimens

Table 5.13: Net total acid-soluble chloride concentration values of LMST-C specimens subjected to 28-day RCPT.

Depth (mm)	Chloride Concentration (% by sample weight)		Correlation Coefficient (r^2)	Average Chloride Concentration (% by sample weight)
	LMST-C-1	LMST-C-2		
3.0	0.259	0.281	0.979	0.270
5.0	0.165	0.182		0.173
7.5	0.158	0.129		0.144
10.5	0.102	0.077		0.089
14.0	0.059	0.063		0.061
18.0	0.035	0.032		0.034
22.0	0.000	0.007		0.004

Table 5.14: Net total acid-soluble chloride concentration values of LMST-C specimens subjected to 56-day RCPT.

Depth (mm)	Chloride Concentration (% by sample weight)		Correlation Coefficient (r^2)	Average Chloride Concentration (% by sample weight)
	LMST-C-1	LMST-C-2		
3.0	0.229	0.122	0.953	0.176
5.0	0.196	0.126		0.161
7.5	0.094	0.090		0.092
10.5	0.061	0.060		0.060
14.0	0.041	0.040		0.040
18.0	0.014	0.010		0.012
22.0	0.000	0.000		0.000

Table 5.15: Net total acid-soluble chloride concentration values of LMST-C specimens subjected to 91-day RCPT.

Depth (mm)	Chloride Concentration (% by sample weight)		Correlation Coefficient (r^2)	Average Chloride Concentration (% by sample weight)
	LMST-C-1	LMST-C-2		
3.0	0.197	0.087	0.998	0.142
5.0	0.115	0.051		0.083
7.5	0.035	0.020		0.028
10.5	0.000	0.000		0.000
14.0	0.000	0.000		0.000
18.0	0.000	0.000		0.000
22.0	0.000	0.000		0.000

5.4 Experimentation on LMST-W Aggregate and Rock

5.4.1 Introduction

This set of experiments was designed to examine the effect of aggregate porosity on RCPT, first, when aggregate particles work as an integral part of the concrete and, second, when a representative rock specimen is solely subjected to RCPT. Because we did not have large representative pieces of rocks for any of the 12 aggregate types provided by Mn/DOT, we decided to do the necessary experimentation on the rock pieces and the corresponding aggregate particles from a local quarry in Wisconsin. With the generous help of Prof. Hani Titi, we obtained approximately 100 kg of limestone aggregate and two large pieces of limestone rock from Waukesha Quarry in Wisconsin. To avoid confusion, this aggregate will be called LMST-W, the concrete made out of this aggregate will be called LMST-W concrete

and the rock pieces will be called LMST-W rocks (Rock-1 and Rock-2). The experimental works are divided into two subgroups:

- Experimentation on LMST-W Aggregate and Concrete
- Experimentation on LMST-W Rocks

5.4.2 Experimentation on LMST-W Aggregate and Concrete

5.4.2.1 Basic Aggregate Properties

Once the aggregate was obtained, the basic physical properties such as specific gravity, absorption and porosity were determined according to the procedures explained in Chapter 4. Similarly, ambient chloride content was also determined according to the RCT method. Table 5.16 provides the calculated physical properties of the LMST-W aggregate.

Table 5.16: Specific gravity, absorption, porosity and ambient chloride content values of LMST-W aggregate.

Aggregate Type	Dry Bulk Specific Gravity	SSD Bulk Specific Gravity	Apparent Specific Gravity	Absorption (%)	Porosity (%)	Chloride Content (% by sample wt)
LMST-W	2.604	2.654	2.740	1.900	4.95	0.049

SSD: Saturated Surface-Dry

5.4.2.2 Mixing, Casting and Curing

Following the same mixing and making procedures as in the Mn/DOT concretes, two batches (about 0.03 m^3 of fresh mix in each batch) were prepared using the LMST-W aggregate. Except for the proportions of coarse and fine aggregates and water (which are dependent on the coarse aggregate density), all other constituent materials and their

proportions remained the same as in Mn/DOT project (Table 4.5 in Chapter 4). The quantities of LMST-W aggregate in different size ranges, sand, grit and water are presented in Table 5.17.

Table 5.17: Quantities of water, fine aggregates and coarse aggregate required to prepare 0.028 m^3 of concrete mix.

Aggregate Type	Weight of 19 mm – 25.4 mm aggregate (kg)	Weight of 12.7 mm – 19.0 mm aggregate (kg)	Weight of 9.5 mm – 12.7 mm aggregate (kg)	Weight of 4.75 mm – 9.5 mm aggregate (kg)	Weight of dry sand (kg)	Weight of dry grit (kg)	Total weight of water (kg)
LMST-W	0.49	7.82	5.86	7.82	10.55	15.91	4.74

The fresh concrete properties such as slump, air content and the unit weight were determined in each of the mixes according to the appropriate ASTM standards. These properties are provided in Table 5.18. Five 100-mm-diameter by 200-mm long cylinders were made in each batch. Casting and curing of cylinders was done in accordance with AASHTO T126.

Table 5.18: Slump, air content and unit weight values of LMST-W concrete.

Concrete Type	Batch Number	Slump (cm)	Air Content (%)	Unit Weight (kg/m^3)
LMST-W	1	8.5	7.5	2246.5
	2	8.5	7.5	2249.1

5.4.2.3 RCPT on LMST-W Concrete

The concrete samples were subjected to RCPT at standard test ages of 28, 56 and 91 days. The standard procedure according to AASHTO T 277 was followed to condition and test the specimens. Table 5.19 provides RCPT results on both batches of concrete at all three test ages.

Table 5.19: RCPT results on LMST-W specimens at different concrete ages.

Concrete Types	Total Charge Passed (Coulomb)		
	28-Day RCPT	56-Day RCPT	91-Day RCPT
LMST-W-1	2039	1152	817
LMST-W-2	1773	1049	846
Average	1906	1101	832

When the RCPT results shown in Table 5.19 were compared with calculated RCPT values based on the linear regression lines in Figure 4.1 (in Chapter 4) for an aggregate porosity value of 4.95% (as shown in Table 5.16), the experimental RCPT values were slightly lower than the calculated values at all ages. Still, the scatter of data points was within the acceptable margin.

5.4.3 Experimentation on LMST-W Rocks

5.4.3.1 Overview

Both Rock-1 and Rock-2 were core-drilled using a diamond saw bit to obtain 100-mm diameter cores. The coring locations in each of these rocks were chosen in such a way that the direction of coring in Rock-1 was approximately perpendicular to the rock strata whereas this direction in Rock-2 was approximately parallel to the strata. Cores were drilled at two

different locations in each of Rock-1 and Rock-2. Cores thus collected were further cut into 50-mm thick disc shapes so that they could be subjected to RCPT. We were able to make 2 specimens from Rock-1 and 3 specimens from Rock-2. The direction of drilling eventually becomes the direction of chloride migration during RCPT. Therefore, chloride ions during RCPT will move approximately perpendicular to the rock strata in Rock-1 specimens whereas chloride movement will be approximately parallel to the strata in Rock-2 specimens.

5.4.3.2 RCPT on Rock Specimens

RCPT was done according to AASHTO T 277. Unfortunately, there was massive leakage of exposure solutions from the device during the RCPT on both specimens of Rock-1 and one specimen (out of 3) of Rock-2 and hence the RCPT results on those specimens were disregarded. RCPT results on the specimens for which the test went smoothly are reported in Table 5.20.

Table 5.20: RCPT values on two Rock-2 specimens.

Rock Type	Total Charge Passed during RCPT (Coulomb)
Rock-2-1	570
Rock-2-2	434
Average	502

5.4.3.3 Chloride Profiling on a Rock Specimen

Rock-2-1 was subjected to chloride profiling according to the procedures explained in Section 5.3. During the profiling, the powder samples were collected from the additional

depths along with the usual average depth of 18- to 22- as explained in Section 5.3. The additional depths were taken at an increment of 4-mm and here again, the average depth is taken as the sampling depth. The powder samples thus collected were subjected not only to the RCT but also to the RCTW (a test method similar to RCT) where RCTW determines the water-soluble chloride content (see Appendix A). RCT determines the total acid-soluble chloride content of the sample whereas RCTW determines only the water-soluble chloride content in the sample (Germann Instruments 2003).

The main objective of chloride profiling on R-2-1 specimen was to determine whether there was visible chloride binding. Estimation of free surface chloride concentration is necessary to determine the level of binding, if any, in the profiled specimen. Free surface chloride concentration (C_{fs}) in % (by weight of material) is estimated as:

$$C_{fs} = \frac{nA_{Cl}M_{NaCl}}{1000\rho} \times 100\% \quad \text{……..…(5.1)}$$

where, A_{Cl} is the atomic weight of chlorine (approximately equal to 35.5), M_{NaCl} is the molarity of NaCl solution (approximately equal to 0.513 for 3% NaCl solution used in RCPT), n is the porosity (in fraction), and ρ is the dry bulk density of the material (rock density in this case) in g/cm^3. For the specific case of LMST-W rock, total porosity (n) is 0.0495 and ρ is 2.604 g/cm^3 (corresponding to a dry bulk specific gravity of 2.604), both from Table 5.16. Using the above numerical values, C_{fs} during RCPT on R-2-1 is found to be approximately equal to 0.035% from Equation 5.1 above. Table 5.21 provides RCT and RCTW values at different depths of Rock-2-1. Figure 5.3 provides a graphical representation of RCT and RCTW values in Table 5.21 with the above-calculated free surface chloride concentration cut-off.

Table 5.21: Acid-soluble chloride content (RCT values) and water-soluble chloride content (RCTW values) values at different depths of Rock-2-1 specimen.

Depth (mm)	RCT			RCTW		
	Background Chloride Content (% by wt)	Gross Chloride Content (% by wt)	Net Chloride Content (% by wt)	Background Chloride Content (% by wt)	Gross Chloride Content (% by wt)	Net Chloride Content (% by wt)
3.0	0.050	0.119	0.069	0.046	0.111	0.065
5.0		0.114	0.064		0.102	0.056
7.5		0.107	0.058		0.098	0.052
10.5		0.095	0.045		0.087	0.041
14		0.087	0.037		0.079	0.033
18		0.085	0.035		0.077	0.031
22		0.083	0.033		0.080	0.035
26		0.049	0.000		0.048	0.002
30		0.056	0.006		0.050	0.004
34		0.052	0.003		0.045	0.000
38		0.055	0.005		0.042	0.000

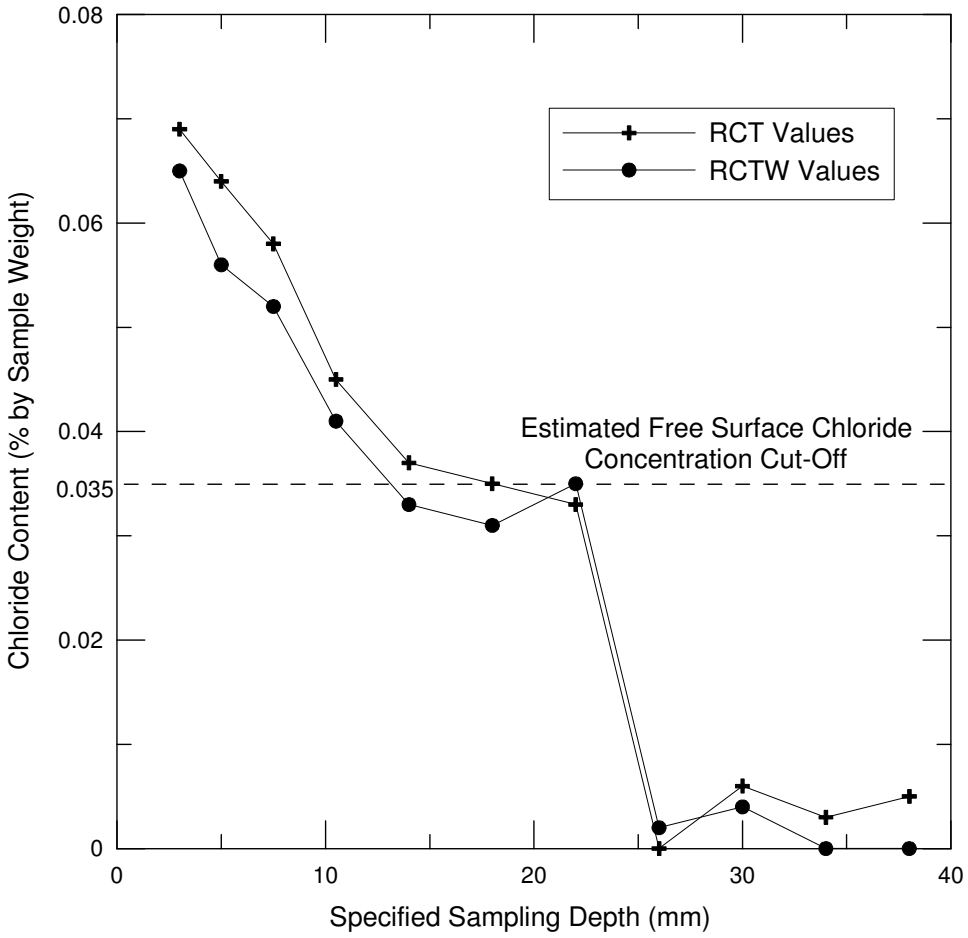

Figure 5.3: Graphical representation of acid-soluble and water-soluble chloride concentrations at different depths of R-2-1 and an estimated free surface chloride concentration cut-off line.

From Figure 5.3, it is seen that the total chloride concentration values (both RCT and RCTW) close to the surface are higher than the estimated free surface chloride concentration. This confirms that there is chloride binding in the R-2-1 specimen. The shape of the chloride profile in Figure 5.3 also confirms the presence of binding. On the other hand, RCT values (total chloride concentration) and RCTW values (water-soluble chloride concentration) are very close to each other at all measured specimen depths.

5.5 Observation of ITZ under SEM and EDX Analysis

5.5.1 Observation of ITZ under SEM

Each of GNSS-A-3, LMST-E-3 and LMST-C-3 specimens that were subjected to 28-day RCPT was observed using a scanning electron microscope (SEM) after necessary sample preparations. The purpose of this observation was to determine the extent of ITZ formation around the aggregate particles and, at the same time, to determine the nature of the chloride migration in the paste-aggregate interface region where the ITZ is most likely to occur. For the purpose of sample preparation, a 12.5-mm thick slice (approximate) along the direction of chloride penetration was cut from the specimen. It was then further cut into a circular shape of about 25-mm diameter, which included the paste-aggregate interface. Figure 5.4 shows a sample preparation technique for the SEM observation.

An experienced technician observed the prepared samples through the SEM at different magnifications. Typical SEM pictures for each of the concrete types are shown in Figures 5.5 to 5.7.

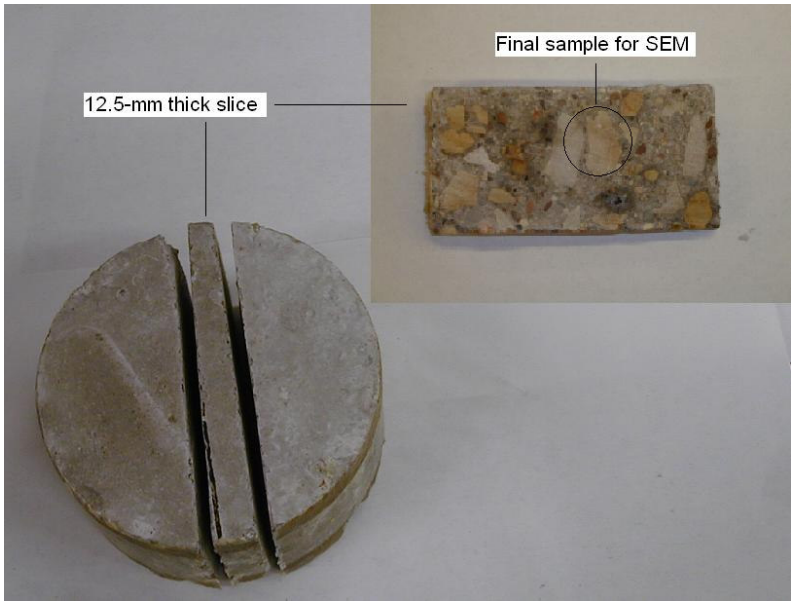

Figure 5.4: A typical sample preparation technique for the SEM observation.

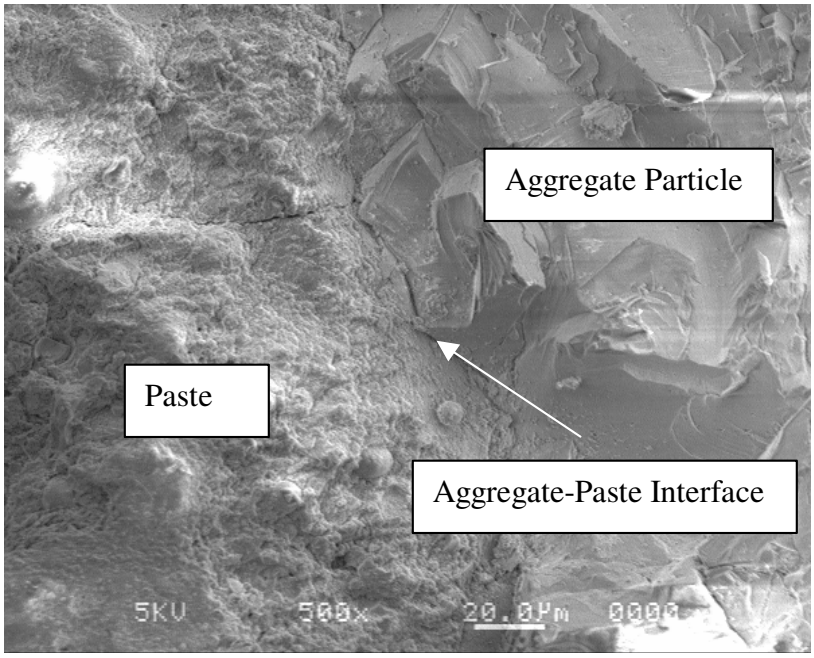

Figure 5.5: A typical paste-aggregate interface in GNSS-A-3 Concrete.

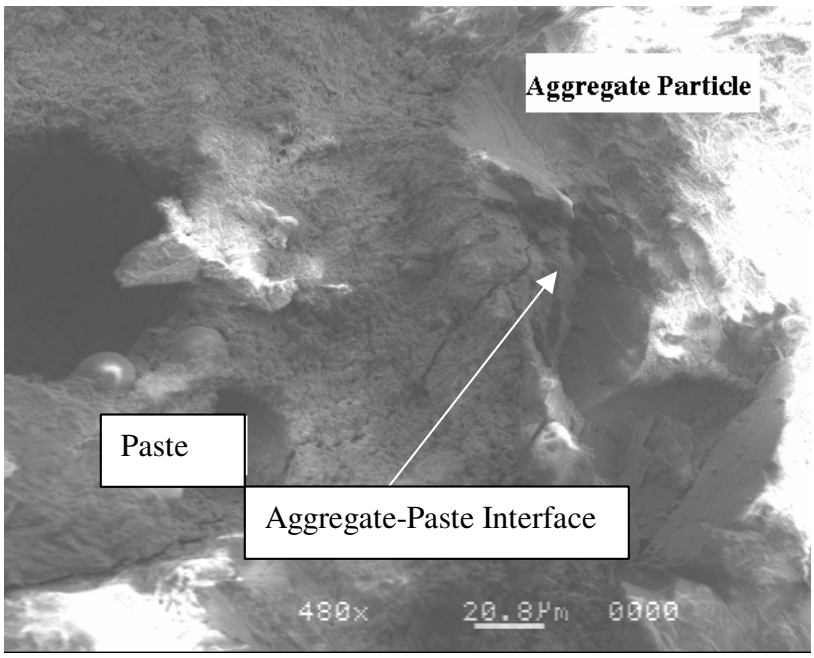

Figure 5.6: A typical paste-aggregate interface in LMST-E-3 Concrete.

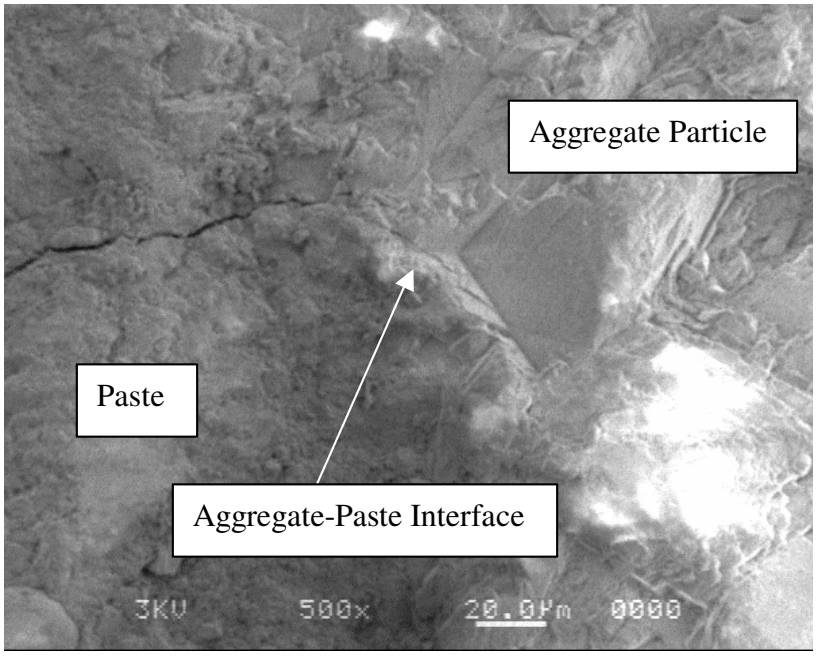

Figure 5.7: A typical paste-aggregate interface in LMST-C-3 Concrete.

To examine the difference in microstructure around the paste-aggregate interface (where the ITZ was supposed to exist) between concretes with and without silica fume/fly ash, the concrete specimens without silica fume/fly ash were also prepared and observed under the SEM. For this purpose, two *cement-alone* concrete mixes were prepared by using cement as the sole binding material (siliaca fume and fly ash not used) with high water-to-cement ratio (approximately 0.55) where one mix used GNSS-A aggregate and the other mix used LMST-C aggregate. One cylinder was cast from each mix and at 28 days, the SEM samples were prepared form each of these cylinders and the paste-aggregate interface was observed under the SEM. Figure 5.8 provides the comparative images showing the paste-aggregate interface of the *cement-alone* concrete versus the paste-aggregate interface of a typical silica fume/fly ash concrete at the same magnification ratio.

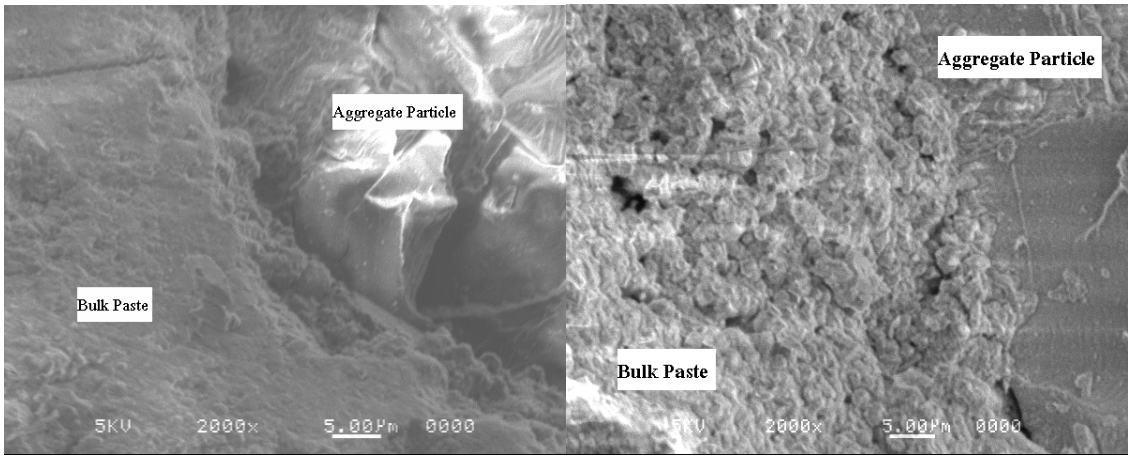

Figure 5.8: Comparative images showing the paste-aggregate interface at 2000× magnification: the left image for the silica fume/fly ash concrete and the right image for the *cement-alone* concrete.

5.5.2 EDX Analysis

Energy Dispersive X-Ray Analysis (EDX Analysis) is done while the sample is still under the SEM. In this analysis method, a narrow sample area (typically less than 1 μm^2) is picked (focused) and the chemical analysis of the material falling under the focused area is done on an elemental basis. The samples for this analysis were prepared from the concrete specimens subjected to 28-day RCPT. This analysis was carried out to assess whether the chloride concentrations in the regions of possible ITZ formation were higher as compared to the chloride concentration in the paste region. To serve this purpose, a number of observation locations were arbitrarily selected assuming a critical interface region of 20 – 30 µm. A conceptual sketch is presented in Figure 5.9. In this sketch, Location 1 can be regarded as a point inside the paste, which is well outside the critical interface region (refer to a 50-µm bar in the sketch). Location 2 is relatively closer to the critical region and Location 3 is well

within the region. Location 4, on the other hand, is on the aggregate surface. In general, the observation locations were selected in such a way that an imaginary line passing through these locations would be approximately perpendicular to the direction of the chloride movement. Typical graphs showing the proportion of each of the elements present at the observation locations are shown in Figures 5.10 to 5.12 (Note that silver (Ag) appears in the graphs because silver nitrate was sprayed on the surfaces of the samples before the observations).

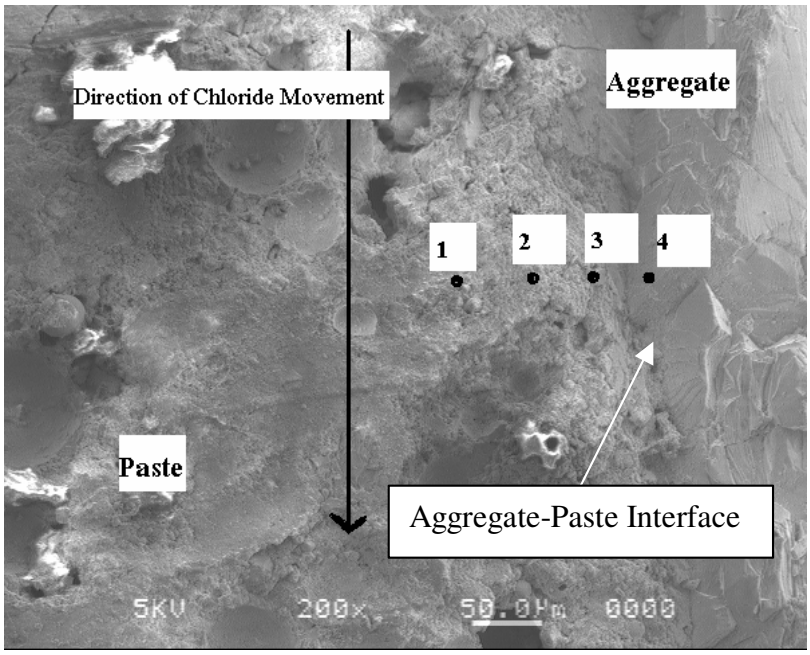

Figure 5.9: A conceptual sketch showing the relative observation locations on a sample under the SEM (locations are only for comparison purposes, not to the exact scale).

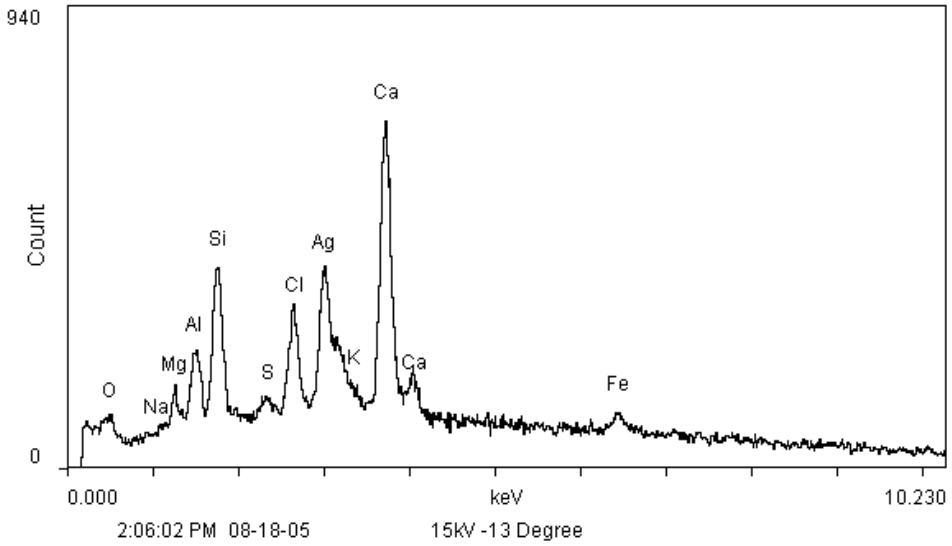

Figure 5.10: A typical graph showing the elemental composition at a location in the bulk paste region, represented by Locations 1 and (possibly) 2 in Figure 5.8 above.

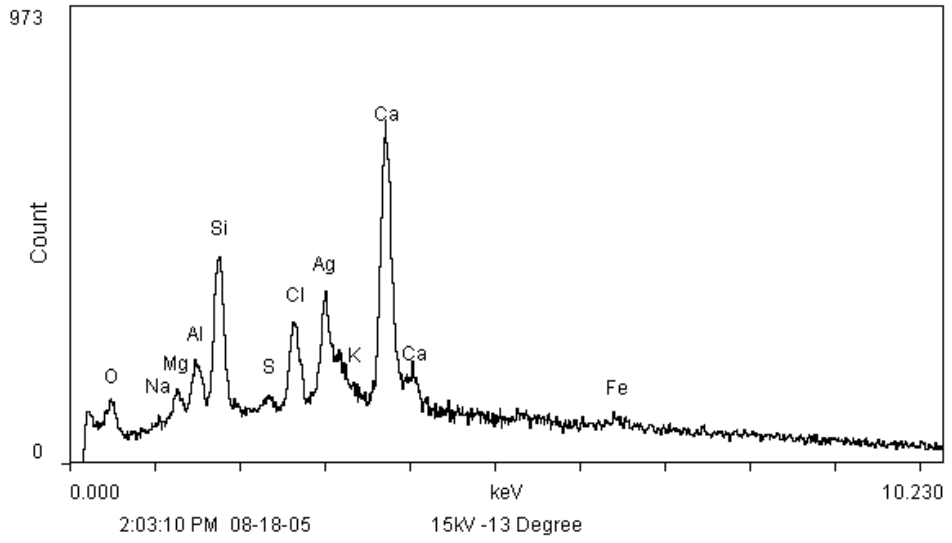

Figure 5.11: A typical graph showing the elemental composition at a location inside the critical interface region, represented by Location 3 in Figure 5.8 above.

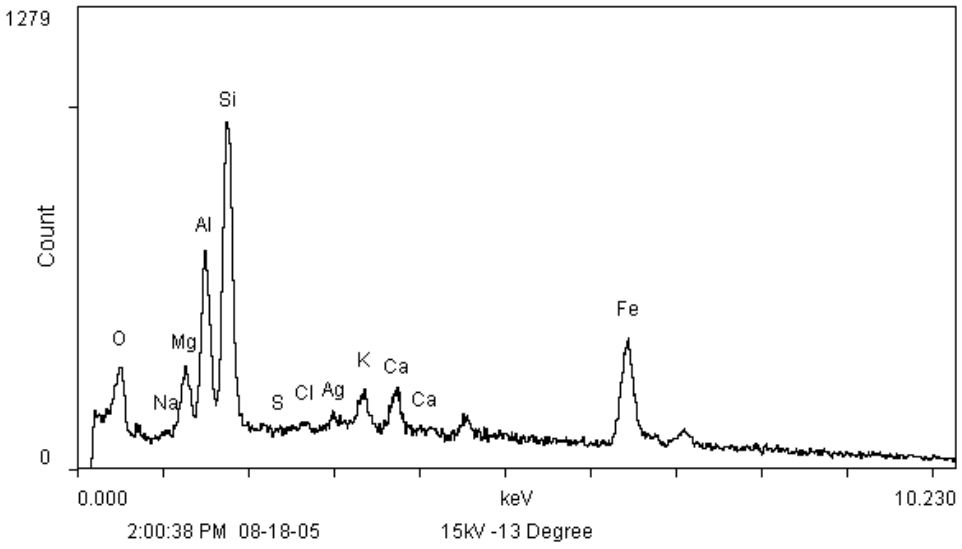

Figure 5.12: A typical graph showing the elemental composition at a location on the aggregate surface (note the high contents of Al and Si), represented by Location 4 in Figure 5.8 above.

Observation of samples using SEM indicated that the ITZ regions were absent or, at least, impossible to detect in the observed concrete types using this method. Similarly, subsequent EDX analysis indicated that the chloride concentration at the aggregate-paste interface is not visibly higher than the paste region as indicated by Figures 5.10 to 5.12. These two tests confirmed that ITZ regions were, most likely, not present in the concretes prepared in the present study.

5.6 Immersion of Aggregate Particles in Salt Solution

Approximately 100 g of aggregate particles (relatively of larger sizes) in each aggregate type (GNSS-A, LMST-E and LMST-C) were left completely immersed in salt solution (10% NaCl by weight) uninterruptedly for 90 days. The positions of the aggregate particles inside the

solution were shifted from time to time to allow the even distribution of local effects such as piling-up of particles and blockages of chloride paths. At the end of 90-day period, the aggregate particles were taken out of the solution, the particle surfaces were washed thoroughly, and left for complete drying. Then a single aggregate particle was selected in each aggregate type in such a way that these particles were similar in sizes and masses to one another. Each of the selected particles was ground to a fine powder using a mortar and pestle. The fine powder samples thus collected were subjected to RCT to determine the bulk chloride content of the selected particle. This procedure was repeated for one more set of particles to obtain statistically viable outcomes. Table 5.22 provides the RCT results on both sets of aggregate particles.

Table 5.22: Acid-soluble chloride contents of aggregate particles immersed in salt solution for 90 days.

Aggregate Types	Background Chloride Content (% by sample wt.)	Porosity (%)	Sample No.	Weight of ground particle (g)	Gross Chloride Content (% by sample wt.)	Net Chloride Content (% by sample wt.)
GNSS-A	0.0035	0.806	1	10.53	0.0107	0.0072
			2	9.30	0.0180	0.0145
LMST-E	0.0100	2.965	1	12.67	0.0655	0.0556
			2	10.51	0.0501	0.0402
LMST-C	0.0501	5.805	1	13.14	0.1135	0.0634
			2	13.73	0.1409	0.0907

Based on the tabulated results, it is not possible to obtain a well-defined relationship between the aggregate porosity and the 90-day chloride content values. However, the results clearly demonstrate that the higher porosities result in the higher chloride contents and so on. Because a single piece of aggregate was selected for the RCT each time, the 90-day chloride content is representative of that particular piece rather than the aggregate type in general. In a single aggregate type, the parameters such as porosity (and possibly the cracks and/or faults) may not be evenly distributed from particle to particle. In this context, the types of results obtained were not completely unexpected.

5.7 Conclusions on Additional Experimental Work

Based on the outcomes of various experiments done in the preceding sections, a number of conclusions can be drawn:

- ITZ regions around the aggregate particles were not present or, at least, were impossible to detect in the concretes we observed under the SEM. Similarly, the Energy Dispersive X-Ray Analysis indicated that the chloride content in the critical interface region was not visibly higher as compared to the nearby paste region suggesting that there was no preferential pathway (or ITZ) for the chloride transport during RCPT in the observed concrete samples.
- As indicated by LMST-W rock specimens subjected to RCPT, this rock type is not completely chloride resistive as indicated by RCPT results. Although the RPCT results on LMST-W rock specimens were very low (even lower than the 91-day RCPT results on LMST-W concretes), aggregates particles, just like their parent rock origin, may have certain level of chloride penetrability. Similarly, 90-day immersion test results showed that the chloride ions were able to penetrate into the aggregate

particles where the levels of penetration, more or less, depended on the aggregate porosities.

- According to the chloride profiling and the subsequent analysis on R-2-1, chloride binding does take place in the limestone rocks (and aggregates) such as LMST-W.

6.0 PHASE III: CHLORIDE MIGRATION SIMULATION

6.1 Overview

As discussed in the previous chapters, the movement of chloride ions during RCPT is governed by the diffusion-migration mechanism coupled with the chloride binding mechanism. The diffusion-migration equation is essentially a partial differential equation. As will be seen in subsequent paragraphs, potential difference (V) is also defined in terms of a partial differential equation. Therefore, a partial differential equation solver is required to properly model the migration of chloride ions in concrete during RCPT. In the present study, a commercially available partial differential software package known as FlexPDE (Backstrom 2004) was used to analytically model the chloride transport mechanisms. This software package uses the finite difference method of solution by rendering the entire structure into a vast number of discrete elements.

6.2 Mathematical Formulation

Using the law of conservation of mass, the one-dimensional (1D) Nernst-Planck equation in Chapter 3 (Equation 3.13) can be generalized to a 2D situation in the following form (Alden 1998):

$$\frac{\partial C}{\partial t} = \left[\frac{\partial}{\partial x}\left(D\frac{\partial C}{\partial x}\right) + \frac{\partial}{\partial y}\left(D\frac{\partial C}{\partial y}\right)\right] + u\left[\frac{\partial}{\partial x}\left(C\frac{\partial V}{\partial x}\right) + \frac{\partial}{\partial y}\left(C\frac{\partial V}{\partial y}\right)\right] \quad \text{.....(6.1)}$$

where, C is the chloride concentration, D is the chloride diffusion coefficient, t is the time, and u is the mobility factor. Rewriting the equation related to mobility factor (u) from Chapter 3 (Equation 3.11), we have:

$$u = \frac{zFD}{RT} \quad \text{.....(6.2)}$$

where, z is the valence of chloride ions (-1), F is the Faraday's constant (96,485 coulomb/mole), R is the gas constant (8.314 Joule/mole-K), and T is the absolute temperature of the pore solution (in K). Equation 6.1 does not account for the binding of chlorides, so the chloride concentration (C) in Equation 6.1 is actually the free chloride concentration (C_f). Hence, Equation 6.1 can be rewritten as:

$$\frac{\partial C_f}{\partial t} = \left[\frac{\partial}{\partial x}\left(D\frac{\partial C_f}{\partial x}\right) + \frac{\partial}{\partial y}\left(D\frac{\partial C_f}{\partial y}\right)\right] + u\left[\frac{\partial}{\partial x}\left(C_f\frac{\partial V}{\partial x}\right) + \frac{\partial}{\partial y}\left(C_f\frac{\partial V}{\partial y}\right)\right] \quad \text{……..……(6.3)}$$

A term accounting for the binding should be added to Equation 6.3 to properly represent the actual diffusion-migration situation in concrete during chloride migration. As bound chlorides are the so-called *lost* chlorides from chloride transport point of view, the rate of binding can be introduced on the right hand side of Equation 6.3 with a negative sign (Buenfeld et al. 1998):

$$\frac{\partial C_f}{\partial t} = \left[\frac{\partial}{\partial x}\left(D\frac{\partial C_f}{\partial x}\right) + \frac{\partial}{\partial y}\left(D\frac{\partial C_f}{\partial y}\right)\right] + u\left[\frac{\partial}{\partial x}\left(C_f\frac{\partial V}{\partial x}\right) + \frac{\partial}{\partial y}\left(C_f\frac{\partial V}{\partial y}\right)\right] - \frac{\partial C_b}{\partial t} \quad \text{…….(6.4)}$$

where, C_b is the bound chloride concentration. Even though Equation (6.4) is complete for a homogeneous material with a constant porosity, the proposed model, which has different porosity values for the paste and aggregate phases, does not represent a homogeneous material. Therefore, all C_f and C_b terms in Equation 6.4 need to be multiplied by porosity (n) to account for the variations in porosities in the model space. After the inclusion of n in Equation (6.4), it is modified into the following form (Samson et al. 2003, Truc et al. 2000):

$$\frac{n\partial C_f}{\partial t} = \left[\frac{\partial}{\partial x}\left(nD\frac{\partial C_f}{\partial x}\right) + \frac{\partial}{\partial y}\left(nD\frac{\partial C_f}{\partial y}\right)\right] + u\left[\frac{\partial}{\partial x}\left(nC_f\frac{\partial V}{\partial x}\right) + \frac{\partial}{\partial y}\left(nC_f\frac{\partial V}{\partial y}\right)\right] - \frac{n\partial C_b}{\partial t} \quad (6.5)$$

At first, it may seem that *n* is a common term on both sides and it will eventually vanish. But in finite difference method, any parameters that might vary in time and/or space should be included in the equation to properly address the situation (Backstrom 2004). Now, the actual free and bound chloride concentrations in the model are nC_f and nC_b, respectively.

As discussed in Chapter 3, chloride binding, initially, is a function of free chloride concentration; but as the binding approaches its upper limit imposed by the finite pore-wall surface area (see Figure 3.5 in Chapter 3), the rate of binding practically reduces to zero. In our study, a relationship between the rate of binding and free and bound chloride concentrations was empirically developed based on the past studies as well as several rounds of trial-and-error execution of the model to match the experimental chloride profile data obtained in Chapter 5. The relationship thus developed can be mathematically expressed as:

$$\frac{\partial C_b}{\partial t} = \alpha.erfc(\beta.C_b).C_f \quad \text{.....(6.6)}$$

where, α is the initial binding-rate constant, β is the binding capacity constant and *erfc* is the complementary error function. Table 6.1 shows *erfc* values corresponding to different numerals. From Equation 6.6 and Table 6.1, it is observed that α determines the initial rate of chloride binding because C_b is zero at the beginning and hence:

$$\left(\frac{\partial C_b}{\partial t}\right)_{t=0} = \alpha.C_f \quad \text{.....(6.7)}$$

When β is kept constant, increase in α leads to a higher binding rate by which binding approaches its saturation limit sooner as compared to the lower values of α. Figure 6.1 below depicts this situation.

Table 6.1: Numerals from 0 to 4 and corresponding complementary error function (*erfc*) values.

x	*erfc*(x)	Graphical Representation
0	1.0	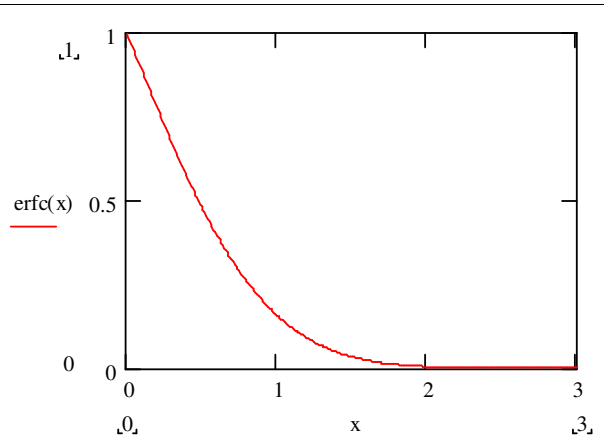
1	0.157	
2	4.678×10^{-3}	
2.5	4.070×10^{-4}	
3	2.209×10^{-5}	
3.5	7.431×10^{-7}	
4	0	

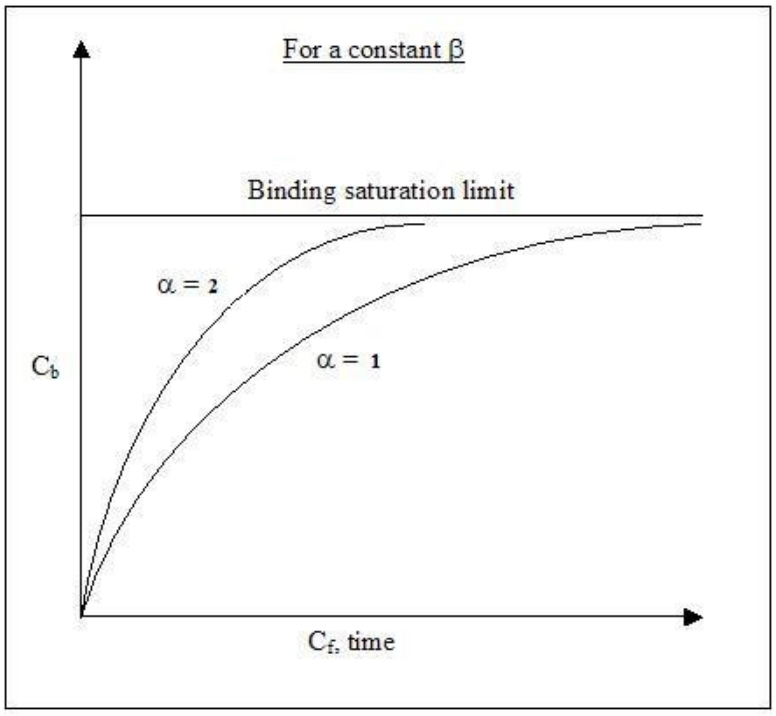

Figure 6.1: Binding isotherms at different values of α for a constant β (α values in the figure are for comparison purposes only).

However, as C_b increases, the rate of binding decreases even at a constant α because *erfc* in Equation 6.6 becomes smaller at higher C_b values. At this stage, β plays an important role in determining how fast the binding approaches its saturation limit. For example, assigning a higher value for β means the binding reaches its saturation point earlier and so on. Additionally, higher β values also mean that the binding ratio (C_b/C_f) is less. This situation is illustrated in Figure 6.2.

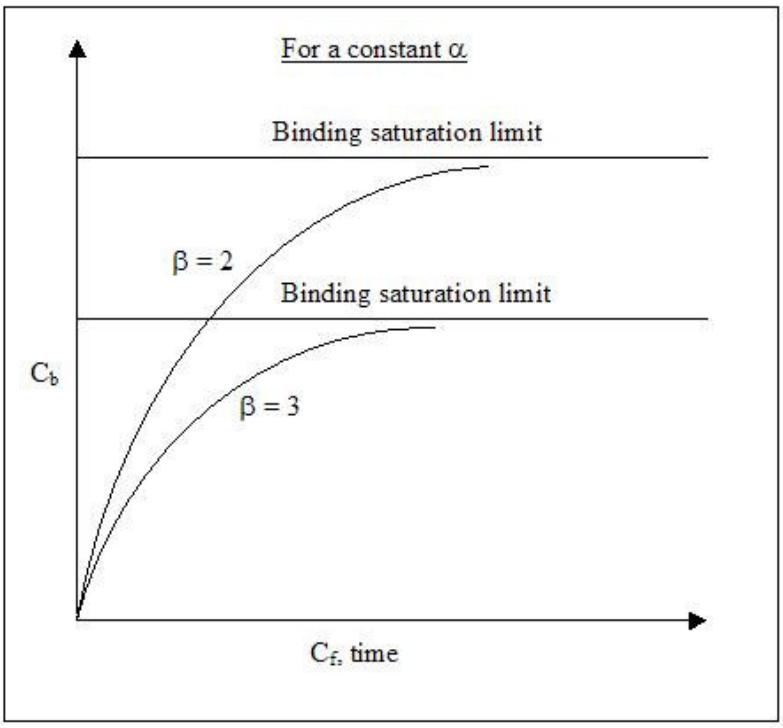

Figure 6.2: Binding isotherms at different values of β for a constant α (β values in the figure are for comparison purposes only).

In Equation (6.5), C_f, C_b and V are the three variables that need to be solved simultaneously. To evaluate the electrical potential (V) in Equation 6.5, Poisson's equation should be

simultaneously solved with Equation 6.5 (Jackson 1975). After including n and D (which vary in space) appropriately in Poisson's equation, the averaged form of Poisson's equation in 2D can be expressed as (Samson et al. 1999):

$$\frac{\partial}{\partial x}\left(nD\frac{\partial V}{\partial x}\right)+\frac{\partial}{\partial y}\left(nD\frac{\partial V}{\partial y}\right)+n\frac{F}{\omega}\sum_{i=1}^{N}z_iC_i=0 \quad \text{.....(6.8)}$$

where, z_i and C_i are the valence and the concentration of i^{th} ion, N is the total number of ions in the pore solution, and ω is the dielectric permittivity of the pore solution (Samson et al. 2003). The third term on the left side of Equation 6.6 is the net charge in the transport solution (sum of positive and negative charges). Under the assumption that the total charge of both positive and negative ions in the solution will be zero, the third term will vanish (Truc et al. 2000). Hence, Equation 6.6 reduces to a simpler form as shown below:

$$\frac{\partial}{\partial x}\left(nD\frac{\partial V}{\partial x}\right)+\frac{\partial}{\partial y}\left(nD\frac{\partial V}{\partial y}\right)=0 \quad \text{.....(6.9)}$$

Equations 6.5, 6.6 and 6.9 are the three fundamental equations that the proposed model will utilize to predict the chloride transport during RCPT.

6.3 Analytical Modeling

6.3.1 Introduction

To reduce the computational complexity, a three-dimensional (3D) situation in the real world is reduced to a two-dimensional (2D) condition in the modeling. To properly represent the changes in both free chloride concentration (C_f) and bound chloride concentration (C_b) with time, the model is developed as a transient model. Although actual concrete has several phases such as aggregate particles (fine and coarse), voids (entrained and entrapped), ITZ and the cement paste, the proposed model is designed to address the effect

of coarse aggregates only. That means the effects of other parameters such as fine aggregates and voids are added in the cement paste itself, resulting in a so-called *smeared-effect* of cement paste, fine aggregates and voids. This *smeared-effect* will be known as the smeared paste henceforth. In fact, the idea behind preparing and testing *paste-alone* mix as discussed in Chapter 5 was to compare the effect of different types of coarse aggregates in concrete during chloride transport in RCPT, keeping the *smeared-effect* of cement paste, fine aggregates and voids constant. In addition, our studies showed that the ITZ regions were either absent or negligible in the high performance concretes prepared in the present study and hence they are not incorporated in the model. This means that the model eventually reduces to a two-phase composite consisting of the smeared paste and the coarse aggregates. Aggregates in the model are represented by circular sections of varying diameters. Figure 6.3 shows the actual concrete phases versus the model representation.

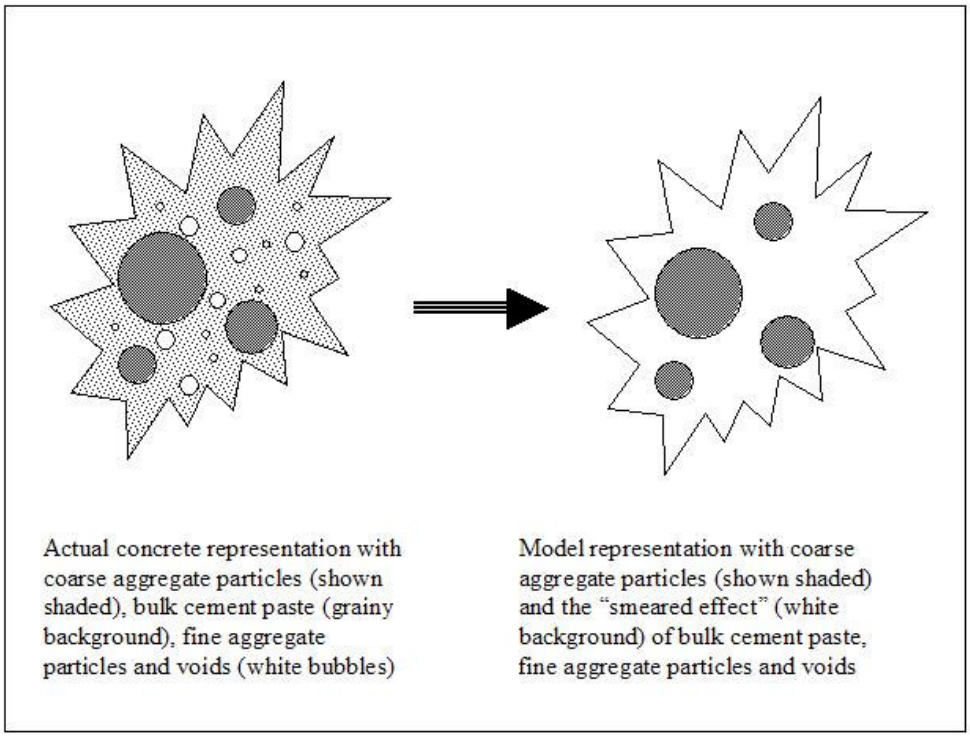

Figure 6.3: Actual concrete representation and the subsequent model representation.

6.3.2 Development and Execution Phases

Development and execution of the chloride transport model can be best described with a flowchart as provided in Figure 6.4 below.

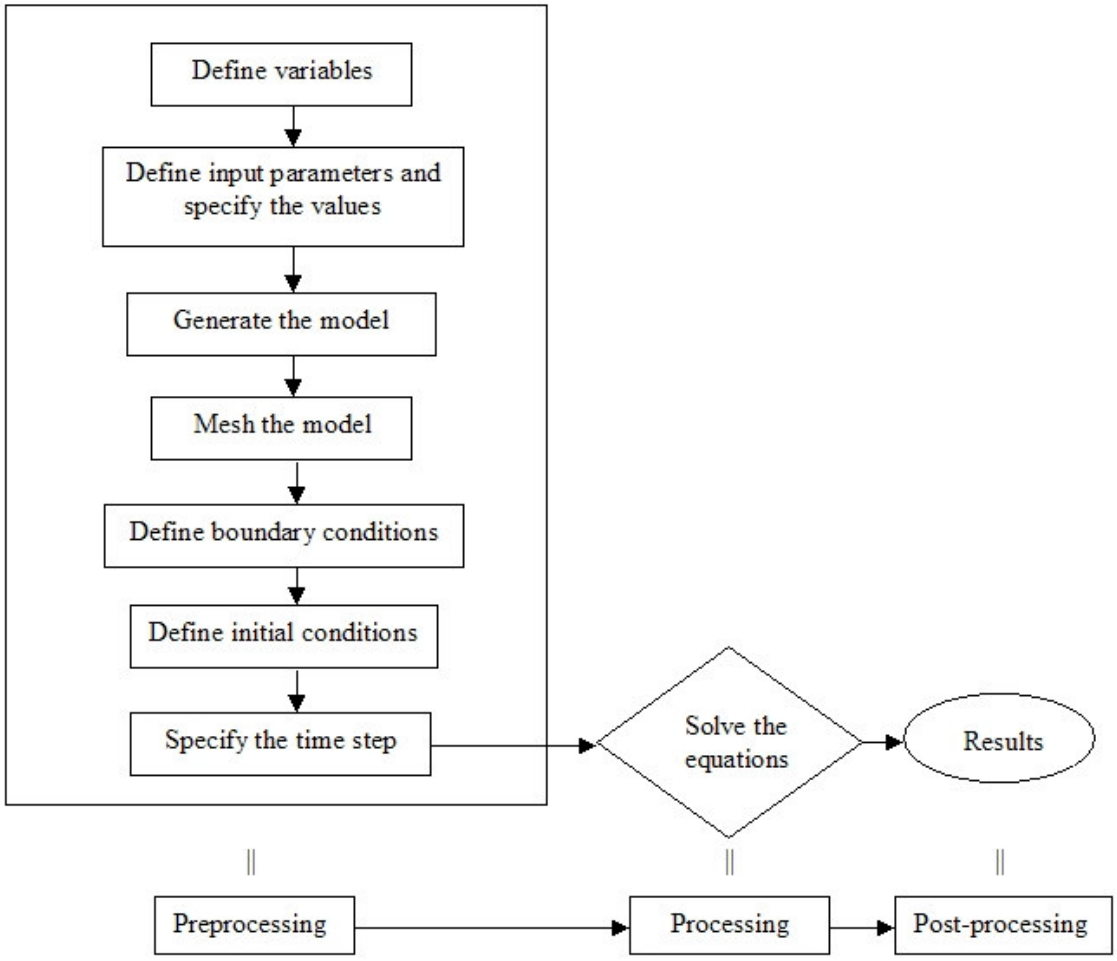

Figure 6.4: A typical flowchart showing the different steps involved in the modeling.

Steps mentioned in the flowchart are described in the following paragraphs.

Define Variables

As C_f and C_b vary with time, they are the two variables that the model should address. Additionally, potential difference (V) is also supplied as a variable in the model. Hence, there are three variables in the model that need to be defined, namely, C_f, C_b and V.

Define Input Parameters and Specify the Values

In this stage, all the parameters that are included in Equations 6.5, 6.6 and 6.9 should be defined and supplied with appropriate values. These parameters include: z (-1), F (96,485 Coulomb/mol), R (8.314 Joule/mol-K), T (in K) and D (in mm^2/hr).

Generate the Model

This stage includes the generation of a 2D model corresponding to the concrete specimen subjected to RCPT. An actual specimen is a short cylindrical disc with a 100 mm diameter cross-section and a thickness of 50 mm. But in the model, this shape is represented by a 100 mm wide and 50 mm thick rectangular area. Figure 6.5 shows the actual 3D concrete specimen and its 2D representation in the model.

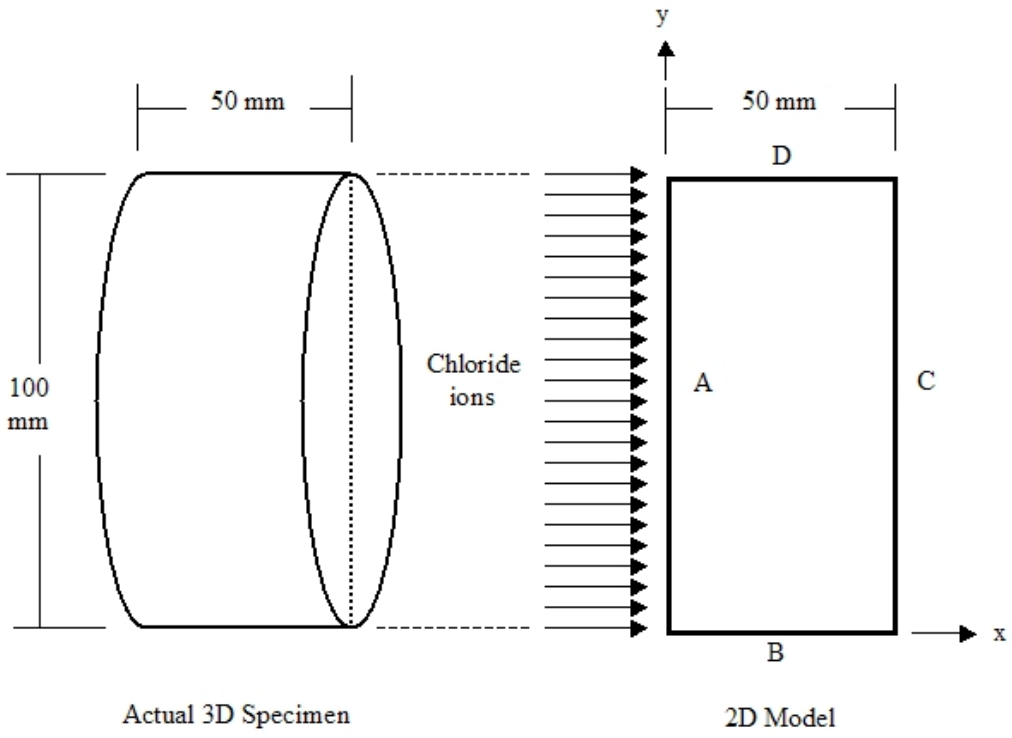

Figure 6.5: An actual three-dimensional (3D) concrete specimen and the corresponding two-dimensional (2D) model representation.

In Figure 6.5, the chloride ion movement is shown to take place in the positive direction along the x-axis of the model. Four boundaries in the model representation are shown as A, B, C and D where chloride ions penetrate through boundary A. Boundaries B and D represent the peripheral surface area of the actual specimen. As the peripheral surface area of the specimen is sealed during the test using epoxy coating, boundaries B and D should be treated accordingly during modeling.

The total aggregate volume fraction (including both coarse and fine aggregates) in the concrete specimens was approximately 65% by concrete volume. On the other hand, assuming total aggregate volume as 100%, the volume fraction of coarse and fine aggregates was 45% and 55% respectively (see Table 4.4 in Chapter 4). Table 6.2 below lists the

calculated area contribution of each of the coarse aggregate particle sizes in the total model area of 5000 mm^2 (100 mm by 50 mm).

Table 6.2: Volume fraction and total aggregate area in different particle size ranges of coarse aggregate.

Coarse Aggregate Particle Size Range	Approximate Volume fraction of individual particle sizes to fine + coarse aggregate volume	Volume fraction of fine + coarse aggregates volume to concrete volume	Actual fraction of individual particle sizes to concrete volume	Theoretical area contribution of individual particle sizes to the model area of 5000 mm^2 (mm^2)
4.75 mm – 9.5 mm	16%	65%	10.4%	520
9.5 mm – 12.7 mm	12%		7.8%	390
12.7 mm – 19.0 mm	16%		10.4%	520
19.0 mm – 25.4 mm	1%		0.65%	32.5
Total	45%		29.25%	1462.5

A statistical approach proposed by Zheng et al. (2003) was used to select and distribute the particle sizes inside the model perimeter. In each particle size range, particles were assumed to follow equal volume (area for 2D) fraction distribution, that is, there would be equal distribution of the total volume among different particle sizes. That would mean that the larger-size particles would have less numbers as compared to smaller-size particles and vice versa. According to the theory of stereology proposed by Zheng (2000), the two-dimensional cumulative distribution function in terms of number of aggregates for an equal volume fraction mix is given as:

$$P(d) = \frac{d^2(d_u^2 - d_l^2)^{1.5} - d_l^2(d_u^2 - d^2)^{1.5}}{d^2(d_u^2 - d_l^2)^{1.5}} \quad \text{.....(6.10)}$$

where, d is the diameter associated with P(d), and d_u and d_l are the upper and lower particle size (diameter) limits. The aggregate distribution in a given particle size range can be summarized in the following manner:

- A random number between 0 and 1 is generated and this number is substituted for P(d) in Equation 6.10.
- The diameter d corresponding to P(d) is calculated based on the upper and lower diameter limits in the range.
- This process is repeated as long as the particles generated result in the total area less than the area allocated for the particle size range. As soon as the total area of particle generated equals or exceeds the allocated area, this process should stop.
- Generated particles are placed in the model according to random number generations for x- and y-coordinates. Here also, random numbers corresponding to x and y coordinates are generated where the lower bound in each direction is the particle radius and the upper bound is the model dimension minus the particle radius.
- As a necessary condition, placement of a newer particle cannot overlap the particles already present.

Table 6.3 below provides the actual particle sizes (diameters) and the number of particles in each size range as determined using the procedure explained above.

Table 6.3: Aggregate particle diameters and numbers in different particle size ranges.

Coarse Aggregate Particle Sizes	Number of Aggregates	Particle Diameters (mm)	Total Area (mm^2)
4.75 mm – 9.5 mm	13	5.6, 5.7, 5.9, 6.2, 6.3, 6.6, 6.9, 7.3, 7.7, 8.1, 8.2, 8.6, 8.7	520.8
9.5 mm – 12.7 mm	5	9.6, 9.7, 9.9, 10.2, 10.4	389.9
12.7 mm – 19.0 mm	3	14.5, 15.2, 16.3	555.3
19.0 mm – 25.4 mm	Area included in 12.7 mm – 19.0 mm range		
Total	21	-	1466.0

Using the particle sizes and numbers provided in Table 6.3, two different aggregate distribution patterns were laid out according to the approach proposed by Zheng et al. (2003). Then, a mirror image pattern about the Y-Y axis was generated for each of these two patterns. Hence, the total number of aggregate distribution patterns used in the simulation was four. Our tests showed that the ITZ regions were not present or negligible in the concretes prepared in the present study (see Section 5.5 in Chapter 5). Therefore, ITZ regions are not included in the model. A typical aggregate distribution pattern in a 2D model generated in FlexPDE with circular aggregate particles is shown in Figure 6.6.

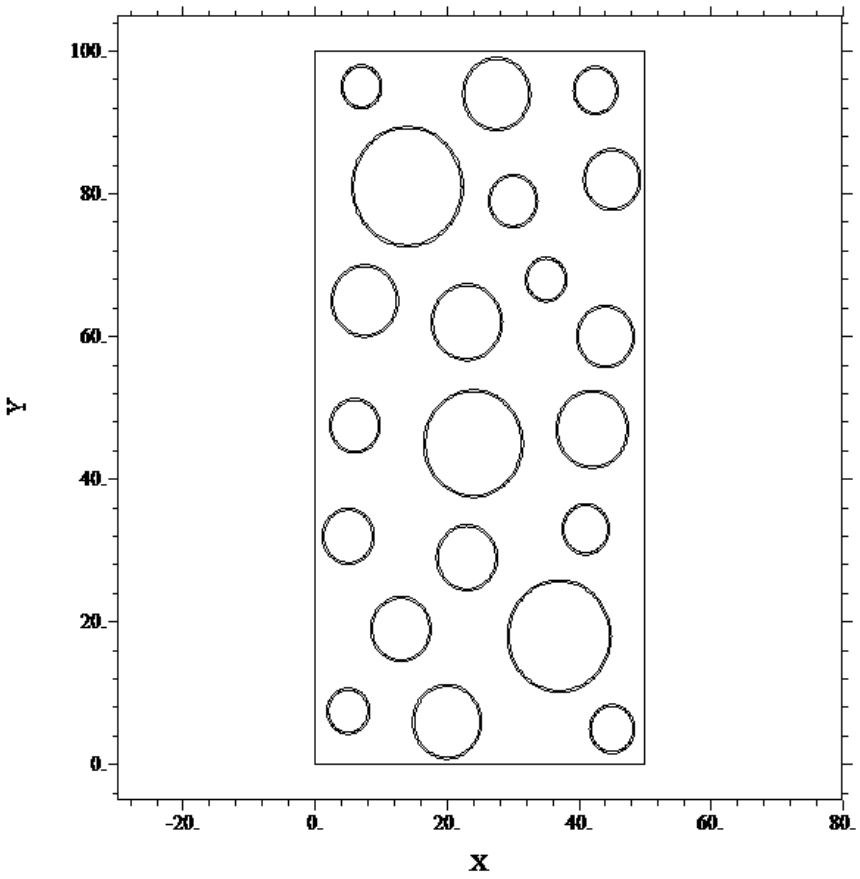

Figure 6.6: A typical aggregate distribution pattern in a 2D model generated in FlexPDE including circular aggregate particles.

Mesh the Model

In the finite difference method of solution, the space (or the model) is divided into small discrete elements. When there is a sharp change in variables at the interface between two boundaries, a finer mesh should be provided. For example, at the boundary where chloride initially penetrates or at the interfaces between the paste and aggregates, finer meshing is always necessary to minimize the solution error. The software used in the present study,

however, is capable of adaptive meshing as the solution progresses thus eliminating the need to specify mesh parameters most of the time.

Define Boundary Conditions

Boundary conditions in the proposed model are defined either as Dirichlet types where the variables are assigned specific values, or as Neumann types where the normal derivatives of the variables are assigned specific values (Backstrom 2004). In the model, free chloride concentration (C_f) on boundary A is a finite value and hence a Dirichlet type boundary condition is applicable on this boundary. But on boundaries B and D, the boundary condition is a Neumann type where the normal derivative of C_f is zero, that is, there are no chlorides going in or out of these surfaces (representative of an actual situation where these faces are epoxy-coated during RCPT). On boundary C, on the other hand, C_f is equal to zero assuming a semi-infinite media (that is, the downstream boundary is far enough to assume a zero value for C_f) and this is, obviously, a Dirichlet type boundary condition. Figure 6.7 shows the boundary conditions assigned to variables C_f, C_b and V on all four boundaries of the model.

In Figure 6.7, N_1 is the estimated free surface chloride concentration and this value is calculated based on the concentration of upstream NaCl solution and the porosity of the test specimen. But, because C_f in Equation 5.5 is a hypothetical free chloride concentration, N_1 is also a hypothetical value, which is given as:

$$N_1 = \frac{C_{fs}}{n} \quad \text{.....(6.11)}$$

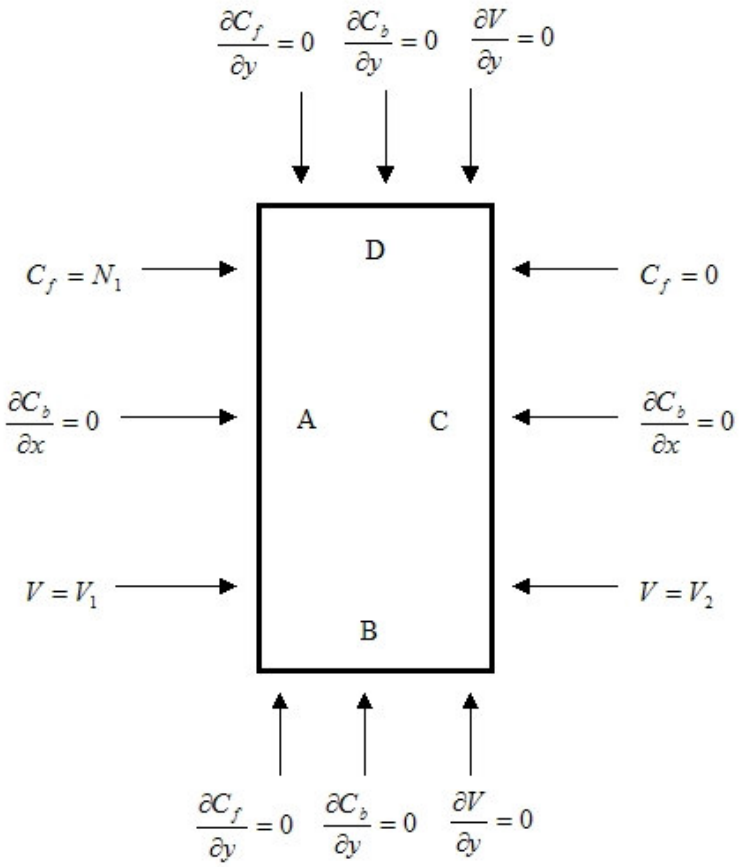

Figure 6.7: Boundary conditions assigned to variables C_f, C_b and V on boundaries A, B, C and D.

where, n is provided as a fraction. The free surface chloride concentration (C_{fs}) can be estimated using Equation 5.1 in Chapter 5. Similarly, V_1 and V_2 are the components of potential difference provided across the specimen where V_1-V_2 should be equal to the actual potential difference during the test (60 V in case of RCPT).

As mentioned earlier, porosity (n) and diffusion coefficient (D) values for aggregate particles are different from the smeared paste. Therefore, appropriate values of both *n* and D should be supplied at the regions that represent smeared paste and aggregate particles in the model.

Define Initial Conditions

Initially (at t = 0), all three variables are equal to zero, that is:

$C_f = C_b = V = 0$

Define Test Duration

The test duration for an RCPT is 6 hours. This duration can be broken down into smaller units such as minutes, but the solution time will significantly increase. On the other hand, when the test duration is specified in hours, all time dependent input parameters such as diffusion coefficient (D) should be specified accordingly (in mm^2/hr etc.).

Solve the Equations and Obtain the Results

Equations 6.5, 6.6 and 6.9 are solved simultaneously to obtain the solutions to the three unknowns that are C_f, C_b and V. The average total chloride concentration (the sum of C_f and C_b) values at different predetermined depths of chloride penetration from the simulation are the most important output parameters as these values can be directly compared with the experimental total chloride concentration values. For example, the average total chloride concentrations are determined at 6 to 7 different depths of concrete and mortar specimens subjected to RCPT (see Chapter 5). A number of parameters will be determined from the simulation based on curve fitting between the simulation and the experimental chloride profile results.

6.4 Simulation Procedures

6.4.1 Simulation in Mortar

Simulation begins with the representative models of mortar samples. At any given age (28-, 56- or 91-day), a model including only the smeared paste, which essentially represents the mortar at that age, is run after supplying the model with all necessary input parameters including boundary conditions. These include u, D, V, α, β and N_1 where α, β and D are supplied as trial values at first. In successive executions of the model, α, β and D are adjusted until the chloride profile from the model comes acceptably close to the experimental chloride profile of the mortar at that age. Parameters (α, β and D), thus determined, should represent, at least theoretically, the paste properties of all three concrete types (GNSS-A, LMST-E and LMST-C) for the age at which the mortar model was run. For example, simulation of a 28-day mortar sample can be performed after supplying all the parameters and boundary values (both known and trial values). Once the final values of input parameters (α, β and D) are determined based on the curve fitting of the simulation results to the experimental chloride profile results on the 28-day mortar, these parameters now become the representative parameter values for the paste portions in the 28-day concrete models of all three aggregate types.

6.4.2 Simulation in Concrete

For the concrete, the porosity (n) and diffusion coefficient (D) values of aggregates are different from those of the paste portion; therefore, aggregate phase in the model requires its own *n* and D values. Here again, *n* for each of the three aggregate types is already determined (see Table 4.2 in Chapter 4) and hence the appropriate *n* values can be provided during

simulation. But D is not known initially and hence the work should begin with a trial value. The final D value is determined based on the curve fitting of the simulation results with the experimental chloride profile results of the respective concrete types. Theoretically speaking, aggregate diffusion coefficient for a given aggregate type should remain constant at all concrete ages because this property does not depend on the concrete age.

6.5 Simulation Results

6.5.1 Simulation in Mortar

For the purpose of simulation, the porosity and the dry bulk specific gravity (or the dry bulk density) values of mortar specimens were taken as 20% and 2.0 (2.0 g/cm^3) respectively, at all three ages. The reason of using single values of porosity and bulk specific gravity at all three ages is due to the fact that these values only marginally changed from one test age to the other as shown in Table 5.2 in Chapter 5. Because of a single porosity value and a single dry bulk density value, a single value of C_{fs} and subsequently a single value of N_1 can be used for all three mortar ages. Using Equation 5.1 in Chapter 5, C_{fs} (by % of sample weight) is calculated as:

$$C_{fs} = \frac{nA_{Cl}M_{NaCl}}{1000\rho} \times 100\% = \frac{(0.20)(35.5)(0.513)}{1000(2.0)} \times 100\% = 0.182\% \quad \text{……..…(6.12)}$$

where, n is the paste porosity in fraction (equal to 0.20), A_{Cl} is the atomic weight of chlorine (approximately equal to 35.5), M_{NaCl} is the molarity of 3% NaCl solution (approximately equal to 0.513) and ρ is the dry bulk density of mortar (equal to 2.0 g/cm^3). Again using Equation 6.11, boundary value, N_1, is calculated as:

$$N_1 = \frac{C_{fs}}{n} = \frac{0.182}{0.20} = 0.91\% \quad \text{……..……(6.13)}$$

Referring to Figure 6.7, V_1 and V_2 are the other two boundary values that need to be specified. In the current modeling, V_1 is assigned a value of 60 (equal to a potential difference of 60 V) and V_2 is assigned a zero value.

Table 6.4 provides a single set of input parameters that is applicable to all three mortar ages. Similarly, Tables 6.5 to 6.7 provide simulation results whereas Table 6.8 provides the corresponding α, β and D values. Experimental chloride concentration values in Tables 6.5, 6.6 and 6.7 are the chloride profile results determined in Section 5.3 of Chapter 5.

Table 6.4: Input parameters for mortar specimens applicable to all three mortar ages.

Input Parameters	Boundary Values	Time
z = -1 F = 96,485 Coulomb/mole R = 8.314 J/mole-K T = 298 K n = 0.20	N_1 = 0.91% V_1 = 60 V V_2 = 0 V	t = 6 hours

Table 6.5: Simulation results in comparison to the experimental results for the 28-day mortar specimens.

Depth (mm)	Total Chloride Concentration (% by Weight)		Correlation Coefficient (r^2)
	Simulation	Experiment	
3.0	0.357	0.356	0.998
5.0	0.323	0.309	
7.5	0.264	0.268	
10.5	0.164	0.167	
14.0	0.053	0.033	
18.0	0.008	0.009	
22.0	0.000	0.001	

Table 6.6: Simulation results in comparison to the experimental results for the 56-day mortar specimens.

Depth (mm)	Total Chloride Concentration (% by Weight)		Correlation Coefficient (r^2)
	Simulation	Experiment	
3.0	0.259	0.259	1.0
5.0	0.159	0.159	
7.5	0.043	0.044	
10.5	0.000	0.000	
14.0	0.000	0.000	
18.0	0.000	0.000	
22.0	0.000	0.000	

Table 6.7: Simulation results in comparison to the experimental results for the 91-day mortar specimens.

Depth (mm)	Total Chloride Concentration (% by Weight)		Correlation Coefficient (r^2)
	Simulation	Experiment	
3.0	0.265	0.265	1.0
5.0	0.101	0.100	
7.5	0.001	0.000	
10.5	0.000	0.000	
14.0	0.000	0.000	
18.0	0.000	0.000	
22.0	0.000	0.001	

Table 6.8: α, β and D values for mortar specimens corresponding to the simulation results as shown in Tables 6.5, 6.6 and 6.7.

Parameters	28-Day Mortar	56-Day Mortar	91-Day Mortar
α	0.75	0.43	1.0
β	1.18	1.30	2.0
D	1.992×10^{-11} m^2/s	8.750×10^{-12} m^2/s	7.472×10^{-12} m^2/s

6.5.2 Migration Simulations in Concrete

Even though the *paste-alone* mix was designed to represent the paste region of all three concretes under consideration, the paste regions in the concretes were found to have different parameter (α, β and D) values than that of mortar specimens in most cases according to the simulation results. Initially the idea was: once the diffusion coefficient value and the binding parameters (α and β) of a mortar specimen at a given age were determined from the migration simulation in mortar, those values were to be used as constant values for the bulk paste regions of all three concrete specimens at that age during the migration simulation in concrete. But during the simulation of chloride migration in concretes, it was not possible to keep these parameters as constant values if we wanted to get the simulation results close enough to the corresponding experimental chloride profile results. Because of this situation, the paste parameters (α, β and D) once again became unknowns and had to be found by trial and error during the simulation of chloride migration in concretes. As it would be almost impossible to work both on the paste parameters and the aggregate parameters on a trial and error basis, aggregate binding parameters (α and β) were preset as 0.1 and 1.0, respectively, for all concrete types and ages. These values should be regarded as the well-acceptable values for the following reasons:

- Binding was observed in LMST-W rock specimen during RCPT (see Section 5.4 in Chapter 5), which is a limestone rock, whereas two of the selected aggregate types (that is, LMST-E and LMST-C) also come from the limestone family.
- On the other hand, the porosity value for GNSS-A aggregate is very low and as a result the analytical model is not noticeably sensitive to the binding parameters for this aggregate type.

Out of four unknowns to be dealt now (that is, α, β and D for the bulk paste region, and D for the aggregate), the ranges for the paste binding parameters (α and β) were more or less known from the simulation in mortar. D for a given aggregate type should be a constant, at least theoretically, regardless of the concrete age or concrete type. Hence for each aggregate type, a single D value (for all concrete ages) was determined from the simulation in such a way that D resulted in the best curve fitting at all test ages. The chloride profile data and the corresponding α, β and D values as obtained from the simulations are provided in Tables 6.9 to 6.18. The set of input parameters presented in Table 6.4 (for mortar) is applicable to concretes as well. Additional input parameters necessary for concretes are provided in Table 6.18. The simulation results are the average values from the four separate models each having its own aggregate distribution pattern (two patterns and two mirror patterns as explained in Section 6.3).

Table 6.9: Simulation results in comparison to the experimental results for 28-day GNSS-A concrete.

Depth (mm)	Total Chloride Concentration (% by Weight)						Correlation Coefficient (r^2)
	Simulation					Experiment	
	Aggregate Distribution Pattern				Average		
	1	2	3	4			
3.0	0.206	0.214	0.202	0.230	0.213	0.202	0.997
5.0	0.122	0.130	0.130	0.146	0.132	0.117	
7.5	0.073	0.075	0.070	0.066	0.071	0.076	
10.5	0.039	0.030	0.043	0.023	0.034	0.022	
14.0	0.005	0.004	0.009	0.002	0.005	0.000	
18.0	0.000	0.000	0.000	0.000	0.000	0.000	
22.0	0.000	0.000	0.000	0.000	0.000	0.000	

Table 6.10: Simulation results in comparison to the experimental results for 56-day GNSS-A concrete.

Depth (mm)	Total Chloride Concentration (% by Weight)						Correlation Coefficient (r^2)
	Simulation					Experiment	
	Aggregate Distribution Pattern				Average		
	1	2	3	4			
3.0	0.208	0.217	0.208	0.234	0.217	0.219	0.999
5.0	0.094	0.100	0.102	0.105	0.100	0.110	
7.5	0.031	0.024	0.032	0.013	0.025	0.030	
10.5	0.003	0.002	0.006	0.001	0.003	0.005	
14.0	0.000	0.000	0.000	0.000	0.000	0.000	
18.0	0.000	0.000	0.000	0.000	0.000	0.000	
22.0	0.000	0.000	0.000	0.000	0.000	0.000	

Table 6.11: Simulation results in comparison to the experimental results for 91-day GNSS-A concrete.

Depth (mm)	Total Chloride Concentration (% by Weight)						Correlation Coefficient (r^2)
	Simulation					Experiment	
	Aggregate Distribution Pattern				Average		
	1	2	3	4			
3.0	0.073	0.082	0.085	0.080	0.080	0.076	1.0
5.0	0.008	0.008	0.009	0.005	0.008	0.008	
7.5	0.000	0.000	0.001	0.000	0.000	0.000	
10.5	0.000	0.000	0.000	0.000	0.000	0.000	
14.0	0.000	0.000	0.000	0.000	0.000	0.000	
18.0	0.000	0.000	0.000	0.000	0.000	0.000	
22.0	0.000	0.000	0.000	0.000	0.000	0.000	

Table 6.12: Simulation results in comparison to the experimental results for 28-day LMST-E concrete.

Depth (mm)	Total Chloride Concentration (% by Weight)						Correlation Coefficient (r^2)
	Simulation					Experiment	
	Aggregate Distribution Pattern				Average		
	1	2	3	4			
3.0	0.267	0.276	0.263	0.276	0.271	0.263	0.999
5.0	0.178	0.187	0.184	0.203	0.188	0.179	
7.5	0.114	0.123	0.112	0.116	0.116	0.112	
10.5	0.075	0.063	0.075	0.066	0.070	0.056	
14.0	0.016	0.013	0.024	0.012	0.016	0.010	
18.0	0.001	0.001	0.002	0.000	0.001	0.000	
22.0	0.000	0.000	0.000	0.000	0.000	0.000	

Table 6.13: Simulation results in comparison to the experimental results for 56-day LMST-E concrete.

Depth (mm)	Total Chloride Concentration (% by Weight)						Correlation Coefficient (r^2)
	Simulation					Experiment	
	Aggregate Distribution Pattern				Average		
	1	2	3	4			
3.0	0.176	0.182	0.175	0.182	0.179	0.136	0.989
5.0	0.120	0.126	0.123	0.134	0.126	0.119	
7.5	0.075	0.081	0.073	0.076	0.076	0.074	
10.5	0.036	0.025	0.040	0.029	0.033	0.026	
14.0	0.001	0.000	0.003	0.000	0.001	0.000	
18.0	0.000	0.000	0.000	0.000	0.000	0.000	
22.0	0.000	0.000	0.000	0.000	0.000	0.000	

Table 6.14: Simulation results in comparison to the experimental results for 91-day LMST-E concrete.

Depth (mm)	Total Chloride Concentration (% by Weight)						Correlation Coefficient (r^2)
	Simulation					Experiment	
	Aggregate Distribution Pattern				Average		
	1	2	3	4			
3.0	0.131	0.136	0.132	0.138	0.134	0.132	1.0
5.0	0.036	0.040	0.040	0.040	0.039	0.039	
7.5	0.004	0.003	0.004	0.003	0.004	0.001	
10.5	0.001	0.000	0.002	0.001	0.001	0.000	
14.0	0.000	0.000	0.000	0.000	0.000	0.000	
18.0	0.000	0.000	0.000	0.000	0.000	0.000	
22.0	0.000	0.000	0.000	0.000	0.000	0.000	

Table 6.15: Simulation results in comparison to the experimental results for 28-day LMST-C concrete.

Depth (mm)	Total Chloride Concentration (% by Weight)						Correlation Coefficient (r^2)
	Simulation					Experiment	
	Aggregate Distribution Pattern				Average		
	1	2	3	4			
3.0	0.267	0.275	0.265	0.289	0.274	0.270	0.989
5.0	0.195	0.200	0.191	0.211	0.199	0.173	
7.5	0.131	0.147	0.134	0.143	0.139	0.144	
10.5	0.128	0.123	0.105	0.119	0.119	0.089	
14.0	0.087	0.076	0.089	0.087	0.085	0.061	
18.0	0.036	0.030	0.052	0.026	0.036	0.034	
22.0	0.010	0.012	0.011	0.003	0.009	0.004	

Table 6.16: Simulation results in comparison to the experimental results for 56-day LMST-C concrete.

Depth (mm)	Total Chloride Concentration (% by Weight)						Correlation Coefficient (r^2)
	Simulation					Experiment	
	Aggregate Distribution Pattern				Average		
	1	2	3	4			
3.0	0.209	0.216	0.208	0.226	0.215	0.176	0.987
5.0	0.152	0.156	0.148	0.163	0.155	0.161	
7.5	0.094	0.105	0.095	0.102	0.099	0.092	
10.5	0.077	0.071	0.057	0.066	0.068	0.060	
14.0	0.041	0.031	0.043	0.036	0.038	0.040	
18.0	0.005	0.005	0.018	0.002	0.008	0.012	
22.0	0.001	0.003	0.001	0.001	0.002	0.000	

Table 6.17: Simulation results in comparison to the experimental results for 91-day LMST-C concrete.

Depth (mm)	Total Chloride Concentration (% by Weight)						Correlation Coefficient (r^2)
	Simulation					Experiment	
	Aggregate Distribution Pattern				Average		
	1	2	3	4			
3.0	0.159	0.164	0.158	0.171	0.163	0.142	0.981
5.0	0.077	0.084	0.074	0.088	0.081	0.083	
7.5	0.024	0.025	0.021	0.017	0.022	0.028	
10.5	0.027	0.025	0.023	0.025	0.025	0.000	
14.0	0.004	0.002	0.007	0.002	0.004	0.000	
18.0	0.000	0.000	0.002	0.000	0.001	0.000	
22.0	0.000	0.000	0.000	0.000	0.000	0.000	

Table 6.18: Parameters for different concrete types corresponding to the simulation results in Tables 6.9 to 6.17.

Concrete Types	Parameters	Aggregate	Paste (28-Day)	Paste (56-Day)	Paste (91-Day)
GNSS-A	n (%)	0.81	20.0	20.0	20.0
	α	0.1	0.45	1.0	0.45
	β	1.0	1.5	1.5	2.0
	D (m^2/s)	5.556×10^{-12}	1.500×10^{-11}	1.250×10^{-11}	5.222×10^{-12}
LMST-E	n (%)	2.97	20.0	20.0	20.0
	α	0.1	0.75	0.15	0.15
	β	1.0	1.18	2.5	2.5
	D (m^2/s)	1.111×10^{-11}	1.972×10^{-11}	1.097×10^{-11}	5.000×10^{-12}
LMST-C	n (%)	5.81	20.0	20.0	20.0
	α	0.1	0.32	0.2	0.06
	β	1.0	0.65	1.5	3.5
	D (m^2/s)	3.611×10^{-11}	1.806×10^{-11}	9.861×10^{-12}	3.889×10^{-12}

6.5.3 Simulation on Concrete Specimens using Averaged Parameter Values

Individual α, β and D values obtained from the simulation on each of mortar, GNSS-A, LMST-E and LMST-C are presented in Table 6.18. As discussed in Section 6.5.2 above, the paste phases in mortar, GNSS-A, LMST-E and LMST-C did not result in identical parameter (α, β and D) values at any given age. Therefore for a given age, these parameters were averaged from all four specimen types and the averaged values were used for each of the concrete types in the next simulation phase. Table 6.19 provides the individual and averaged α, β and D values in the paste regions for 28-, 56- and 91-day specimens.

Table 6.19: Individual and averaged α, β and D values at different specimen ages.

Parameters	Specimen Types	Parameter Values for the Paste Phases		
		28-Day	56-Day	91-Day
α	Mortar	0.75	0.43	1.00
	GNSS-A	0.45	1.00	0.45
	LMST-E	0.75	0.15	0.15
	LMST-C	0.32	0.20	0.06
	Average	**0.57**	**0.45**	**0.42**
β	Mortar	1.18	1.30	2.00
	GNSS-A	1.50	1.50	2.00
	LMST-E	1.18	2.50	2.50
	LMST-C	0.65	1.50	3.50
	Average	**1.13**	**1.70**	**2.50**
D (m^2/s)	Mortar	1.991×10^{-11}	8.750×10^{-12}	7.472×10^{-12}
	GNSS-A	1.500×10^{-11}	1.250×10^{-11}	5.222×10^{-12}
	LMST-E	1.972×10^{-11}	1.097×10^{-11}	5.000×10^{-12}
	LMST-C	1.806×10^{-11}	9.861×10^{-12}	3.889×10^{-12}
	Average	$\mathbf{1.817\times10^{-11}}$	$\mathbf{1.052\times10^{-11}}$	$\mathbf{5.396\times10^{-12}}$

Except for the averaged α, β and D as obtained from Table 6.19 for the paste region of the concretes, other general input parameters including aggregate parameters and the paste porosity values during chloride migration simulation in concretes in this phase were used as provided in Tables 6.4 and 6.18. Simulation results in comparison to the experimental results are provided in Appendix C. The simulation results are the average of four aggregate distribution patterns as explained in Section 6.3. Correlation coefficients between the simulation and the experimental results were found to be higher than 0.9 and, in most cases, higher than 0.95 (see Appendix C).

6.5.4 Determination of Paste Chloride Concentrations from Simulation

In real life situations, the embedded reinforcing bars in concretes are surrounded by the paste and hence the chloride concentration in the paste becomes an issue of interest rather than the average chloride concentration (average of the paste and aggregates). For example, the average chloride concentration at any given concrete depth is the average of the concentrations in the paste portion and in aggregate particles. However, aggregate is always less porous than the paste and has much less chloride concentration as compared to the paste portion. As a result, the actual chloride concentration in the paste is noticeably higher than the average concentration. This situation is illustrated in Figure 6.8 where the chloride concentration in the paste is much higher than in the aggregate particles.

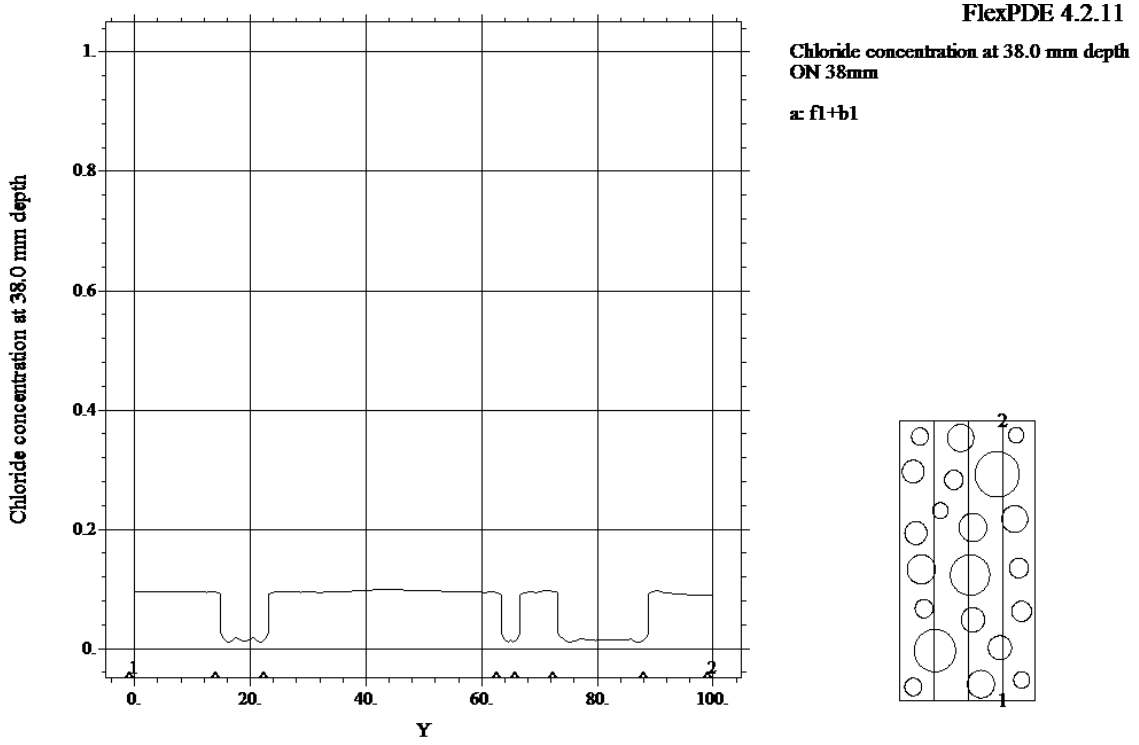

Figure 6.8: A typical chloride profile curve at 38.0 mm depth along the direction of migration (at location 1-2 as indicated in the thumbnail figure to the right) where the recessed regions in the curve indicate the chloride concentrations in aggregates.

In this section, the paste chloride concentration in comparison to the average concentration is determined at a pre-selected concrete depth using the analytical simulation method for two different chloride transport situations as follows:

- Short-term diffusion-migration, and
- Long-term diffusion

6.5.4.1 Short-Term Diffusion-Migration

The analytical model proposed in the present study is primarily developed for the simulation of chloride migration during RCPT and this test represents a short-term diffusion-migration of chlorides in concretes. However, the proposed model is developed in such a way that all the input parameters including potential difference (V), test duration and surface chloride concentration can be changed without any difficulty. Moreover, both diffusion and migration terms are included in the equation that governs the simulation process (Equation 6.5). Therefore, this model can be used to simulate chloride diffusion/migration during other short- and long-term test methods as well, as long as these methods follow non-steady state transport mechanisms. They include NT Build 492/RMT (diffusion-migration) and Bulk Diffusion Test (diffusion).

A depth of 12.7 mm was selected for viewing the paste and average chloride concentrations in all three concrete types (GNSS-A, LMST-E and LMST-C). Simulations were done on 28-day concretes using aggregate distribution pattern-1 (see Figure C.1 in Appendix C) and the averaged parameter values (α, β and D) for 28-day concretes were used (see Table 6.19). Except for the averaged parameters, other necessary input parameters were used as provided in Tables 6.4 and 6.18. Table 6.20 provides the overall average, in-paste average and in-aggregate average chloride concentration values at 12.7 mm for each of three concrete types at 28 days as obtained from the simulation. Graphical presentations of different levels of chloride concentrations along the concrete depth are provided in Figure 6.8.

Table 6.20: Average total chloride concentration values (overall, in-paste and in-aggregate) at 12.7 mm depth from the 28-day RCPT simulations on all three concrete types.

Concrete Types	Porosity (%)	Diffusion Coefficient (m^2/s)	Total Chloride Concentrations at 12.7 mm Depth (% of Concrete Weight)		
			Overall Average	In-Paste Average	In-Aggregate Average
GNSS-A	0.81	5.556×10^{-12}	0.025	0.033	Negligible
LMST-E	2.97	1.111×10^{-11}	0.031	0.041	Negligible
LMST-C	5.81	3.611×10^{-11}	0.101	0.118	0.043

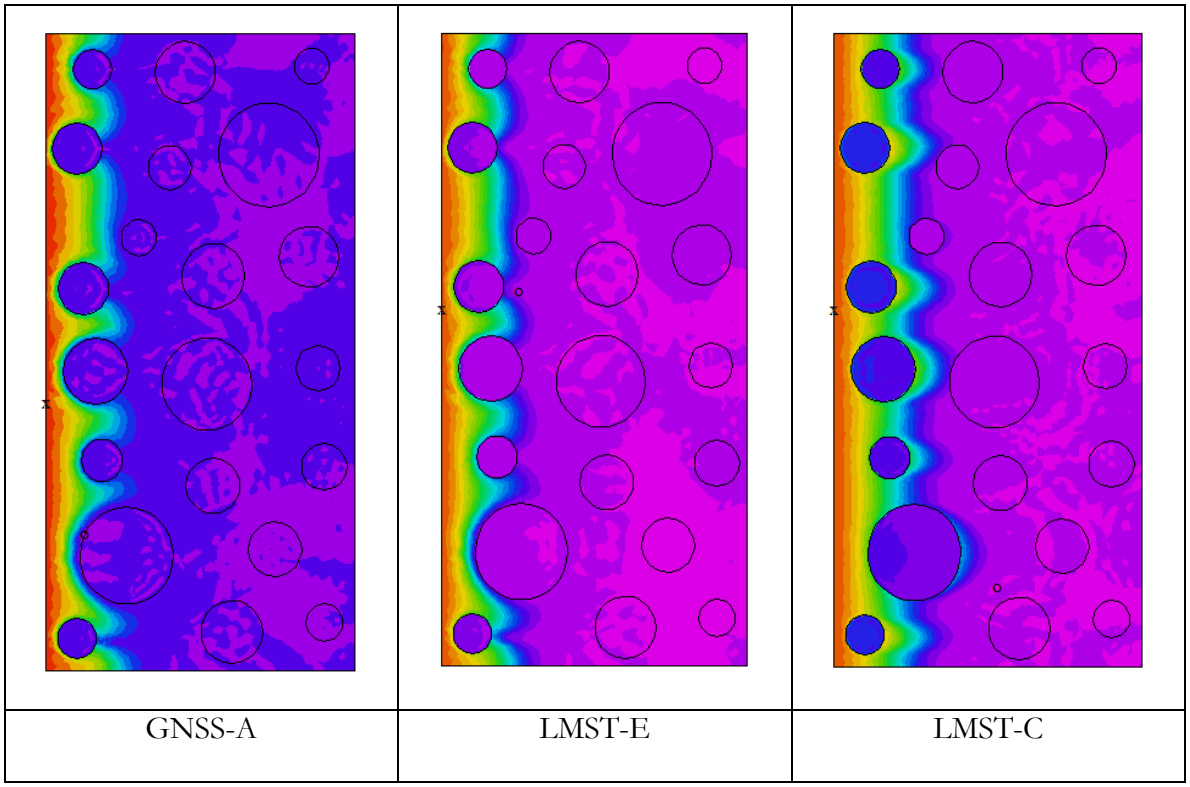

GNSS-A | LMST-E | LMST-C

Figure 6.9: Contour plots of chloride concentrations from simulation along the path of chloride migration in 28-day GNSS-A, LMST-E and LMST-C concretes.

6.5.4.1 Long-Term Diffusion

A long-term diffusion process was simulated using the proposed model. Because there is no electrical potential (V) during this process, this parameter (V) was set to zero. During long-term diffusion, the binding pattern may or may not be similar to the pattern during migration. However, binding parameters (α and β) and N_1 (a parameter corresponding the surface chloride concentration) the simulation were selected as 1.5, 3.5 and 0.5, respectively, which in turn, result in the total (free and bound) surface chloride concentrations in the neighborhood of 0.15% by concrete weight (approximately equal to 3.5 kg of chloride/m^3 of concrete) at the end of the test duration. We wanted to see the overall and in-paste chloride concentrations at a depth of 38.0 mm in all three concretes at the end of 12-year period. According to ACI 222R-96 (1997), threshold chloride concentration for the corrosion initiation in reinforcing bars in dry conditions is estimated to be about 0.2% by cement weight, which corresponds to 0.03% by concrete weight assuming 15% cement by concrete weight (Hussain et al. 1996). It should be noted that 0.03% (by concrete weight) is an overall average concentration, not just the paste concentration. A diffusion coefficient of 2.0×10^{-12} m^2/s was selected which is less than half the 91-day average diffusion coefficient from simulation (5.4×10^{-12} m^2/s, see Table 6.19). This selection was based on the trial running of the proposed model, which resulted in the average chloride concentrations in the neighborhood of 0.03% by concrete weight, at least, for GNSS-A. Simulations were run using aggregate distribution pattern-1 (see Figure C.1 in Appendix C). The simulation results in terms of overall, in-paste and in-aggregate chloride concentrations at 38.0 mm depth for each concrete type is presented in Table 6.21.

Table 6.21: Average total chloride concentration values (overall, in-paste and in-aggregate) at 38.0 mm depth from the simulations for a long-term (12-year period) diffusion process on all three concrete types.

Concrete Types	Porosity (%)	Diffusion Coefficient (m^2/s)	Total Chloride Concentrations at 38.0 mm Depth (% of Concrete Weight)		
			Overall Average	In-Paste Average	In-Aggregate Average
GNSS-A	0.81	5.556×10^{-12}	0.020	0.027	Negligible
LMST-E	2.97	1.111×10^{-11}	0.042	0.058	Negligible
LMST-C	5.81	3.611×10^{-11}	0.073	0.095	0.014

7.0 RESULTS AND DISCUSSION

This chapter is divided into two sections: discussion on the experimental chloride profile results (see Chapter 5) and discussion on the simulation results (see Chapter 6). The first section analyzes the general trends on the experimental chloride profile data and the chloride penetration depths among the specimens under consideration. Similarly, the second section makes a comprehensive analysis of the simulated paste diffusion coefficient values of concretes in relation to the simulated mortar diffusion coefficient values and the estimated paste RCPT values (based on the RCPT results in Chapter 4). The correlation between aggregate porosity and aggregate diffusion coefficient values as obtained from the simulation is also discussed in this section. Similarly, the effect of aggregate porosity on the paste chloride concentration in concrete is briefly discussed.

7.1 Discussion on Experimental Chloride Profile Results

Experimental chloride profile results are analyzed from two different perspectives: the comparative study of chloride profile results on mortar and concrete specimens at a given test age (various specimens at a given test age), and the comparative study of the chloride profile results on a given specimen type (mortar, GNSS-A, LMST-E and LMST-C) at all three test ages (a given specimen at various test ages).

7.1.1 Various Specimens at a Given Test Age

The experimental chloride profile results on all four specimen types at the test ages of 28, 56 and 91 days are graphically presented in Figures 7.1 to 7.3.

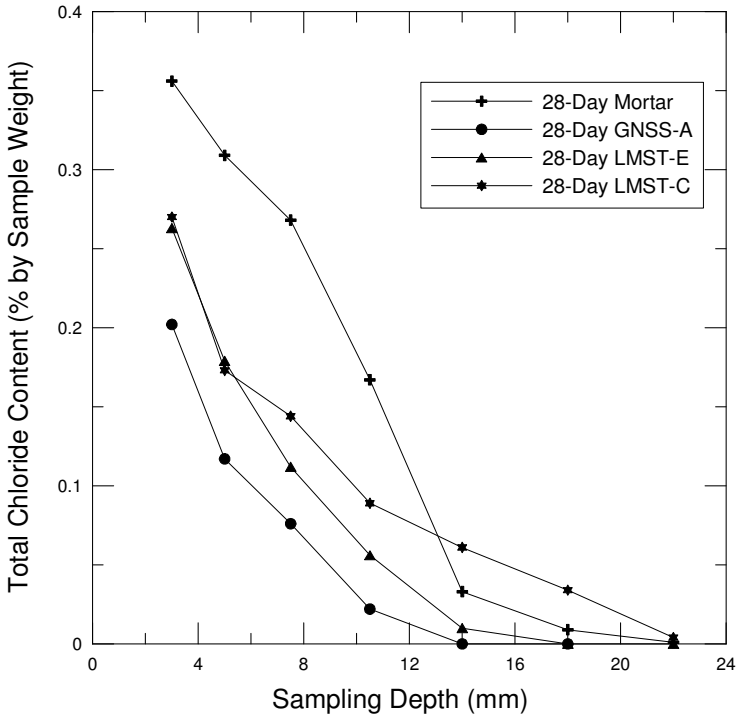

Figure 7.1: Total chloride profile results for various specimens subjected to 28-day RCPT.

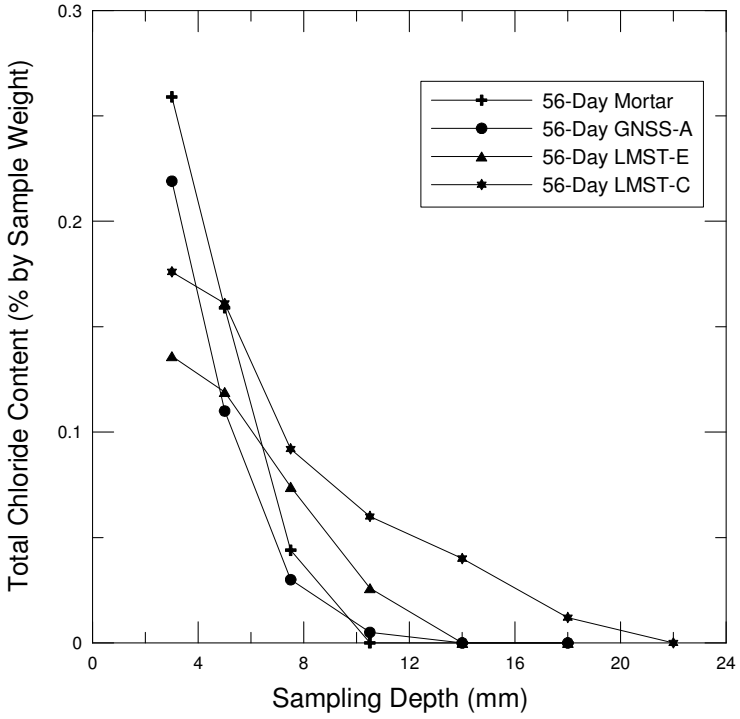

Figure 7.2: Total chloride profile results for various specimens subjected to 56-day RCPT.

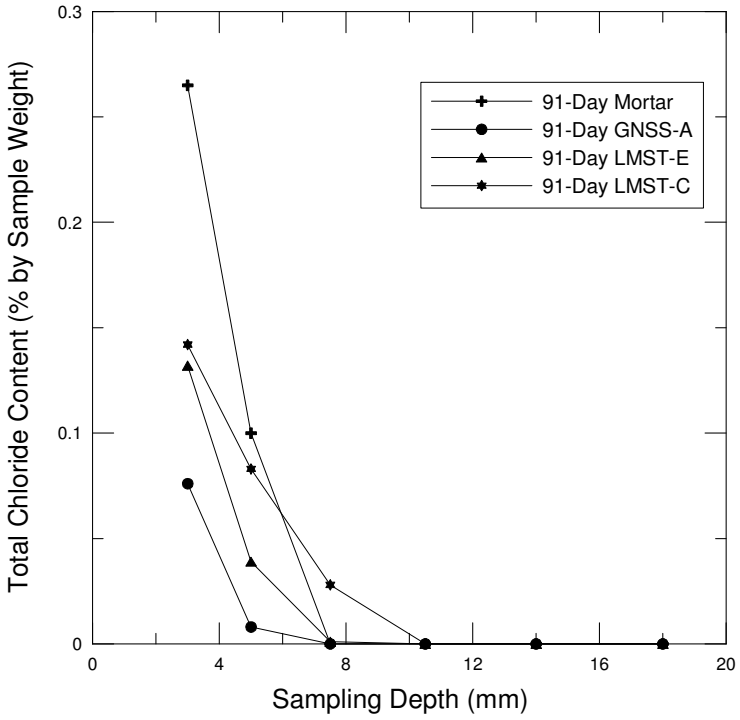

Figure 7.3: Total chloride profile results for various specimens subjected to 91-day RCPT.

Mortar specimens have a porosity of about 20% throughout the specimen volume at all three test ages (see Table 5.2 in Chapter 5). In concrete specimens, however, only about 71% of the specimen volume is the paste (which is assumed to have the same porosity as that of mortar specimens) and about 29% of the volume is occupied by the aggregate particles (see Figure 5.1 in Chapter 5). Moreover, porosity values of GNSS-A, LMST-E and LMST-C aggregates are 0.81%, 2.97% and 5.81% respectively (see Table 4.2 in Chapter 4). In view of the differences in the average porosity values (including paste and aggregate porosities where applicable) in each of these specimen types, chloride concentration values at any specified depth would not be the same in these specimens even if the chloride diffusivities in the aggregates (not applicable to mortar) and the paste were to remain constant. In each of the above figures, the mortar specimen has the highest chloride concentration near the surface,

followed by the concrete specimens made with the LMST-C, LMST-E and GNSS-A aggregates, respectively. This is a usual trend because of the fact that average porosity for the mortar specimens is the highest among all specimen types, followed by the LMST-C, LMST-E and GNSS-A concretes, respectively. In general, chloride profile results seem to obey the rule of more porosity leading to more chloride content at any given depth of concrete specimen under identical test conditions.

7.1.2 A Given Specimen at Various Test Ages

Experimental chloride profile results of mortar, GNSS-A, LMST-E and LMST-C specimens at various test ages are graphically presented in Figures 7.4 to 7.7.

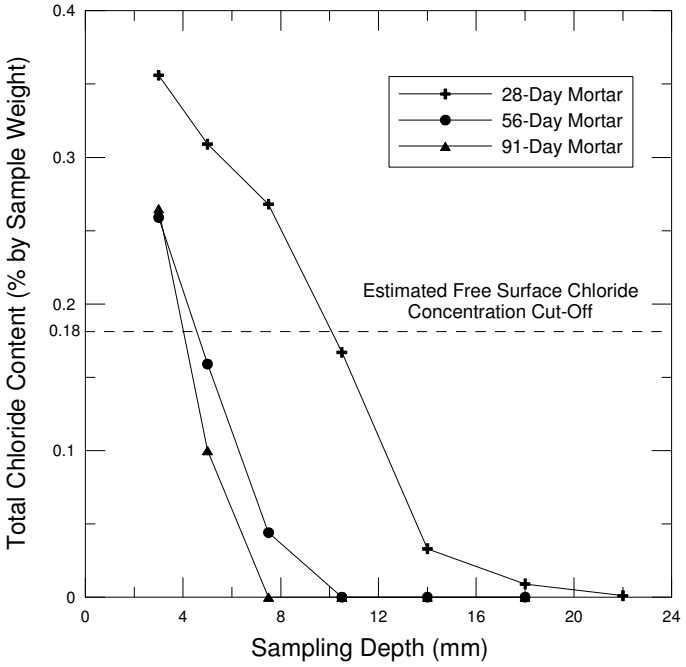

Figure 7.4: Total chloride profile results on the mortar specimens subjected to 28-, 56- and 91-day RCPT.

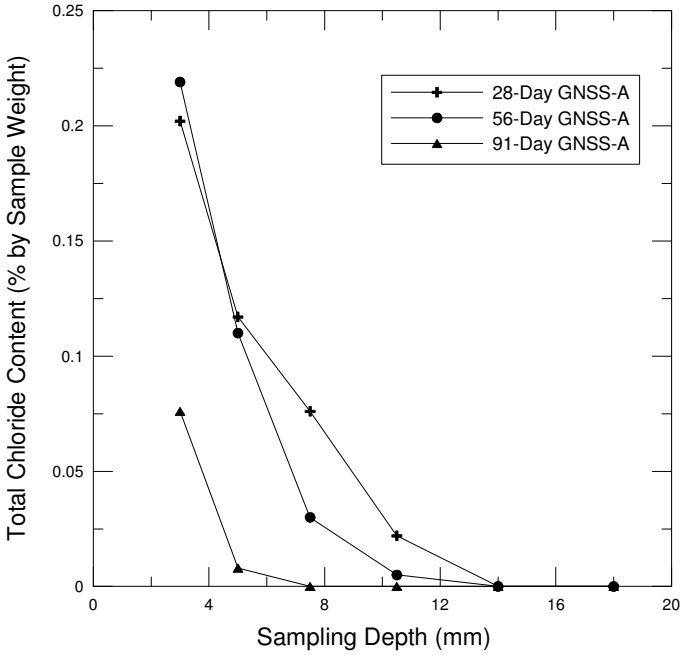

Figure 7.5: Total chloride profile results on the GNSS-A specimens subjected to 28-, 56- and 91-day RCPT.

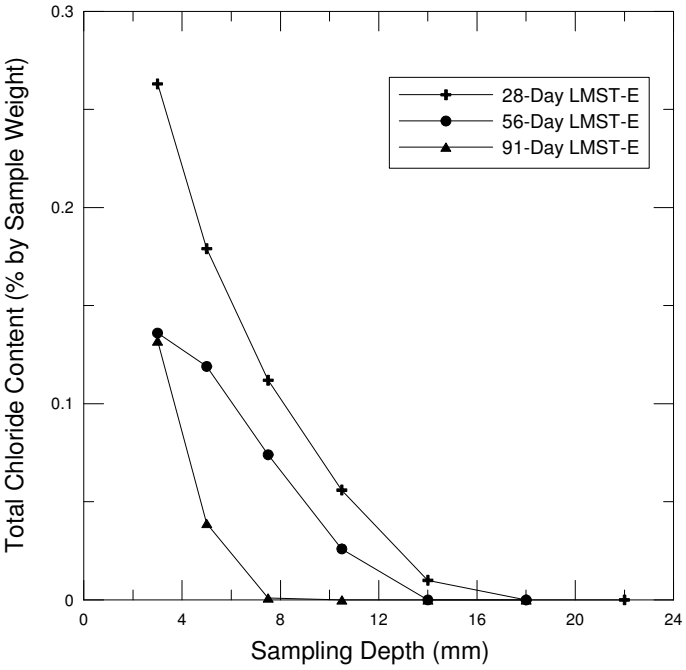

Figure 7.6: Total chloride profile results on LMST-E specimens subjected to 28-, 56- and 91-day RCPT.

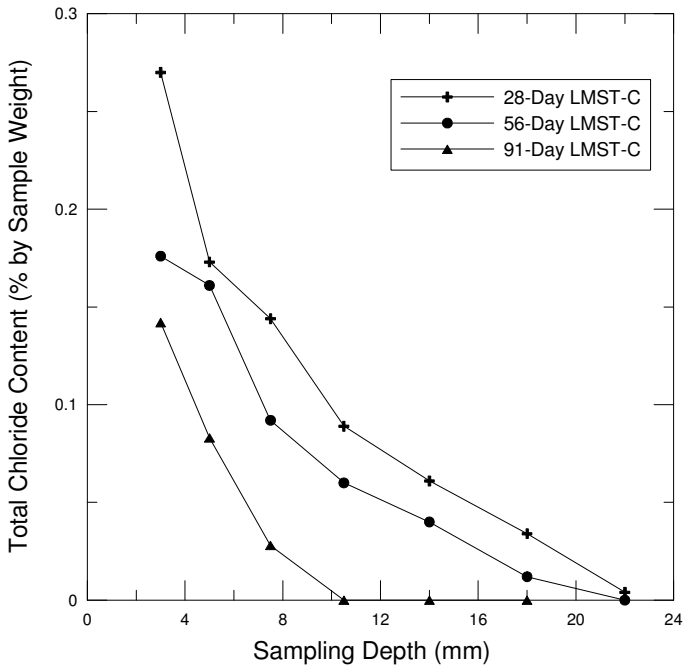

Figure 7.7: Total chloride profile results on LMST-C specimens subjected to 28-, 56- and 91-day RCPT.

The general trend of decrease in chloride penetration depths at increasing specimen ages in Figures 7.4 to 7.7 is in line with the reduction in RCPT values with the increasing ages (see Section 4.2 in Chapter 4). Theoretically, the reduction in penetration depths with the increase in age can attributed to the reduction and refinement of pores in the bulk paste region because of more hydration of cement particles with aging.

7.2 Discussion on Analytical Simulation Results

The diffusion coefficients obtained from the analytical modeling are the values that are independent of the chloride binding. Therefore, these values are not the same as the diffusion coefficient values that would be obtained from the long-term test methods such as the bulk diffusion test and the salt ponding test. Since binding slows down the diffusion

process, the bulk diffusion values from these long-term test methods are the so-called apparent diffusion coefficients, which will be less than the diffusion coefficient values obtained from our simulation method.

7.2.1 Correlation between Mortar and Concrete Paste Diffusion Coefficients

As mentioned in Chapter 6, the binding parameters (α and β) for aggregates were preset values assuming that a moderate level of chloride binding would take place during RCPT in all three aggregate types. Similarly for each of the three aggregate types, a single diffusion coefficient value (for all three test ages) was determined on a trial-and-error basis from the simulation process that resulted in the best curve fitting with the experimental data at all three specimen ages. The diffusion coefficient values and the binding parameters for the three aggregate types used in the simulation processes are given in Table 6.18 in Chapter 6.

The diffusion coefficient values of mortar and the paste regions of all three concrete types as obtained from the simulations in Chapter 6 are summarized in Table 7.1 and these values are graphically presented in Figure 7.8 at various specimen ages.

The diffusion coefficient values show a general trend of decrease in values at increasing ages. However, these values somewhat differ from one specimen type to another at any given age. The mixing parameters were controlled during the mixing phases for each of these mortar and concrete types in such a way that the mortar and concrete paste diffusion coefficient values should be representing identical microstructural phases and, therefore, should be numerically very similar to one another at any given age. For example, the diffusion coefficient value of 28-day mortar should be close (within the statistically permissible range) to the 28-day diffusion coefficient values of the paste regions of GNSS-A, LMST-E and LMST-C specimens and so on.

Table 7.1: Diffusion coefficients at different ages of mortar and concrete specimens at 25°C as obtained from the analytical simulation, and the average of four specimens.

Specimen Types	Diffusion Coefficient, D (m^2/s)		
	28-Day	56-Day	91-Day
Mortar	1.991×10^{-11}	8.750×10^{-12}	7.472×10^{-12}
GNSS-A (Paste Region)	1.500×10^{-11}	1.250×10^{-11}	5.222×10^{-12}
LMST-E (Paste Region)	1.972×10^{-11}	1.097×10^{-11}	5.000×10^{-12}
LMST-C (Paste Region)	1.806×10^{-11}	9.861×10^{-12}	3.889×10^{-12}
Average	1.817×10^{-11}	1.052×10^{-11}	5.396×10^{-12}

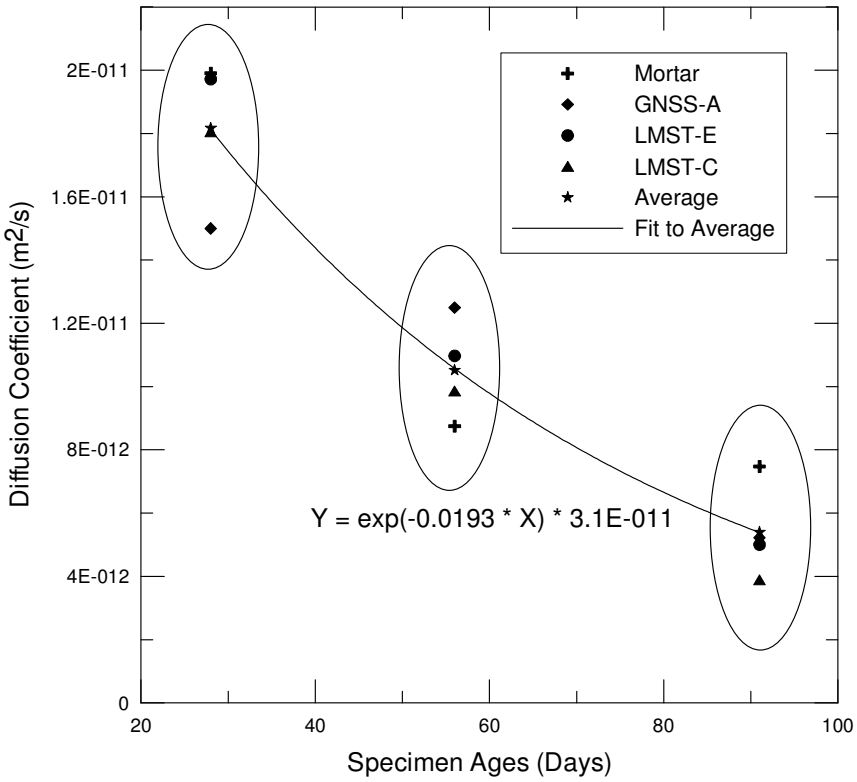

Figure 7.8: Mortar diffusion coefficient and concrete paste diffusion coefficient values at test ages of 28, 56 and 91 days.

Among the three concrete types (excluding the mortar), the only variable in each of the concrete types during the mixing was the coarse aggregate. However, the simulation results show that the paste diffusion coefficient values in these concretes somewhat vary at any given age. But the variations in the paste diffusivities in these concretes did not follow any specific trend. For example, for the 28-day specimens, GNSS-A had lower paste diffusion coefficient as compared to LMST-E and LMST-C whereas for the 56-day specimens, the paste diffusion coefficient of GNSS-A was higher than that of LMST-E and LMST-C (see Table 7.2). Therefore, the variations in the paste diffusion coefficient values cannot be attributed to the possible presence and/or variations in ITZ phases; instead, these variations might be the result of the variations during concrete mixing, curing, testing, profiling etc. In short, in spite of the fact that the mortar and paste diffusion coefficient values differ somewhat, they are generally in the same range with a reasonable data scatter.

In the second phase of simulations, individual α and β and D values of mortar and concrete specimens were averaged for each of the test ages and these averaged parameters were used in the paste of all three concrete types. The second phase of simulations on concretes (that used averaged values of the parameters) resulted in a good correlation with the experimental chloride profile data (see Section 6.5.3 and Appendix C). Therefore, it is safe at this point to conclude that at identical concrete ages, a single set of parameters (α, β and D) represents the paste properties of all three concrete types (GNSS-A, LMST-E and LMST-C) within a reasonable statistical variation.

7.2.2 Correlation between Paste RCPT and Paste Diffusion Coefficients

In this section, the paste RCPT values of each of the concrete types under investigation are determined and compared against the diffusion coefficient values from the analytical

simulation. The RCPT value (total charge passed in Coulombs) is the total charge passed through both the paste region and the aggregate particles. To estimate the charge passed through the aggregate particles, the regression (curve-fitted) lines in Figure 4.1 in Chapter 4 can be used at each specimen age. Using appropriate notations to the fitted regression lines in Figure 4.1, we get:

For 28-day specimens (all aggregate types): $Q = 225.8n + 1239$ …… (7.1)

For 56-day specimens (all aggregate types): $Q = 122.5n + 739$ ……...(7.2)

For 91-day specimens (all aggregate types): $Q = 126.5n + 456$ ……..…..(7.3)

where, Q is the total charge passed through the specimen during RCPT (in Coulombs) and *n* is the aggregate porosity (in percentage). The first term in the right hand side of each of the above relationships represents the contribution of the aggregate fraction towards the total RCPT value whereas the second term represents the contribution of the paste region. Hypothetically speaking, if an aggregate type with zero porosity is used in a concrete, then the first term on the right hand side of each of these equations vanishes, leaving behind only the second term (a numerical value), which is equal to the charge passed through the paste region during RCPT. Hence, the charge passed through the aggregate fraction is given as:

For the specimens subjected to 28-day RCPT: $Q_f = 225.8n$ ……..……(7.4)

For the specimens subjected to 56-day RCPT: $Q_f = 122.5n$ ……..(7.5)

And, for the specimens subjected to 91-day RCPT: $Q_f = 126.5n$ ……..(7.6)

where, Q_f is the total charge attributable to the aggregate fraction. The averaged experimental chloride profile data represent the average values of only the first and second batches of specimens for any given concrete type and age because specimens from the third batch were not used for chloride profiling (see Chapter 5). Therefore, the RCPT values of

only those two batches are used to determine the average value. The total average RCPT values from Batch-1 and Batch-2, charge attributable to the aggregate portions and the net charge passed through the paste regions are provided in Table 7.2.

Table 7.2: Computed paste RCPT values of GNSS-A, LMST-E and LMST-C concretes at 28, 56 and 91 days.

Specimen Types	Concrete Specimens	RCPT Values (Coulomb)		
		28-Day	56-Day	91-Day
GNSS-A (n = 0.81%)	GNSS-A-1	1550	1116	677
	GNSS-A-2	1341	872	691
	Average	1446	994	684
	Aggregate Contribution (Eq. 7.4)	183	99	102
	Paste Contribution	**1263**	**895**	**582**
LMST-E (n = 2.97%)	LMST-E-1	2096	1175	974
	LMST-E-2	1941	1174	827
	Average	2019	1175	901
	Aggregate Contribution (Eq. 7.5)	671	364	376
	Paste Contribution	**1348**	**811**	**525**
LMST-C (n = 5.81%)	LMST-C-1	2598	1668	1206
	LMST-C-2	2332	1163	1110
	Average	2465	1416	1158
	Aggregate Contribution (Eq. 7.6)	1312	712	735
	Paste Contribution	**1153**	**704**	**423**

A sketch showing the correlation between the paste RCPT value (bold-face values in Table 7.2) and the paste diffusion coefficient values of different concrete specimens as obtained from the simulation (Table 7.1) is provided in Figure 7.9.

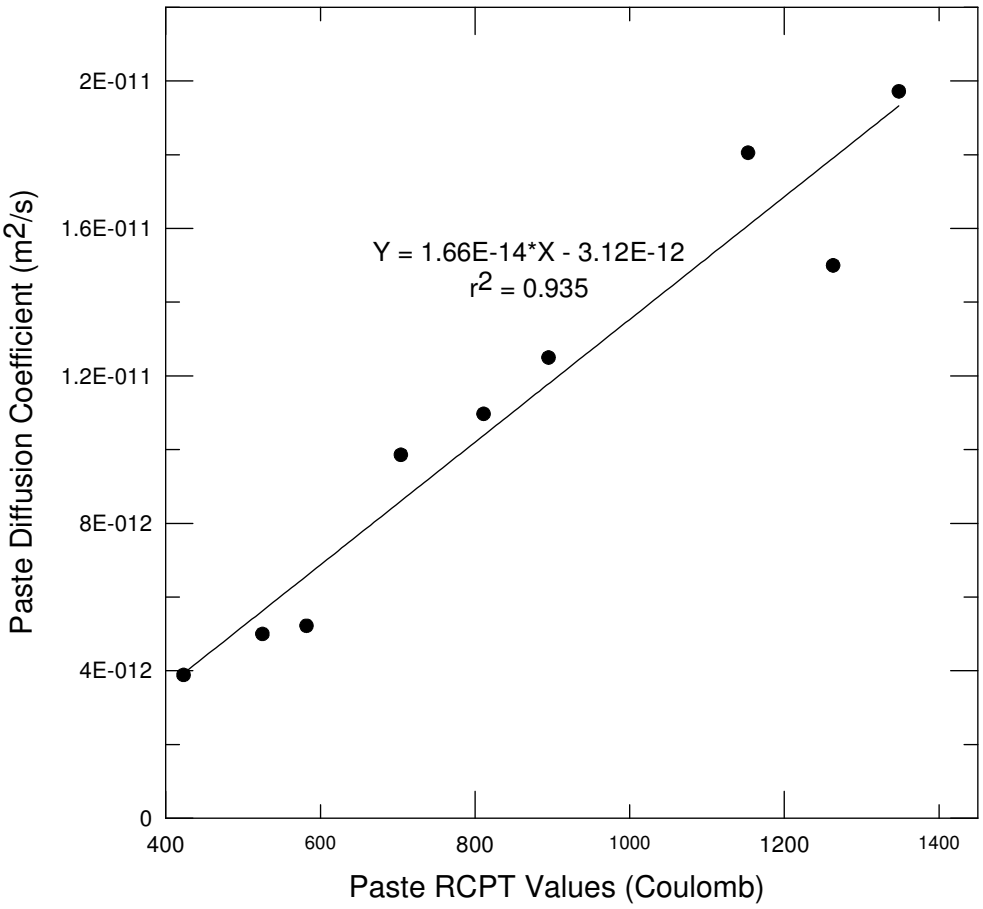

Figure 7.9: Correlation between the experimental paste RCPT values and the simulated paste diffusion coefficient values.

Figure 7.9 demonstrates that there is a good correlation between the experimental paste RCPT values and the simulated paste diffusion coefficient values. In retrospective, this figure demonstrates that the model developed in the present study (see Chapter 6) was able to predict the paste diffusion coefficient values in concretes reasonably well (correlation coefficient, $r^2 = 0.935$). In fact, only the 28-day paste diffusion coefficient value for GNSS-A concrete seems to be noticeably deviating from the linear regression line.

Even though the proposed model is able to predict the paste diffusion coefficients in concretes with a high level of accuracy, there are several parameters that this model has to deal with during the execution phase, namely, the chloride binding parameters and the diffusion coefficients of both aggregate and the paste phases. As a rule of thumb, if the simulation procedure is carried out with less number of unknown parameters, it becomes possible to significantly reduce the amount of time required to run the model on a trial and error basis and at the same time, get the results with high levels of accuracy. For example, if the aggregate diffusivity, the aggregate binding parameters and the chloride migration profile are experimentally known for a concrete specimen at a given age, we would be able to determine the paste diffusion coefficient and the paste binding parameters with higher accuracy and so on. In other words, the number of unknown parameters should be kept at a minimum to ensure accurate simulation results.

7.2.3 Correlation between Aggregate Porosity and Aggregate Diffusion Coefficient

Since the paste diffusion coefficients derived from the analytical simulations are found to have good correlation with the paste RCPT values, the diffusion coefficients for the aggregates as determined on a trial-and-error basis during the analytical simulation could also be considered reasonably accurate. The diffusion coefficient for the LMST-C is more than 3 times the diffusion coefficient for the LMST-E and more than 6 times the diffusion coefficient for the GNSS-A. However, we need to compare these diffusion coefficients with aggregate porosities to arrive at a more comprehensive conclusion. Table 7.3 provides both porosity and diffusion coefficients for all three aggregates under investigation.

Table 7.3: Porosity and diffusion coefficient values of GNSS-A, LMST-E and LMST-C aggregates.

Aggregate Types	Aggregate Porosity (%)	Diffusion Coefficient (m^2/s)
GNSS-A	0.81	5.556×10^{-12}
LMST-E	2.97	1.111×10^{-11}
LMST-C	5.81	3.611×10^{-11}

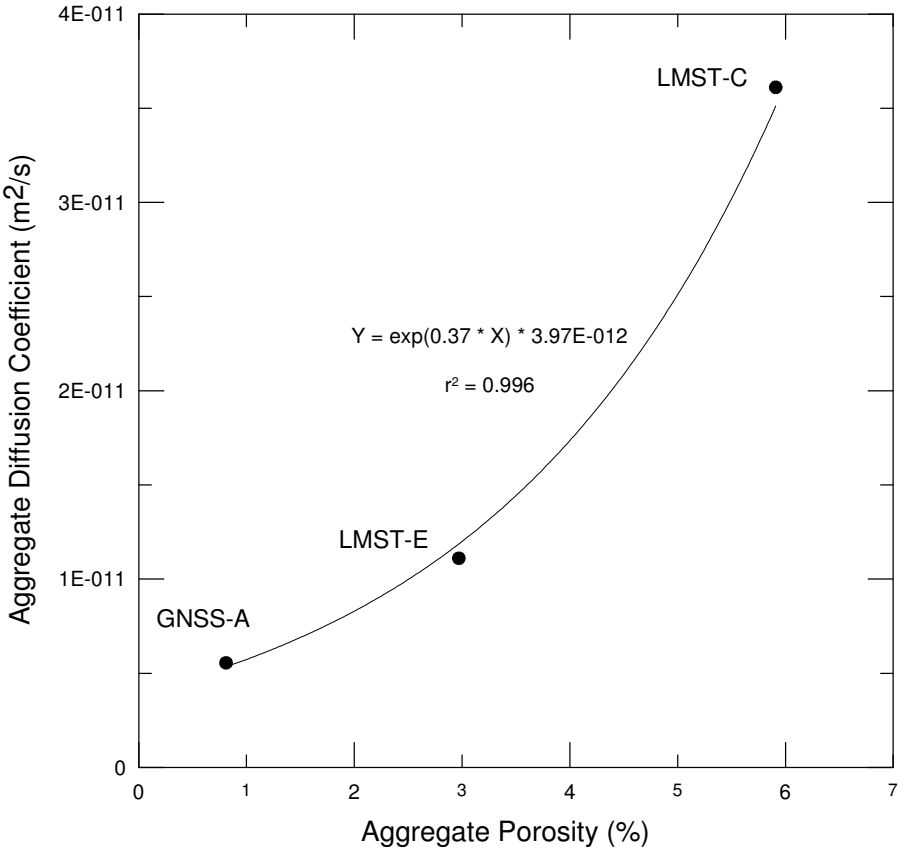

Figure 7.10: Correlation between aggregate porosity and diffusion coefficient values for GNSS-A, LMST-E and LMST-C Aggregates.

According to Figure 7.10, the aggregate diffusivity is not linearly dependent on the porosity. The regression curve shows that it is, in fact, exponentially dependent on porosity. This relationship should be regarded as a normal microstructural behavior because the higher porosity generally means less tortuosity and constrictivity, and a higher connectivity among the pores. However, it should be noted that the chloride diffusion coefficient does not become an infinite value at higher porosities. In fact, the chloride diffusion coefficient in an aqueous solution at infinite dilution is equal to 2.032×10^{-9} m^2/s at 25°C (Lide 2003). At higher ionic concentrations, this value will decrease due to ionic interaction (Buenfeld et al. 1998). Similarly, if the chloride binding is assumed to take place, then the effective chloride diffusion further decreases. Therefore, the estimation of diffusion coefficients at higher aggregate porosities based on the regression curve in Figure 7.10 should be made with caution.

7.2.4 Effect of Aggregate Porosity on the In-Paste Chloride Concentration

Chloride concentrations at pre-selected depths of concretes during short-term and long-term simulations demonstrate a strong correlation between aggregate porosity and chloride concentration at any given concrete depth (see Tables 6.20 and 6.21 in Chapter 6). Both in short-term and long-term simulations, higher aggregate porosities resulted in higher in-paste (and overall) chloride concentrations and lower aggregate porosities resulted in lower concentrations. However, higher in-paste chloride concentrations are attributable not only to higher porosities but also to higher diffusion coefficients (for those aggregates which have higher porosities). For example, simulation results gave us an aggregate diffusion coefficient of 5.556×10^{-12} m^2/s for GNSS-A, which has a porosity of 0.81%. On the other hand, for LMST-C, which has a porosity of 5.81%, simulation results gave an aggregate diffusion

coefficient of 3.611×10^{-11} m^2/s. Therefore, the overall effect of aggregate porosity on the chloride concentration (both in-paste and overall) is, in fact, the result of two parameters: aggregate porosity and aggregate diffusion coefficient.

8.0 CONCLUSIONS AND RECOMMENDATIONS

8.1 Conclusions

In the Mn/DOT project, twelve different concrete types were prepared from 12 different coarse aggregate types where each concrete type used a particular aggregate type (Titi et al. 2004). The RCPT results showed a strong correlation between aggregate porosity and RCPT values. Out of 12 aggregate types, three types that resulted in the lowest, mid-range and the highest aggregate porosities/RCPT results (namely, GNSS-A, LMST-E and LMST-C respectively) were selected for further study. Since coarse aggregates were the only variable in these concrete mixes, aggregate porosity and/or ITZ regions could be responsible for the correlation between aggregate porosity and RCPT values. However, observations of aggregate-paste interfaces under a scanning electron microscope (SEM) showed that the ITZ regions were either absent or, at least, so small as to be impossible to detect in the concretes prepared in the present study. Similarly, the Energy Dispersive X-Ray analysis (EDX analysis) confirmed that there was no such preferential pathway for chloride migration (ITZ region) at the aggregate-paste interface. Hence, the variations in the RCPT results could solely be attributed to the aggregate porosities. Another test where the representative aggregate particles from each aggregate type were immersed in the salt solution continuously for 90 days showed that the pores in aggregates allowed the chloride penetration into aggregate particles. The level of penetration depended more or less on individual aggregate porosity; in other words, more aggregate porosity led to more chloride penetration. In another test, a representative rock (LMST-W) was cut into a number of RCPT specimens and subjected to RCPT. Since there was a low level of charge passed through the specimens, this set of tests confirmed that there was a certain level of chloride migration in this rock during RCPT. This indicated that aggregates allow chloride migration with the level of

migration depending on the porosity of the individual aggregate types. Another important observation from this set of tests was that a moderate level of chloride binding was found to take place in this rock type during RCPT.

A two-phase (bulk paste region and aggregate fraction) analytical model was developed that was able to account for chloride diffusion, migration and binding in concrete. In the model, not only the smeared paste but also the aggregate fraction (which includes all aggregate particles) could be treated as a porous phase. In other words, separate porosity and diffusion coefficient values could be assigned to the bulk paste region and the aggregate fraction. Additionally, all the relevant findings from the experimentations were incorporated in the model. For example, because the ITZ regions were not detected in the representative concrete samples, the ITZ regions were not analytically treated as a separate phase; rather, both porosity and the diffusion coefficient values for ITZ were kept the same as that of the bulk paste. The general perception is that the aggregate particles do not allow chloride binding in them. But according to the chloride profiling on a limestone rock specimen (LMST-W) subjected to RCPT in the present study, a moderate level of chloride binding is possible, at least, in limestone aggregates. Therefore, the binding parameter values for aggregate phase were selected in such a way that those values represented a moderate level of binding in aggregate particles. It should be noted that the above model without ITZ is only applicable to high performance concretes. The presence of ITZ is a well-known fact in conventional (OPC) concretes. In addition to the above experimentations, a *paste-alone* mix was prepared that would be representative of the bulk paste regions of the concretes under investigation. Chloride profiling was done to representative mortar and concrete specimens subjected to 28-, 56- and 91-day RCPT.

The analytical simulation results indicated that the mortar microstructure did not perfectly represent the bulk paste regions of the concretes under investigation. Moreover, the paste regions of different concretes resulted in somewhat variable diffusion coefficients. However, a single set of averaged diffusion coefficient and binding parameter values resulted in the simulation results that were very close to the experimental chloride profile results. Similarly, there was a good correlation between the paste RCPT values and the simulated bulk paste diffusion coefficient values. This correlation demonstrated that the proposed analytical model was able to predict the paste diffusivity with reasonable accuracy. Similarly, aggregate diffusion coefficients of all three aggregate types were determined from the simulation process. Comparison of the aggregate diffusion coefficients with the aggregate porosities showed that the diffusion coefficient is very sensitive to porosity and diffusion coefficients increase significantly with an increase in porosity.

According to both short-term diffusion-migration (RCPT) and long-term diffusion simulations, the average in-paste chloride concentrations are higher than the overall average chloride concentrations for each concrete type. Moreover, both overall and in-paste concentrations increase sharply with an increase in aggregate porosity. In fact, these sharp increases in the chloride concentrations are not only attributable to higher aggregate porosities but also to higher aggregate diffusion coefficients, which increase significantly as a result of increases in aggregate porosities.

8.2 Recommendations For Future Studies

Based on the results of the present study, the following recommendations are made for future studies:

1. It is possible to estimate the binding pattern in a given concrete/mortar type if appropriate experimentations are carried out. For example, at a given age, representative concrete/mortar specimens can be subjected to different durations of RCPT (say, 2, 4, 6, 8 hours etc.). Once the chloride profiling is done in each of these specimens, the chloride binding parameters, α and β (which theoretically should be the same for all four RCPT durations), can be determined using the simulation techniques such as the one used in the present study. In this case, however, the so-called high performance concretes at later ages may not be suitable because there might not be enough chloride migration into the specimens at shorter duration tests such as 2-hour and 4-hour RCPT.
2. The author envisions the development of an analytical technique in the future that is able to determine the chloride diffusion coefficient values based on the extracted pore solution chemistry and the RCPT results. For this purpose, the concept of multi-species migration techniques such as the ones proposed by Truc (2000) and Tang and Truc (2000) can be used.
3. According to the chloride profiling on a limestone rock specimen subjected to RCPT in the present study, chloride binding is possible, at least, in limestone aggregates. Therefore, a study is needed to further evaluate the issue of chloride binding in aggregates.
4. Even though the effect of different proportions of air entrainment in the concrete/mortar was not analyzed in the present study, this issue might be an

interesting topic for a future study. In fact, the concrete/mortar mixes with, say, 3%, 6%, 9% etc. can be prepared and subjected, first, to RCPT, and then to chloride profiling. An analytical model similar to the one proposed in the present study can be developed that can predict the chloride diffusion coefficient values at much wider range of air-entrainment values, say, 0% to 15% etc.

REFERENCES

AASHTO T126 (2002). "Making and Curing Concrete Test Specimens in the Laboratory," *AASHTO Standard Specifications – Part II Tests*, American Association of States Highway and Transportation Officials, Washington, D. C.

AASHTO T259 (2002). "Resistance of Concrete to Chloride Ion Penetration," *AASHTO Standard Specifications – Part II Tests*, American Association of States Highway and Transportation Officials, Washington, D. C.

AASHTO T277 (2000). "Electrical Indication of Concrete's Ability to Resist Chloride Ion Penetration," *AASHTO Standard Specifications – Part II Tests*, American Association of States Highway and Transportation Officials, Washington, D. C.

Abou-Zeid, Mohamed Nagib, Meggers, David, and McCabe, Steven L., (2003). "Parameters Affecting Rapid Chloride Permeability Testing," *Concrete International*, November.

ACI 221R-96 (1997). "Guide for Use of Normal Weight and Heavyweight Aggregates in Concrete," *ACI Manual of Concrete Practice*, Part I: Materials and General Properties of Concrete, American Concrete Institute, Farmington Hills, MI.

ACI 222R-96 (1997). "Corrosion of Metals in Concrete," *ACI Manual of Concrete Practice*, Part I: Materials and General Properties of Concrete, American Concrete Institute, Farmington Hills, MI.

Alden, John (1998). "Computational Electrochemistry," *D. Phil. Thesis*, Physical and Theoretical Chemistry Laboratory, Oxford University, United Kingdom.

Alexander, M. D., Mindess, S., Diamond, S., and Qu, L. (1995). "Properties of Paste-Rock Interfaces and Their Influence on Composite Behavior," *Materials of Structures*, Vol. 28, pp. 497 – 506.

Andrade, C., (1993). "Calculation of Chloride Diffusion Coefficients in Concrete From Ionic Migration Measurements," *Cement and Concrete Research*, Vol. 23, No. 3, pp. 724 – 742.

Andrade, C., Sanjuan, M. A., Recuero, A., and Rio, O. (1994). "Calculation of Chloride Diffusivity in Concrete from Migration Experiments in Non-Steady State Conditions," *Cement and Concrete Research*, Vol. 24, No. 7, pp. 1214 – 1222.

ASTM C39 (1997). "Standard Test Method for Compressive Strength of Cylindrical Concrete Specimens," *Annual Book of ASTM Standards*, V 04.02, ASTM, Philadelphia.

ASTM C127 (1997). "Standard Test Method for Specific Gravity and Absorption of Coarse Aggregate," *Annual Book of ASTM Standards*, V 04.02, ASTM, Philadelphia.

ASTM C128 (1997). "Standard Test Method for Specific Gravity and Absorption of Fine Aggregate," *Annual Book of ASTM Standards*, V 04.02, ASTM, Philadelphia.

ASTM C136 (1997). "Standard Test Method for Sieve Analysis of Fine and Coarse Aggregates," *Annual Book of ASTM Standards*, V 04.02, ASTM, Philadelphia.

ASTM C143 (1997). "Standard Test Method Slump of Hudraulic-Cement Concrete," *Annual Book of ASTM Standards*, V 04.02, ASTM, Philadelphia.

ASTM C150 (1997). "Standard Specification for Portland Cement," *Annual Book of ASTM Standards*, V 04.01, ASTM, Philadelphia.

ASTM C231 (1997). "Standard Test Method for Air Content of Freshly Mixed Concrete by Pressure Method," *Annual Book of ASTM Standards*, V 04.02, ASTM, Philadelphia.

ASTM C618 (2003). "Standard Specification for Coal Fly Ash and Raw or Calcined Natural Pozzolan for Use in Concrete," *Annual Book of ASTM Standards*, V 04.01, ASTM, Philadelphia.

ASTM C1202 (1997). "Standard Test Method for Electrical Indication of Chloride's Ability to Resist Chloride," *Annual Book of ASTM Standards*, V 04.02, ASTM, Philadelphia, pp. 620-625.

ASTM C1556 (2003). "Standard Test Method for Determining the Apparent Chloride Diffusion Coefficient of Cementitious Mixtures by Bulk Diffusion," *Annual Book of ASTM Standards*, V 04.02, ASTM, Philadelphia, pp. 1 – 7.

Atkins, P. W. (1994). "Physical Chemistry," 5th Edition, Oxford University Press, Oxford, United Kingdom.

Atkinson, A. and Nickerson, A. K. (1984). "The Diffusion of Ions through Water-Saturated Cement," *Journal of Material Science*, London, Vol. 19, No. 9, pp. 3068 – 3078.

Attewell, P. B. and Farmer, I. W. (1976). "Principles of Engineering Geology," *First Edition*, Chapman and Hall, ISBN: 0470036419, pp. 1045.

Backstrom, G. (2004). "Field of Physics by Finite Element Analysis: Electricity, Magnetism and Heat in 2D and 3D Using FlexPDE Version 4," GB Publishing and Gunnar Backstrom, Malmo, Sweden.

Bentur, A., Goldman, A. and Cohen, M. D. (1988). "The Contributions of the Transition Zones to the Strength of High Quality Silica Fume Concretes," *Proceedings: Symposium on Bonding in Cementitious Composites*, Boston, Ed. S. Mindess and S. P. Shah, Vol. 114, Materials Research Society, Pittsburgh, pp. 97 – 103.

Benz, D. P. (2000). "Influence of Silica Fume on Diffusivity in Cement-Based Materials. II. Multi-Scale Modeling of Concrete Diffusivity," *Cement and Concrete Research*, Vol. 30, No. 7, pp. 1121 – 1129, July.

Bentz, D. P., Detwiler, R. J., Garboczi, E. J., Halamickova, P., and Schwartz, L. M. (1997). "Multi Scale Modeling of the Diffusivity of Mortar and Concrete," *Proceedings of Chloride Penetration into Concrete*, Ed. L. O. Nilsson and J. P. Ollivier, RILEM.

Bentz, D. P., Garboczi, E. J., and Lagergren, E. S. (1998). "Multi-Scale Microstructural Modeling of Concrete Diffusivity: Identification of Significant Variables," *Journal of Cement, Concrete Aggregates*, CCAGDP, Vol. 20, No. 1, pp. 129 – 139, June.

Buenfeld, N. R., Glass, G. K., Hassanein, A. M. and Zhang, J. (1998). "Chloride Transport in Concrete Subjected to Electric Field," *Journal of Materials in Civil Engineering*, Vol. 10, No. 4, pp. 220 – 228, Nov.

Cocke, D. L. and Mollah, M. Y. A. (1993). "The Chemistry and Leaching Mechanisms of Hazardous Substances in Cementitious Solidification/Stabilization Systems," *Chemistry and Microstructure of Solidified Waste Forms*, R. D. Spence, Ed., Lewis Publishers, Boca Raton, Florida, pp. 187 – 242.

Cohen, M. D., Olek, J., and Dolch, W. L. (1990). "Mechanism of Plastic Shrinkage Cracking in Portland Cement and Portland Cement-Silica Fume Paste and Mortar," *Cement and Concrete Research*, Vol. 20, No. 1, pp. 103 – 119.

Delagrave, A., Bigas, J. P., Olliver, J. P., Marchand, J., and Pigeon, M. (1997). "Influence of the Interfacial Zone on the Chloride Diffusivity of Mortars," *Advanced Cement Based Materials*, Vol. 5, No. 1, pp. 86 – 92.

Engineering Bulletin-1 (2002). "Force 10,000 Microsilica and Its Uses in Concrete," *Grace Construction Products*, W. R. Grace and Co., Cambridge, Massachusetts.

Garboczi, E. J. and Bentz, D. P. (1996a). "Modeling of the Microstructure and Transport Properties of Concrete," *Construction and Building Materials*, Vol. 10, No. 5, pp. 293 – 300.

Garboczi, E. J. and Bentz, D. P. (1996b). "Multiscale Analytical/Numerical Theory of the Diffusivity of Concrete," *Advanced Cement Based Materials*, Vol. 8, pp. 77 – 88.

Garboczi, E. J. and Bentz, D. P. (1999). "Computer Simulation and Percolation Theory Applied to Concrete," *Annual Reviews of Computational Physics*, VII, Edited by Dietrich Stauffer, World Scientific Publishing Company, pp. 85 – 123.

Germann Instruments, (2000). "RCT – Instruction and Maintenance Manual," *RCT-1029*, November, Evanston, Illinois.

Germann Instruments, (2003). "NDT Systems for Durability of New Structures, Service Life Estimation, Fast Track Construction, Structural Integrity, Repair Quality, and Monitoring," *Catalog NDT-2003*, Copenhagen, Denmark.

Halamickova, Pavla, Detwiler, Rachel J., Bentz, Dale P., Garboczi, Edward J., (1995). "Water Permeability and Chloride Ion Diffusion in Portland Cement Mortars: Relationship to Sand Content and Critical Pore Diameter," *Cement and Concrete Research*, Vol. 25, No. 4, pp. 790 – 802.

Hooton, R. D., Pun, P., Kojundic, T., and Fidjestol, P., (1997). "Influence of Silica Fume on Chloride Resistance of Concrete," *Presented at the PCI/FHWA International Symposium on HPC*, New Orleans, LA, Oct.

Hooton, R. D., Thomas, M. D. A., and Stanish, K. (2001). "Prediction of Chloride Penetration in Concrete," *Final Report*, Report No.: FHWA-RD-00-142, Grant No.: DTFH61-97-R-00022, Federal Highway Administration, McLean, Virginia, USA, Oct.

Hussain, S. E., Al-Gahtani, A. S., and Rasheeduzzafar, D. (1996). "Chloride Threshold for Corrosion of Reinforcement in Concrete," *ACI Materials Journal*, Vol. 94, No. 6, pp. 534 – 538.

Jackson, J. D. (1975). "Classical Electrodynamics," 2nd Edition, John Wiley and Sons, New York, USA.

Jaiswal, S. S., Picka, J. D., Igusa, T., Karr, A. F., Shah, S. P., Ankenman, B. E., and Styder, P. (1998). "Statistical Studies of the Conductivity of Concrete Using ASTM C1202 – 94," *Grants DMS – 9313013 and DMS – 9208758*, National Institute of Statistical Sciences.

Justnes, Dr. H. (1998). "A Review of Chloride Binding in Cementitious Systems," *Nordic Concrete Research (NCR)*, Publication No. 21, The Nordic Concrete Federation, Jan.

Lide, D. R. (2003). "Handbook of Chemistry and Physics," 84th Edition, 2003 – 2004, CRC Press LLC, Boca Raton, Florida.

Maruya, T., Hsu, K., Takeda, H. and Tangtermsirikul, S. (2003). "Numerical Modeling of Steel Corrosion in Concrete Structures due to Chloride Ion, Oxygen and Water Movement," *Journal of Advanced Concrete Technology*, Japan Concrete Institute, Vol. 1, No. 2, pp. 147 – 160, July.

Maso, J. C. (1980). "The Bond between Aggregates and Hydrated Cement Paste," *Proceedings, 7th International Congress on the Chemistry of Cement I*, VII-1/3, Paris.

McGrath, P. and Hooton, R. D. (1996). "Influence of Voltage on Chloride Diffusion Coefficients from Chloride Migration Tests," *Cement and Concrete Research*, Vol. 26, No. 8, pp. 1239 – 1244.

Midgley, H. G. and Illston, J. M. (1984). "The Penetration of Chlorides into Hardened Cement Pastes," *Cement and Concrete Research*, Vol. 15, pp. 546 – 558.

MoDOT (2003). "Laboratory Testing of Bridge Deck Mixes," *Research Development and Technology (RDT)*, Missouri Department of Transportation, Research Investigation 01-044, Research Report 03-004, April.

Monteiro, P. J. M. (2004). "Structure and Properties of Civil Engineering Materials" *Course ID: CE 60 (Undergraduate)*, Department of Civil and Environmental Engineering, University of California – Berkeley, California, USA.

Myers, J. J. (2001). "Permeability Performance of High Performance Concrete Subjected to Various Curing Regimes," *National Research Council, Journal of the Transportation Research Board*, Washington D. C., Accepted for Publication, Feb.

Nagele, E. (1985). "The Zeta-Potential of Cement," *Cement and Concrete Research*, Vol. 15, No. 3, pp. 453 – 462.

Nagele, E. (1986). "The Zeta-Potential of Cement, Part II" *Cement and Concrete Research*, Vol. 16, No. 6, pp. 853 – 863.

Nagele, E. (1987). "The Zeta-Potential of Cement, Part III" *Cement and Concrete Research*, Vol. 17, No. 4, pp. 573 – 580.

Nawy, Edward G. (1997). "Concrete Construction Engineering Handbook," ISBN: 0-8493-2664-4, CRC Press LLC, Boca Raton, Florida.

Neubauer, C. M., Bergstrom, T. B, Sujata, K., Xi, Y., Garboczi, E. J. and Jennings, H. M. (1997). "Drying Shrinkage of Cement Paste as Measured in an ESEM and Comparison with Microstructural Models," *Journal of Material Science*, Vol. 32, pp. 6415 – 6427.

Neuwald, Adam D. (2004). "Supplementary Cementitious Materials Part I: Pozzolanic SCMs," *MC Magazine*, The association of the Manufactured Concrete Products Industry, NPCA, Sept/Oct.

NT Build 492 (1999). "Concrete, Mortar and Cement-Based Repair Materials: Chloride Migration Coefficient from Non-Steady-State Migration Experiments," *Nordtest Method*, Published by NORDTEST, ISSN 0283-7153, FIN-02151, Espoo, Finland.

Oh, B. H., Jang, B. S. and Lee, S. C. (2004). "Chloride Diffusion and Corrosion Initiation Time of Reinforced Concrete Structures," *Proceedings of the International Workshop on Microstructure and Durability to Predict Service Life of Concrete Structures*, Sapporo, Japan, Feb.

Orlova, N. V., Westall, J. C., Rehani, M. and Koretsky, D. (1999). "The Study of Chloride Ion Migration in Reinforced Concrete under Cathodic Protection," *Final Report (SPR 357)*, Oregon Department of Transportation, Salem, Oregon, September.

Ozyildirim, Celik, (1998). "Fabricating and Testing Low-Permeability Concrete for Transportation Structures," *USDOT/Federal Highway Administration, Virginia*, Aug.

Page, C. L. and Vennesland, ϕ. (1983). "Pore Solution Composition and Chloride Binding Capacity of Silica-Fume Cement Pastes," *Materials and Structures*, Vol. 16, No. 91, pp. 19 – 25.

Petersen, C. G., (1991). "Rapid Chloride Test, The RCT-Method," *Concrete Repair Bulletin*, Sept/Oct.

Pfeiffer, D. W., McDonald, D. B., and Krauss, P. D., (1994). "The Rapid Chloride Permeability Test and Its Correlation to the 90-Day Chloride Ponding Test," *PCI Journal*, No. 1, January/February, pp. 38 – 47.

Poon, C. S, Lam, L. and Wong, Y. L. (1999). "Effects of Fly Ash and Silica Fume on Interfacial Porosity of Concrete," *Journal of Materials in Civil Engineering*, Vol. 11, No. 3, pp. 197 – 205, Aug.

Regourd, M. (1985). "Microstructure of High Strength Cement Systems," *Proceedings, Symposium on Very High-Strength Cement-Based Materials*, Ed. J. F. Young, Vol. 42, Materials Research Society, Pittsburgh, pp. 3 – 17.

Russell, Henry G., (2001). "Measuring Chloride Penetration Resistance," *Concrete Products*, Feb.

Samson, E., Marchand, J. and Beaudoin, J. J. (1999). "Describing Ion Diffusion Mechanisms in Cement-Based Materials Using the Homogenization Technique," *Cement and Concrete Research*, Vol. 29, pp. 1341 – 1345.

Samson, E., Marchand, J., and Snyder, K. A., (2003). "Calculation of ionic diffusion coefficients on the basis of migration test results," *Materials and Structures*, National Institute of Standards and Technology, Vol. 36, No. 257, pp. 156 – 165, April.

Sarkar, S. L., Diatta, Y. and Aitcin, P. C. (1988). "Micro-structural Study of Aggregate/Hydrated Paste Interface in Very High Strength River Gravel Concretes," *Proceedings, Symposium on Bonding in Cementitious Composites*, Boston, Ed. S. Mindess and S. P. Shah, Vol. 114, Materials Research Society, Pittsburgh, pp. 111 – 116.

SCA, (2002). "Reducing Permeability," *Slag Cement in Concrete*, Slag Cement Association, No. 6.

Schwartz, L. M., Garboczi, E. J., and Bentz, D. P. (1995). "Interfacial Transport in Porous Media: Application to DC Electrical Conductivity of Mortars," *Journal of Applied Physics*, Vol. 78, No. 10, November.

Scrivener, K. L. and Gartner, E. (1988). "Microstructural Gradients in Cement Paste around Aggregate Particles," *Materials Research Society Symposium Proceedings*, Vol. 114, pp. 77 –85.

Scrivener, K. L. and Nemati, K. M. (1996). "The Percolation of Pore Space in the Cement Paste/Aggregate Interfacial Zone of Concrete," *Cement and Concrete Research*, Vol. 26, No. 1, pp. 35 – 40.

Scrivener, K. L., Bentur, A. and Pratt, P. L. (1988). "Quantitative Characterization of the Transition Zone in High Strength Concretes," *Advances in Cement Research*, Vol. 1, No. 4, pp. 230 – 237.

Sellevolt, E. J. and Nilsen, T. (1987). "Condensed Silica Fume in Concrete: A World Review," *Supplementary Cementing Materials for Concrete*, Ed. V. M. Malhotra, CAN-MET, Ottawa, Canada, pp. 165 – 243.

Shane, J. D., Hwang, J-H., Sohn, D., Maon, T. O., Jennings, H. M., and Garboczi, E. J. (1997). "Recent Development in the Measurement of Transport Properties in Cement-Based Materials," *Mechanisms of Chemical Degradation of Cement-Based Systems*, Edited by K. L. Scrivener and J. F. Young, E and FN Spon, 2-6 Boundary Road, London.

Shane, J. D., Maosn, T. O., Jennings, H. M., Garboczi, E. D., and Bentz, D. P. (2000). "Effect of Interfacial Transition Zone on the Conductivity of Portland Cement Mortars," *Journal of American Ceramics Society*, Vol. 83, No. 5, pp. 1137 – 1144.

Shehata, M. H. and Thomas, M. D. A. (2000). "The Effects of Fly Ash Composition on the Expansion of Concrete due to Alkali-Silica reaction," *Cement and Concrete Research*, Vol. 30, pp. 1063 – 1072.

Shehata, M. H. and Thomas, M. D. A. (2002). "Use of Ternary Blends Containing Silica Fume and Fly Ash to Suppress Expansion due to Alkali-Silica Reaction in Concrete," *Cement and Concrete Research*, Vol. 32, No. 3, pp. 341 – 349, March.

Shi, Caijun, (2001). "Another Look at the Rapid Chloride Permeability Test (ASTM C1202 or AASHTO T277)," *CJS Technology Inc.*, Burlington, Ontario, Canada.

Snyder, K. A., Feng, X., Keen, B. D., and Mason, T. O. (2003). "Estimating the Electrical Conductivity of Cement Paste Pore Solutions from OH^-, K^+ and Na^+ Concentrations," *Cement and Concrete Research*, Vol. 33, No. 6, pp. 793 – 798, June.

Stanish, K. D. (2002). "The Migration of Chloride Ions in Concrete," *Ph. D. Thesis*, University of Toronto, Toronto, Canada.

Stanish, K. D., Hootan, R. D., and Thomas, M. D. A., (1997). "Testing the Chloride Penetration Resistance of Concrete: A Literature Review," *FHWA Contract DTFH61-97-R-00022 "Prediction of Chloride Penetration in Concrete"*

Stanish, K. D., Hootan, R. D., and Thomas, M. D. A., (2005). "The Rapid Migration Test for HPC," *HPC Bridge Views*, Issue No. 37, Jan/Feb.

Sujata, K., Xi, Y. and Jennings, H. M. (1996). "Interfacial Shrinkage Cracks and the Mechanisms," *Proceedings, Mat. Conf. in 1996 ASCE Convension*, ASCE, Reston, Virginia.

Takewaka, Koji, Yamaguchi, Toshinobu, and Maeda, Satoshi, (2003). "Simulation Model for Deterioration of Concrete Structures to Chloride Attack," *Journal of Advanced Concrete Technology*, Japan Concrete Institute, Vol. 1, No. 2, pp. 139 – 146, July.

Tang, L. (1996). "Chloride Transport in Concrete – Measurement and Prediction," *Ph. D. Thesis*, Department of Building Materials, Chalmers University of Technology, Goteborg, Sweden.

Tang, L. (1999). "Concentration Dependence of Diffusion and Migration of Chloride Ions – Part 1 & 2," *Cement and Concrete Research*, Vol. 29, pp. 1463 – 1474.

Tang, L. and Nilsson, L. O. (1992). "Rapid Determination of the Chloride Diffusivity in Concrete by Applying an Electrical Field," *ACI Materials Journal* 89, pp. 49 – 53.

Tang, L. and Nilsson, L. O. (1993). "Chloride Binding Capacity and Binding Isotherms of OPC Pastes and Mortars," *Cement and Concrete Research*, Vol. 23, pp. 247 – 253.

Tang L. and Nilsson, L. O. (1999). "Ionic Migration and Its Relation to Diffusion," *Presented at the International Conference on Mass and Ion Transport in Cement-Based Materials*, Toronto, Oct.

Tang, L. and Truc, O. (2000). "Effect of Exposure Solution on Chloride Penetration Test Methods," *Dept. of Building and Materials*, Chalmers University of Technology, Goteborg, Sweden.

Thoft-Christensen, P. (2002). "Stochastic Modeling of the Diffusion Coefficient for Concrete," *IFIP Working Conference*, Osaka, Japan, March.

Thomas, M. D. A. (1996). "Field Studies of Fly Ash Concrete Structures Containing Reactive Aggregates," *Magazine of Concrete Research*, Vol. 48, No. 177, pp. 265 – 279.

Thomas, M. D. A., Hopkins, D. S., Girn, G., Munro, R. and Muhl, E. (2003). "The Use of High Volume Fly Ash in Concrete," *Technical Report*, EcoSmart™ Concrete, Canada.

Thomas, M. D. A., Pantazopoulu, S. J., and Martin-Perez, B., (1995). "Service Life Modeling of Concretes Exposed to Chlorides – A Literature Review," *Prepared for the Ministry of Transportation*, Ontario, at the University of Ontario.

Titi, H. H., Tabatabai, H., Ghorbanpoor, A., Lamichhane, K., and Elias, M. (2004). "The Effect of Minnesota Aggregates on Rapid Chloride Permeability Tests," *Final Report*, Minnesota Department of Transportation, Research Services Section, St. Paul, Minnesota, Sep.

Truc, O. (2000). "Prediction of Chloride Penetration into Saturated Concrete – Multi-Species Approach," *Ph. D. Thesis*, Department of Building Materials, Chalmers University of Technology, Goteborg, Sweden.

Truc, O., Ollivier, J. P. and Nilsson, L. O. (2000). "Multi-Species Transport in Saturated Cement-Based Materials," Building Materials, Chalmers, Goteborg, Sweden.

Whiting, D. A., (1981). "Rapid Determination of the Chloride Permeability of Concrete," *Report No. FHWA/RD-81/119*, Federal Highway Administration, Washington, DC, August.

Winslow, D. N., Cohen, M. D., Bentz, D. P., Snyder, K. A., and Garboczi, A. J. (1994). "Percolation and Pore Structure in Mortars and Concrete," *Cement and Concrete Research*, Vol. 24, No. 1, pp. 25 – 37.

Xi, Y. and Bazant, Z. P. (1999). "Modeling Chloride Penetration in Saturated Concrete," *Journal of Materials in Civil Engineering*, Vol. 11, No. 1, pp. 58 – 65, Feb.

Xu, A. and Chandra, S. (1994). "Calculation of Chloride Diffusion-Coefficients in Concrete from Ionic Migration Measurements – Discussion," *Cement and Concrete Research*, Vol. 24, No. 2, pp. 375 – 379.

Yaman, I. O., Hearn, N., Aktan, H. M. (2000). "Active and Non-Active Porosity in Concrete. Part I: Experimental Evidence," *Materials and Structures*, RILEM.

Zhang, J-Z. (1997). "Developments of Test Methods for Assessment of Chloride Diffusion Resistance of Surface Treatments of Concrete," *Ph. D. Thesis*, Imperial College, London.

Zheng, J. J. (2000). "Mesostructure of Concrete-Stereological Analysis and Some Mechanical Implications," Delft University, Delft, The Netherlands.

Zheng, J. J., Li, C. Q., and Zhao, L. Y. (2003). "Simulation of Two-Dimensional Aggregate Distribution with Wall Effect," *Journal of Materials Engineering in Civil Engineering*, Vol. 15, No. 5, October.

APPENDIX A: RCT and RCTW Methods

Rapid Chloride Test (RCT) and Rapid Water-Soluble Chloride Test (RCTW) Methods

Introduction

Rapid Chloride Test (RCT) is primarily designed for rapid in-situ measurement of chloride content of fine particles including concrete powder drilled from hardened concrete in the field. This test can be done on freshly mixed concrete as well. Application of RCT is not only limited to measuring chloride content at the concrete surface, but this test can be used to prepare a chloride content profile with respect to concrete depth as well. RCT results are not influenced by the types of binders in the concrete. The results have been found equally consistent whether portland cement, fly ash or slag are used. Germann Instruments developed this test method and patented it in 1987 (German Instruments 2000). With this test method, the acid soluble amount of chlorides is measured as the percent of total mass of concrete. RCT method is relatively simple, quick and easy to handle as compared to the traditional chloride test methods of such as potentiometric titration (Petersen 1991). Chloride ions are found to be present in the concrete in three different states: free chloride ions, chemically bound chloride ions, and physically bound chloride ions. RCT, being a test method that uses an acid as the chloride extraction liquid, is capable of extracting both free and bound chloride ions. Hence, this test method gives total chloride content in the tested sample.

Rapid Water-Soluble Chloride Test (RCTW) is another test method similar to RCT. The difference, however, lies in the sample preparation and the test results. Sample preparation for each of these test methods is explained in the following section. In general, RCT, as mentioned above, determines the acid-soluble chloride content (which is regarded as the total chloride content) where as RCTW determines only water-soluble chloride content (which is regarded as the free chloride content).

Description of the Test Methods

Sample preparation techniques for RCT and RCTW are slightly different from one another. They are explained in the following paragraphs.

> RCT: 1.5 g of powder sample is added into 10 ml of extraction liquid (10% acetic acid) in a vial, the vial is secured with a lid and then shaken vigorously for 5 minutes. The vial is ready for the testing.
>
> RCTW: 1.5 g of powder sample is added into 9 ml of extraction liquid (10% acetic acid) in a vial, the vial is secured with a lid and then shaken vigorously for 5 minutes. Once the shaking is complete, the solution in the vial is poured into another vial, which has 1 ml of buffer solution. A filter paper is used during this process to allow only the clear liquid to pass into the vial with buffer solution; the residue on the filter paper is discarded. The new vial is gently shaken to mix the extraction solution with the buffer solution. Now the solution in the vial is ready for the testing.

The reading can be taken immediately in which case the chloride extraction is estimated to be about 90% of the total chloride content in the sample. Alternatively, the vial is left overnight and the reading is taken the next day in which case the chloride extraction is regarded to be 100% of the chloride content in the sample. The reading is done with the help of an electrode connected to an electronic meter where the electrode is dipped into the solution in the vial and the response in the meter is read. The reading provided by the meter is in mV (mili-Volt) and it needs to be converted into chloride content value (chloride percent by weight of the sample) with the help of a calibration chart. Calibration chart is prepared right before the RCT or RCTW by recording the response of the electrode (in mV) to four chloride solutions of known concentrations (0.005%, 0.02%, 0.05%, and 0.5% by weight). A typical calibration chart is shown in Figure A.1.

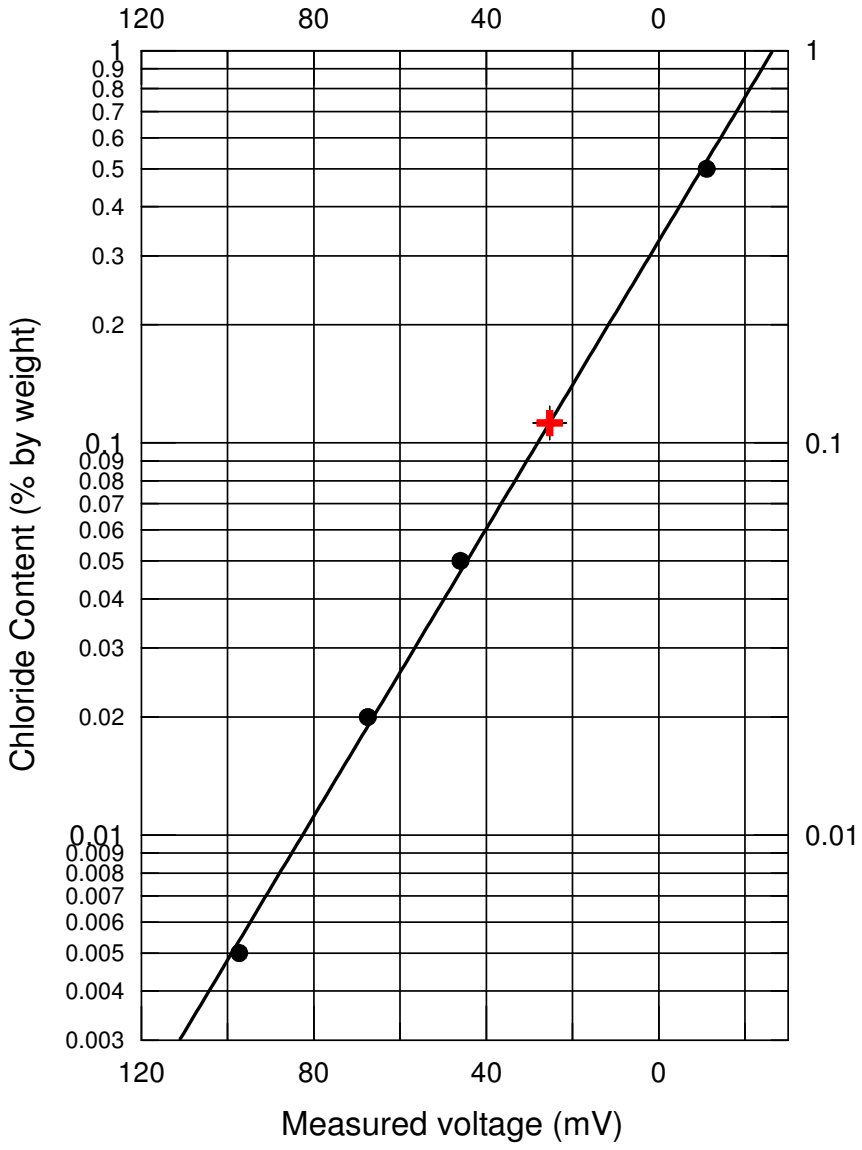

Figure A.1: A typical calibration chart showing a data point (marked +) on the chart.

Correlation Between RCT and Other Standard Test Methods

Ever since the development of RCT method some 15 years ago, numerous studies have been conducted to establish correlations between this test and other standard laboratory chloride extraction test methods such as AASHTO T260, ASTM C114-81 and some other European standards (Germann Instruments 2000). The correlation between RCT and various other test methods is illustrated in Figure A.2.

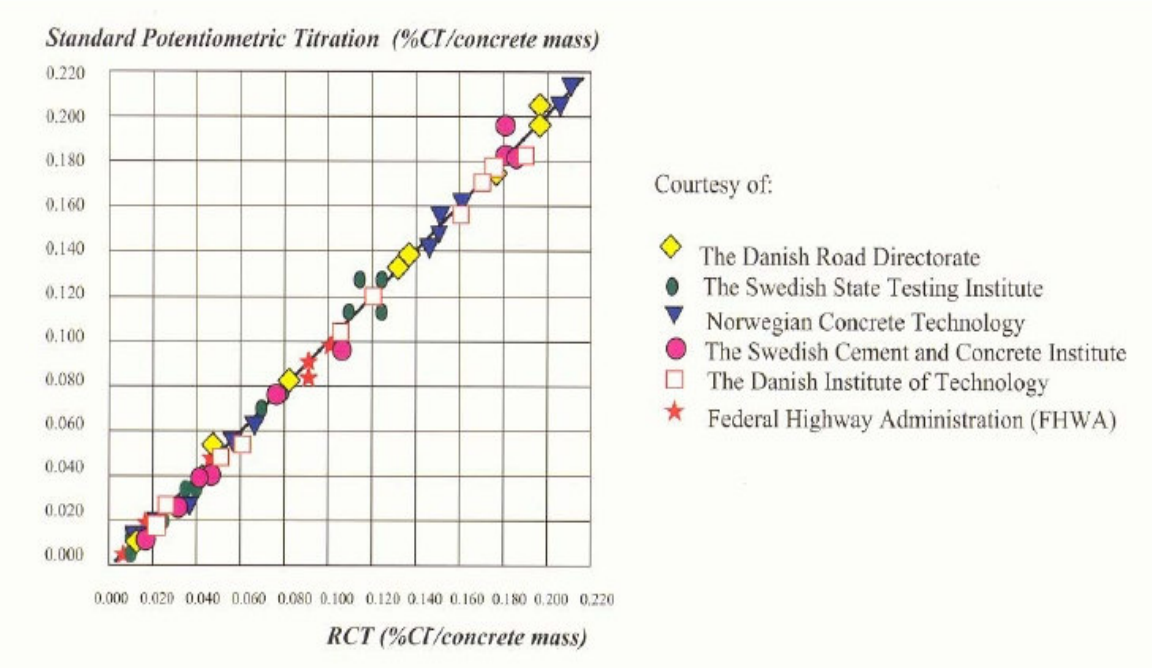

Figure A.2: Correlation between various chloride extraction test methods (Germann Instruments 2000).

In another study, three different types of cement with known chloride contents were subjected to RCT and AASHTO T260 separately (Germann Instruments 2003). Test results from both of these tests came very close to the known amount of chlorides in these cement types, and hence close to each other as well. The test result is summarized in Table A.1.

Table A.1: Comparison of test results by AASHTO T260 and RCT on the cements of known chloride contents (German Instruments 2003).

Cement Type	Known Chloride Amount (% Cl/mass)	AASHTO T260 (% Cl/mass)	RCT (12-Hr) (% Cl/mass)
Portland Cement (CEM I)	0.023	0.024	0.022
	0.071	0.070	0.072
	0.328	0.314	0.321
Flyash Cement (CEM II/B-V)	0.020	0.019	0.019
	0.057	0.052	0.061
	0.244	0.229	0.238
Slag Cement (CEM III/B)	0.020	0.019	0.019
	0.056	0.052	0.059
	0.244	0.231	0.238

APPENDIX B: A Simulation Example

The following algorithm is an actual program written for FlexPDE Version 4.2.11. Supplied numerical values of different parameters are for LMST-C specimen subjected to 28-day RCPT and this particular example uses aggregate distribution pattern-1. Typical graphical results from this simulation example immediately follow this algorithm.

(Note that an entire line of texts can be disabled by placing an exclamation mark (!) in front of the line, or an entire paragraph can be disabled by putting the paragraph within a pair of spiral brackets ({}).)

```
TITLE
'Chloride Migration in Concrete: 28-Day LMST-C Pattern-1'

SELECT
errlim = 0.01
smoothinit = ON
nodelimit = 4000

VARIABLES
f(threshold=0.01)       {Free Chloride}
b(threshold=0.01)       {Bound Chloride}
V                       {Voltage}

DEFINITIONS
C=0.91                  {N1: Surface Chloride Concentration divided by Porosity (% by
material weight)}
L=50                    {Sample thickness (mm)}
W=100           {Sample width (mm)}
V1=60 V2=0              {Voltages applied (V)}
n       porosity1=0.2           porosity2=0.0581        {Porosity (in fraction)}
alpha   alpha1=0.32             alpha2=0.1              {Initial Binding Rate Constant}
beta    beta1=0.65              beta2=1.0               {Binding Capacity Constant}
D       diffusion1=0.065        diffusion2=0.13         {Diffusion Coefficient (mm**2/hr)}
z=-1            Faraday=96485                   Gas_const=8.314
{Valence}       {F: Coulomb/mole}               {R: Joule/mole*Kelvin}
{Note: Volt=Joule/Coulomb}
temp=298                        u=(z*Faraday*D)/(Gas_const*temp)
{T: Kelvin, (25°C)}             {Mobility Factor: u=zFD/RT}
f1=n*f                  b1=n*b                          E=-grad(V)              test_time=6
{Aggregate distribution patterns. Note that {2} is a mirror distribution of {1} and {4} is a
mirror distribution of {3}. n1, n2 etc are x-coordinates; m1, m2 etc are y-coordinates; and
p1, p2 etc are particle radii.}
```

{1} n1=13 n2=36 n3=30 n4=8 n5=27 n6=42.5 n7=22.5 n8=37 n9=45 n10=26 n11=44 n12=6 n13=5 n14=20 n15=5 n16=45 n17=9 n18=27 n19=15 n20=7.5 n21=43
{2} {n1=37 n2=14 n3=20 n4=42 n5=23 n6=7.5 n7=27.5 n8=13 n9=5 n10=24 n11=6 n12=44 n13=45 n14=30 n15=45 n16=5 n17=41 n18=23 n19=35 n20=42.5 n21=7}
{3} {n1=23 n2=28 n3=6 n4=28 n5=7 n6=41.5 n7=11.5 n8=44 n9=39 n10=10 n11=42 n12=28 n13=44 n14=11 n15=29 n16=39 n17=25 n18=7 n19=19 n20=26.5 n21=41}
{4} {n1=27 n2=22 n3=44 n4=22 n5=43 n6=8.5 n7=38.5 n8=6 n9=11 n10=40 n11=8 n12=22 n13=6 n14=39 n15=21 n16=11 n17=25 n18=43 n19=31 n20=23.5 n21=9}
m1=18 m2=81 m3=6 m4=47 m5=62 m6=65 m7=94 m8=19 m9=32 m10=45 m11=47.5 m12=60 m13=82 m14=79 m15=5 m16=7.5 m17=33 m18=29 m19=68 m20=94.5 m21=95
p1=7.6 p2=8.15 p3=4.95 p4=5.2 p5=5.1 p6=4.8 p7=4.85 p8=4.3 p9=3.65 p10=7.25 p11=3.55 p12=4.1 p13=4.05 p14=3.45 p15=3.15 p16=2.95 p17=3.3 p18=4.35 p19=2.85 p20=3.1 p21=2.8 s=0.1 {ITZ thickness}

INITIAL VALUES
f=0
b=0
V=0

EQUATIONS
f: dt(f1)=div(D*grad(f1))+div(u*f1*E)-dt(b1)
b: dt(b1)=alpha*erfc(beta*b)*f1
V: div(n*D*E)=0

BOUNDARIES
region 'Bulk Paste' n=porosity1 D=diffusion1 alpha=alpha1 beta=beta1 start(0,0)
natural(f)=0 natural(b)=0 natural(V)=0 line to (L,0) value(f)=0 value(V)=V2 line to (L,W)
natural(f)=0 natural(V)=0 line to (0,W) value(f)=C value(V)=V1 line to finish
{ITZ region is disabled here by putting within spiral brackets}
{region 'ITZ' n=porosity1 D=diffusion1 alpha=alpha1 beta=beta1
start (n1+p1+s,m1) arc(center = n1,m1) angle = 360 finish start (n2+p2+s,m2) arc(center = n2,m2) angle = 360 finish
start (n3+p3+s,m3) arc(center = n3,m3) angle = 360 finish start (n4+p4+s,m4) arc(center = n4,m4) angle = 360 finish
start (n5+p5+s,m5) arc(center = n5,m5) angle = 360 finish start (n6+p6+s,m6) arc(center = n6,m6) angle = 360 finish
start (n7+p7+s,m7) arc(center = n7,m7) angle = 360 finish start (n8+p8+s,m8) arc(center = n8,m8) angle = 360 finish
start (n9+p9+s,m9) arc(center = n9,m9) angle = 360 finish start (n10+p10+s,m10) arc(center = n10,m10) angle = 360 finish
start (n11+p11+s,m11) arc(center = n11,m11) angle = 360 finish start (n12+p12+s,m12) arc(center = n12,m12) angle = 360 finish
start (n13+p13+s,m13) arc(center = n13,m13) angle = 360 finish start (n14+p14+s,m14) arc(center = n14,m14) angle = 360 finish
start (n15+p15+s,m15) arc(center = n15,m15) angle = 360 finish start (n16+p16+s,m16) arc(center = n16,m16) angle = 360 finish
start (n17+p17+s,m17) arc(center = n17,m17) angle = 360 finish start (n18+p18+s,m18) arc(center = n18,m18) angle = 360 finish

```
start (n19+p19+s,m19) arc(center = n19,m19) angle = 360 finish start (n20+p20+s,m20)
arc(center = n20,m20) angle = 360 finish
start (n21+p21+s,m21) arc(center = n21,m21) angle = 360 finish}

region 'Aggregate' n=porosity2 D=diffusion2 alpha=alpha2 beta=beta2
start(n1+p1,m1) arc(center = n1,m1) angle = 360 finish
start(n2+p2,m2) arc(center = n2,m2) angle = 360 finish
start(n3+p3,m3) arc(center = n3,m3) angle = 360 finish
start(n4+p4,m4) arc(center = n4,m4) angle = 360 finish
start(n5+p5,m5) arc(center = n5,m5) angle = 360 finish
start(n6+p6,m6) arc(center = n6,m6) angle = 360 finish
start(n7+p7,m7) arc(center = n7,m7) angle = 360 finish
start(n8+p8,m8) arc(center = n8,m8) angle = 360 finish
start(n9+p9,m9) arc(center = n9,m9) angle = 360 finish
start(n10+p10,m10) arc(center = n10,m10) angle = 360 finish
start(n11+p11,m11) arc(center = n11,m11) angle = 360 finish
start(n12+p12,m12) arc(center = n12,m12) angle = 360 finish
start(n13+p13,m13) arc(center = n13,m13) angle = 360 finish
start(n14+p14,m14) arc(center = n14,m14) angle = 360 finish
start(n15+p15,m15) arc(center = n15,m15) angle = 360 finish
start(n16+p16,m16) arc(center = n16,m16) angle = 360 finish
start(n17+p17,m17) arc(center = n17,m17) angle = 360 finish
start(n18+p18,m18) arc(center = n18,m18) angle = 360 finish
start(n19+p19,m19) arc(center = n19,m19) angle = 360 finish
start(n20+p20,m20) arc(center = n20,m20) angle = 360 finish
start(n21+p21,m21) arc(center = n21,m21) angle = 360 finish

FEATURE
start '3mm' (3,0) line to (3,W)
start '5mm' (5,0) line to (5,W)
start '7.5mm' (7.5,0) line to (7.5,W)
start '10.5mm' (10.5,0) line to (10.5,W)
start '14mm' (14,0) line to (14,W)
start '18mm' (18,0) line to (18,W)
start '22mm' (22,0) line to (22,W)

TIME
0 to test_time by 0.01

PLOTS
for t = 1e-5 1e-4 1e-3 1e-2 0.05 by 0.05 to 0.2 by 0.1 to endtime
grid(x,y) as "Meshing"
contour(f1+b1) as "Total Chloride Concentration" painted
elevation(f1) from (0,W/2) to (L,W/2) as "Free Chloride Concentration"
elevation(b1) from (0,W/2) to (L,W/2) as "Bound Chloride Concentration"
elevation(f1+b1) from (0,W/2) to (L,W/2) as "Total Chloride Concentration"
elevation(V) from (0,W/2) to (L,W/2) as "Voltage"
elevation(f1+b1) on '3mm' as "Chloride concentration at 3 mm depth" range = (0,1)
```

```
elevation(f1+b1) on '5mm' as "Chloride concentration at 5 mm depth" range = (0,1)
elevation(f1+b1) on '7.5mm' as "Chloride concentration at 7.5 mm depth" range = (0,1)
elevation(f1+b1) on '10.5mm' as "Chloride concentration at 10.5 mm depth" range = (0,1)
elevation(f1+b1) on '14mm' as "Chloride concentration at 14 mm depth" range = (0,1)
elevation(f1+b1) on '18mm' as "Chloride concentration at 18 mm depth" range = (0,1)
elevation(f1+b1) on '22mm' as "Chloride concentration at 22 mm depth" range = (0,1)

SUMMARY ('Simulation Report')
report('Input Parameters:')
report(z) as "z" report(Faraday) as "F"
report(gas_const) as "R"
report(temp) as "T"
report(porosity1) as "Bulk Paste: n"
report(porosity2) as "Aggregate: n"
report('----------------------------------------------------------------')
report('Boundary Values:')
report(C) as "N1"
report(V1) as "V1"
report(V2) as "V2"
report('----------------------------------------------------------------')
report('Time Step:')
report(test_time) as "t"
report('----------------------------------------------------------------')
report('Total Chloride Concentration (% by weight):')
report((1/W)*line_integral(f1+b1,'3mm')) as "3.0 mm "
report((1/W)*line_integral(f1+b1,'5mm')) as "5.0 mm "
report((1/W)*line_integral(f1+b1,'7.5mm')) as "7.5 mm "
report((1/W)*line_integral(f1+b1,'10.5mm')) as "10.5 mm "
report((1/W)*line_integral(f1+b1,'14mm')) as "14.0 mm "
report((1/W)*line_integral(f1+b1,'18mm')) as "18.0 mm "
report((1/W)*line_integral(f1+b1,'22mm')) as "22.0 mm "
report('----------------------------------------------------------------')
report('Bulk Paste:')
report(alpha1) as "Alpha "
report(beta1) as "Beta"
report(2.7778e-10*diffusion1) as "D (m2/s) "
report(' ')
report('Aggregate:')
report(alpha2) as "Alpha "
report(beta2) as "Beta"
report(2.7778e-10*Diffusion2) as "D (m2/s) "

END
```

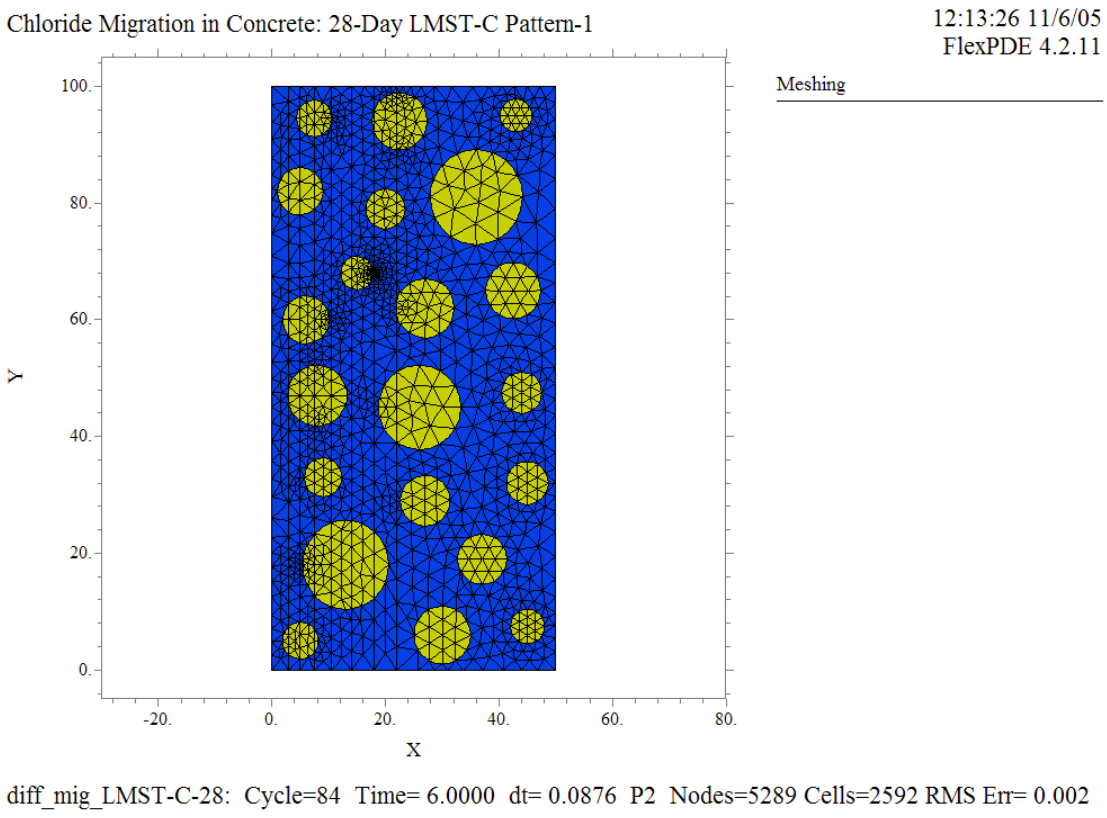

Figure B.1: A typical meshing pattern generated by the software.

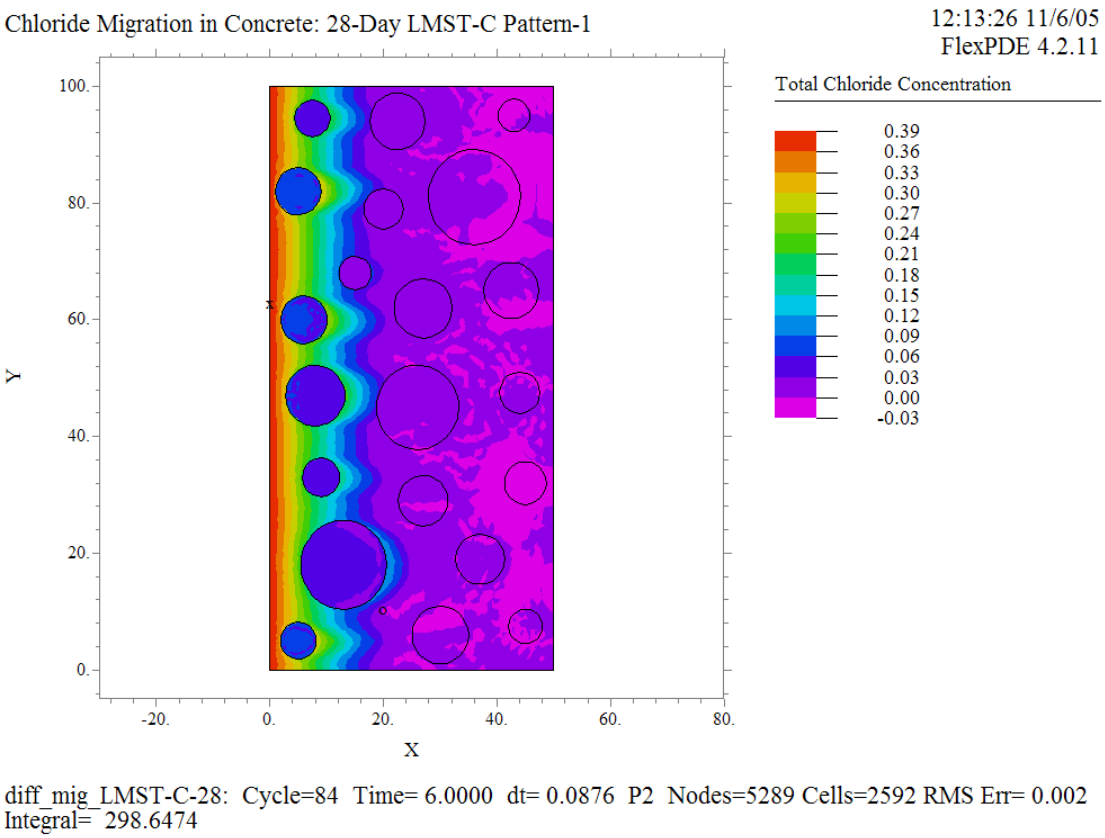

Figure B.2: Final chloride migration profile from the RCPT simulation.

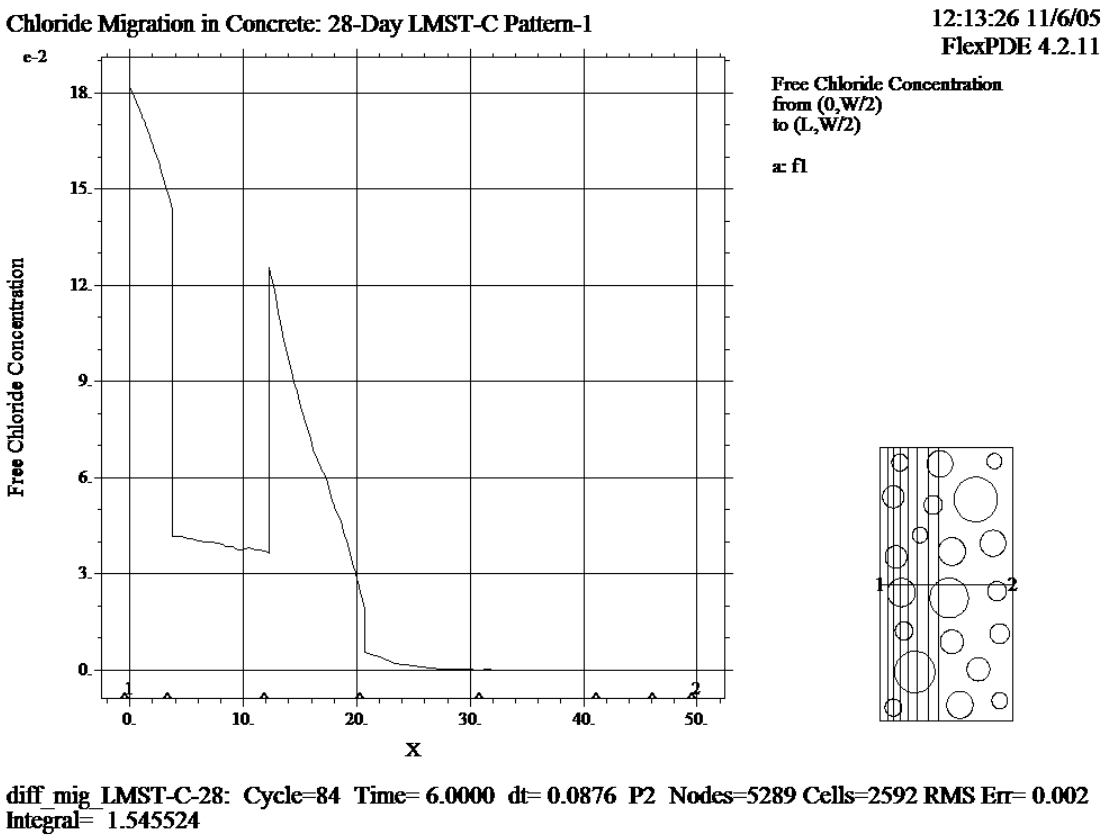

Figure B.3: Free chloride concentration profile from the RCPT simulation along the path indicated by 1-2.

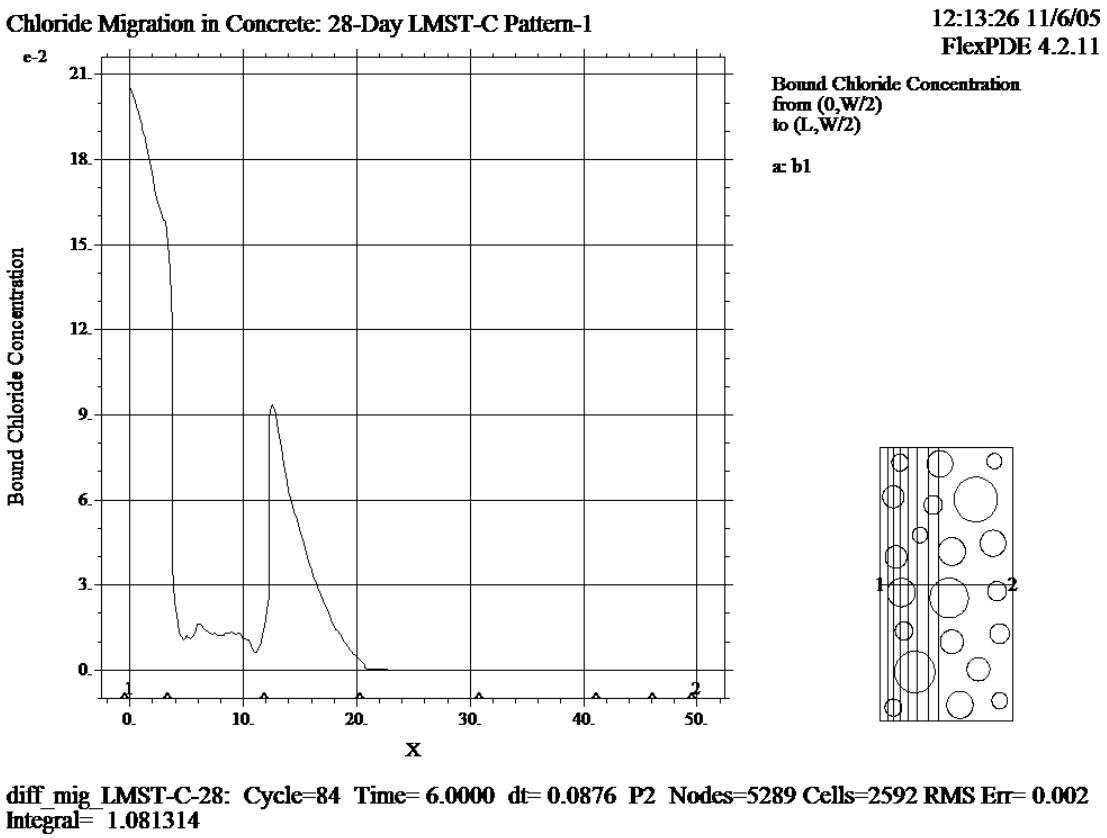

Figure B.4: Bound chloride concentration profile from the RCPT simulation along the path indicated by 1-2.

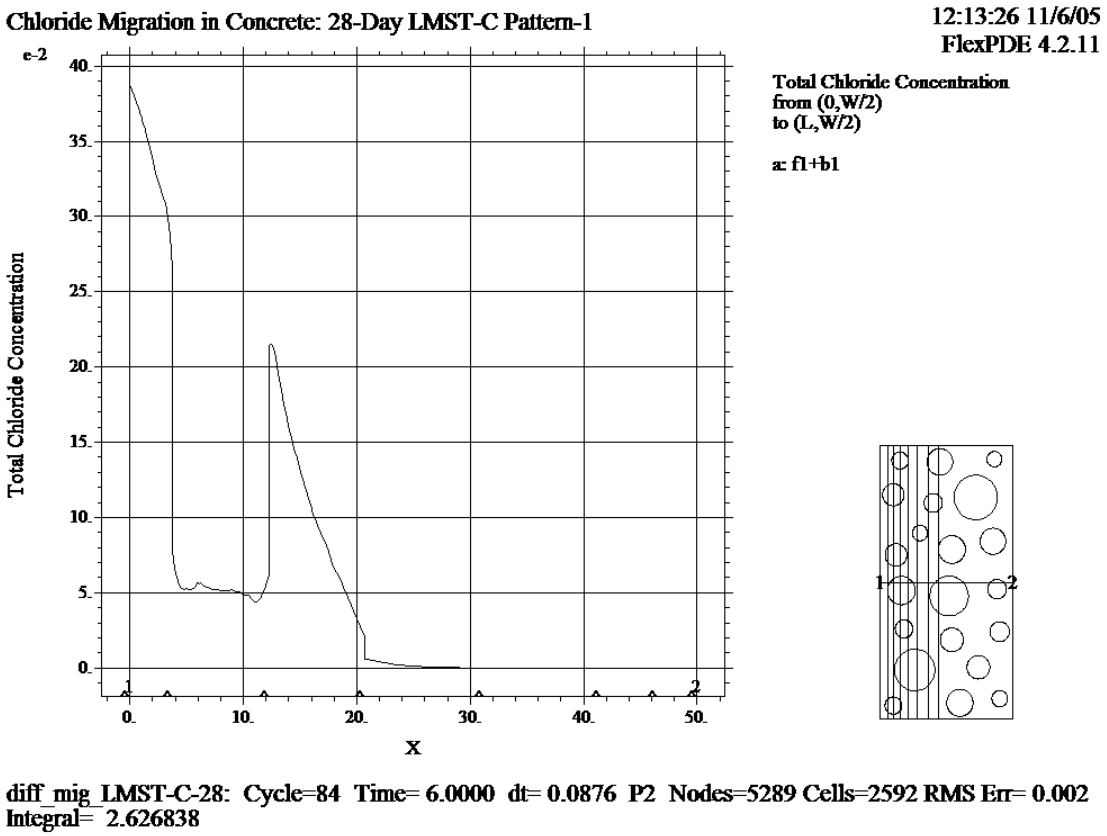

Figure B.5: Total chloride concentration profile from the RCPT simulation along the path indicated by 1-2.

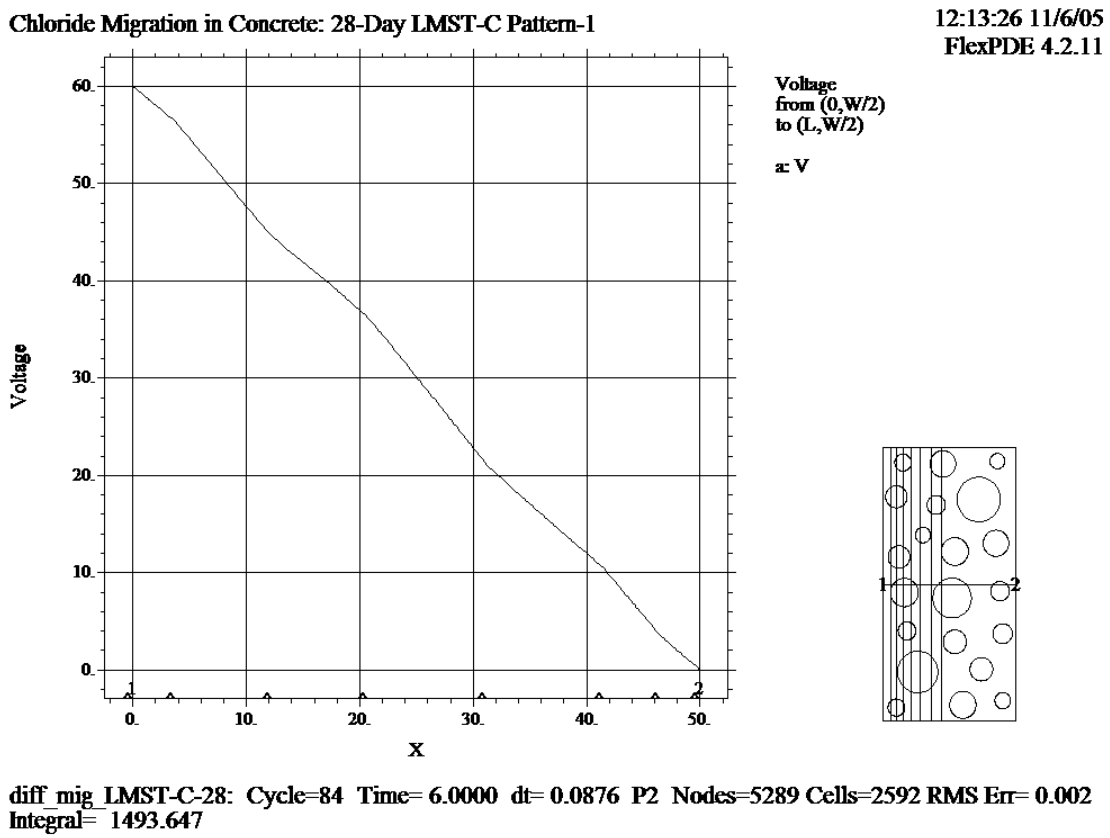

Figure B.6: Applied voltage during the RCPT simulation along the path indicated by 1-2 (note that the voltage is influenced by the local variations in porosity and diffusivity).

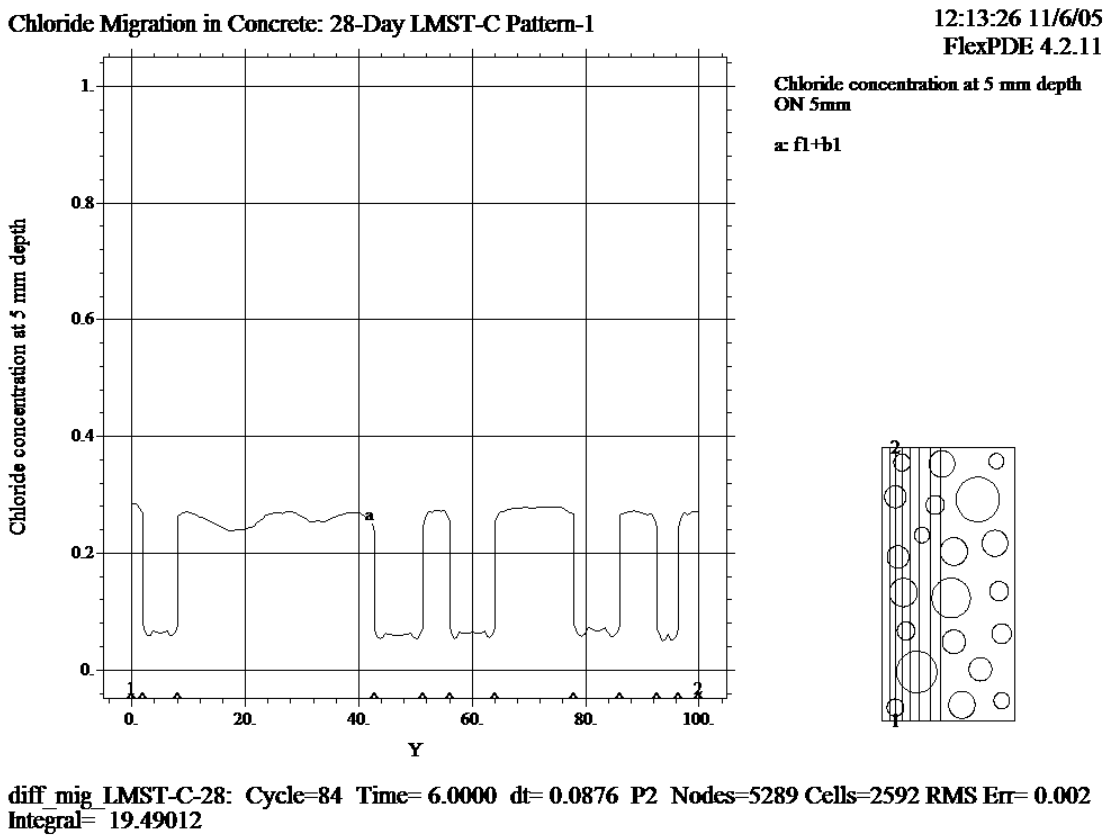

Figure B.7: A typical total chloride concentration profile from the simulation at 5-mm depth of specimen cross-section (along the path indicated by 1-2).

Chloride Migration in Concrete: 28-Day LMST-C Pattern-1 12:13:26 11/6/05
FlexPDE 4.2.11

Simulation Report

Input Parameters:
z= -1.000000
F= 96485.00
R= 8.314000
T= 298.0000
Bulk Paste: n= 0.200000
Aggregate: n= 0.058100

Boundary Values:
N1= 0.910000
V1= 60.00000
V2= 0.00

Time Step:
t= 6.000000

Total Chloride Concentration (% by weight):
3.0 mm= 0.267187
5.0 mm= 0.194853
7.5 mm= 0.131297
10.5 mm= 0.128429
14.0 mm= 0.087451
18.0 mm= 0.035730
22.0 mm= 0.010099

Bulk Paste:
Alpha= 0.320000
Beta= 0.650000
D (m2/s)= 1.805570e-11

Aggregate:
Alpha= 0.100000
Beta= 1.000000
D (m2/s)= 3.611140e-11

diff_mig_LMST-C-28: Cycle=84 Time= 6.0000 dt= 0.0876 P2 Nodes=5289 Cells=2592 RMS Err= 0.002

Figure B.8: A typical simulation report at the end of the RCPT simulation.

APPENDIX C: Individual Simulation Results Using Average α, β and D

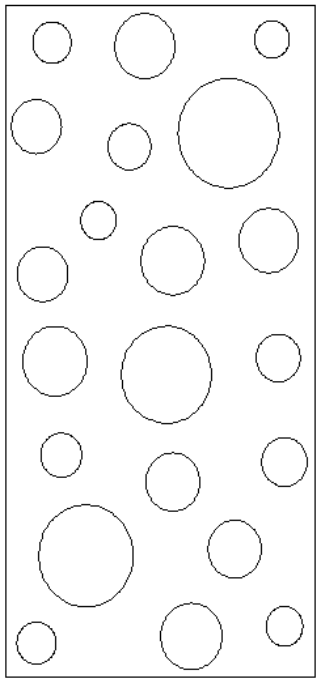

Aggregate Distribution Pattern-1

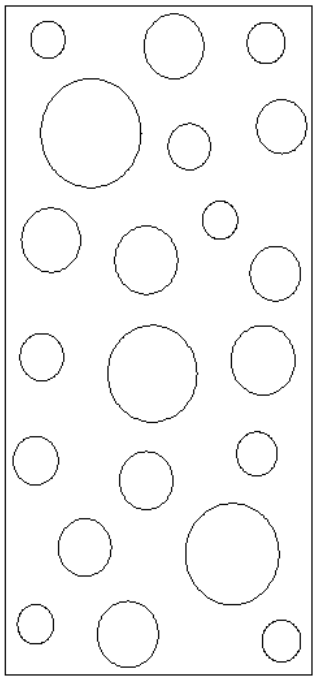

Aggregate Distribution Pattern-2

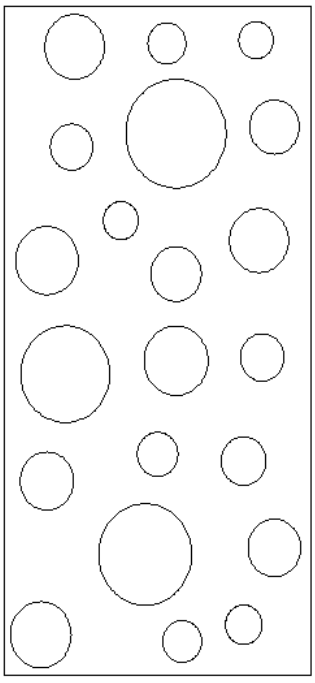

Aggregate Distribution Pattern-3

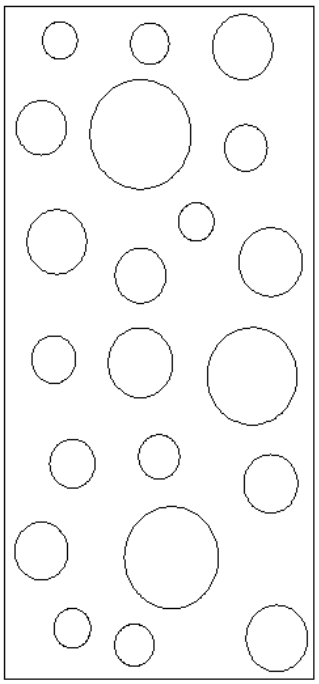

Aggregate Distribution Pattern-4

Figure C.1: Aggregate distribution patterns.

Table C.1: Simulation and Experimental Results on 28-Day GNSS-A

Depth (mm)	Total Chloride Concentration (% by Weight)						Correlation Coefficient (r^2)
	Simulation					Experiment	
	Aggregate Distribution Pattern				Average		
	1	2	3	4			
3.0	0.234	0.243	0.229	0.262	0.242	0.202	0.995
5.0	0.142	0.151	0.150	0.169	0.153	0.117	
7.5	0.088	0.093	0.085	0.084	0.088	0.076	
10.5	0.055	0.045	0.057	0.037	0.049	0.022	
14.0	0.012	0.009	0.019	0.008	0.012	0.000	
18.0	0.001	0.001	0.002	0.001	0.000	0.000	
22.0	0.000	0.000	0.000	0.000	0.000	0.000	

Table C.2: Simulation and Experimental Results on 56-Day GNSS-A

Depth (mm)	Total Chloride Concentration (% by Weight)						Correlation Coefficient (r^2)
	Simulation					Experiment	
	Aggregate Distribution Pattern				Average		
	1	2	3	4			
3.0	0.172	0.181	0.173	0.194	0.180	0.219	1.0
5.0	0.080	0.086	0.087	0.090	0.086	0.110	
7.5	0.032	0.028	0.031	0.018	0.027	0.030	
10.5	0.005	0.003	0.008	0.001	0.004	0.005	
14.0	0.000	0.000	0.000	0.000	0.000	0.000	
18.0	0.000	0.000	0.000	0.000	0.000	0.000	
22.0	0.000	0.000	0.000	0.000	0.000	0.000	

Table C.3: Simulation and Experimental Results on 91-Day GNSS-A

Depth (mm)	Total Chloride Concentration (% by Weight)						Correlation Coefficient (r^2)
	Simulation					Experiment	
	Aggregate Distribution Pattern				Average		
	1	2	3	4			
3.0	0.086	0.096	0.098	0.096	0.094	0.076	1.0
5.0	0.011	0.011	0.013	0.007	0.011	0.008	
7.5	0.001	0.000	0.001	0.000	0.001	0.000	
10.5	0.000	0.000	0.000	0.000	0.000	0.000	
14.0	0.000	0.000	0.000	0.000	0.000	0.000	
18.0	0.000	0.000	0.000	0.000	0.000	0.000	
22.0	0.000	0.000	0.000	0.000	0.000	0.000	

Table C.4: Simulation and Experimental Results on 28-Day LMST-E

Depth (mm)	Total Chloride Concentration (% by Weight)						Correlation Coefficient (r^2)
	Simulation					Experiment	
	Aggregate Distribution Pattern				Average		
	1	2	3	4			
3.0	0.251	0.260	0.248	0.261	0.255	0.263	0.999
5.0	0.164	0.172	0.169	0.186	0.173	0.179	
7.5	0.102	0.110	0.101	0.103	0.104	0.112	
10.5	0.066	0.056	0.066	0.059	0.062	0.056	
14.0	0.016	0.012	0.023	0.012	0.016	0.010	
18.0	0.001	0.001	0.002	0.000	0.001	0.000	
22.0	0.000	0.000	0.000	0.000	0.000	0.000	

Table C.5: Simulation and Experimental Results on 56-Day LMST-E

Depth (mm)	Total Chloride Concentration (% by Weight)						Correlation Coefficient (r^2)
	Simulation					Experiment	
	Aggregate Distribution Pattern				Average		
	1	2	3	4			
3.0	0.199	0.206	0.198	0.208	0.203	0.136	0.935
5.0	0.106	0.113	0.112	0.121	0.113	0.119	
7.5	0.045	0.042	0.043	0.038	0.042	0.074	
10.5	0.008	0.005	0.012	0.006	0.008	0.026	
14.0	0.000	0.000	0.000	0.000	0.000	0.000	
18.0	0.000	0.000	0.000	0.000	0.000	0.000	
22.0	0.000	0.000	0.000	0.000	0.000	0.000	

Table C.6: Simulation and Experimental Results on 91-Day LMST-E

Depth (mm)	Total Chloride Concentration (% by Weight)						Correlation Coefficient (r^2)
	Simulation					Experiment	
	Aggregate Distribution Pattern				Average		
	1	2	3	4			
3.0	0.135	0.143	0.140	0.146	0.141	0.132	0.992
5.0	0.023	0.025	0.026	0.024	0.025	0.039	
7.5	0.002	0.002	0.003	0.002	0.002	0.001	
10.5	0.000	0.000	0.001	0.001	0.001	0.000	
14.0	0.000	0.000	0.000	0.000	0.000	0.000	
18.0	0.000	0.000	0.000	0.000	0.000	0.000	
22.0	0.000	0.000	0.000	0.000	0.000	0.000	

Table C.7: Simulation and Experimental Results on 28-Day LMST-C

Depth (mm)	Total Chloride Concentration (% by Weight)						Correlation Coefficient (r^2)
	Simulation					Experiment	
	Aggregate Distribution Pattern				Average		
	1	2	3	4			
3.0	0.282	0.290	0.280	0.305	0.289	0.270	0.987
5.0	0.214	0.221	0.210	0.232	0.219	0.173	
7.5	0.146	0.164	0.148	0.160	0.155	0.144	
10.5	0.136	0.128	0.109	0.124	0.124	0.089	
14.0	0.076	0.061	0.080	0.071	0.072	0.061	
18.0	0.020	0.017	0.038	0.012	0.022	0.034	
22.0	0.006	0.008	0.006	0.002	0.006	0.004	

Table C.8: Simulation and Experimental Results on 56-Day LMST-C

Depth (mm)	Total Chloride Concentration (% by Weight)						Correlation Coefficient (r^2)
	Simulation					Experiment	
	Aggregate Distribution Pattern				Average		
	1	2	3	4			
3.0	0.236	0.243	0.235	0.255	0.242	0.176	0.983
5.0	0.169	0.175	0.165	0.183	0.173	0.161	
7.5	0.091	0.102	0.091	0.097	0.095	0.092	
10.5	0.071	0.063	0.050	0.058	0.061	0.060	
14.0	0.032	0.023	0.039	0.028	0.031	0.040	
18.0	0.003	0.003	0.015	0.001	0.006	0.012	
22.0	0.001	0.002	0.001	0.001	0.000	0.000	

Table C.9: Simulation and Experimental Results on 91-Day LMST-C

Depth (mm)	Total Chloride Concentration (% by Weight)						Correlation Coefficient (r^2)
	Simulation					Experiment	
	Aggregate Distribution Pattern				Average		
	1	2	3	4			
3.0	0.198	0.205	0.196	0.215	0.204	0.142	0.976
5.0	0.088	0.095	0.086	0.099	0.092	0.083	
7.5	0.026	0.027	0.022	0.018	0.023	0.028	
10.5	0.034	0.028	0.025	0.030	0.029	0.000	
14.0	0.007	0.004	0.012	0.005	0.007	0.000	
18.0	0.000	0.000	0.004	0.000	0.001	0.000	
22.0	0.000	0.000	0.000	0.000	0.000	0.000	

APPENDIX D: Test Results on Mn/DOT Concretes

Table D.1: Slump, air content and unit weight values of fresh concretes (Titi et al. 2004).

Concrete Types	Batch Number	Slump (cm)	Air Content (%)	Unit Weight (kg/m^3)
GRNT-A	1	7.6	6.8	2275.0
	2	8.6	7.0	2276.7
	3	10.9	7.8	2257.4
GNSS-A	1	9.1	8.0	2202.9
	2	4.6	6.8	2251.0
	3	8.4	7.5	2295.9
GRNT-B	1	8.6	6.3	2271.8
	2	7.9	6.8	2262.2
	3	6.4	5.0	2331.2
LMST-A	1	7.4	6.2	2297.5
	2	8.4	7.4	2233.4
	3	8.9	7.3	2254.2
LMST-B	1	7.4	6.6	2263.8
	2	8.4	6.3	2286.3
	3	9.7	6.8	2271.8
GRNT-C	1	7.6	6.1	2318.3
	2	9.4	6.7	2295.9
	3	10.9	7.2	2270.2
LMST-C	1	7.9	6.5	2265.4
	2	7.9	6.8	2276.7
	3	8.4	6.5	2278.3
GRNT-D	1	7.1	6.4	2283.1
	2	7.6	6.6	2276.7
	3	7.1	6.0	2287.9
GRNT-E	1	11.2	6.8	2278.3
	2	9.7	6.8	2273.4
	3	11.7	7.3	2252.6
LMST-D	1	9.9	7.4	2271.8
	3	7.1	6.2	2303.9
QRTZ-A	1	7.1	6.4	2257.4
	2	7.1	6.0	2268.6
	3	7.9	6.8	2254.2
LMST-E	1	8.13	6.8	2273.4
	2	6.35	6.1	2286.3
	3	8.89	7.0	2265.4

Table D.2: 28-day compressive strength test results on cylinders (Titi et al. 2004).

Concrete Types	Batch Number	28-day Ultimate Compressive Load (kg)	28-day Ultimate Compressive Strength (Mpa)	Failure Mode
GRNT-A	1	31416.8	38.0	Cone
	2	31961.6	38.7	Cone
	3	31598.4	38.2	Cone
GNSS-A	1	25287.8	30.6	Columnar
	2	29146.8	35.3	Cone
	3	21020.2	25.4	Cone
GRNT-B	1	33005.8	39.9	Cone
	2	31008.2	37.5	Cone
	3	39452.6	47.7	Columnar
LMST-A	1	37364.2	45.2	Cone
	2	32234.0	39.0	Cone
	3	32324.8	39.1	Cone
LMST-B	1	22382.2	27.1	Cone
	2	35775.2	43.3	Cone
	3	36320.0	44.0	Cone
GRNT-C	1	33051.2	40.0	Cone
	2	29373.8	35.5	Cone
	3	29782.4	36.0	Cone
LMST-C	1	35003.4	42.4	Cone
	2	27058.4	32.7	Columnar
	3	24833.8	30.1	Cone
GRNT-D	1	32234.0	39.0	Cone
	2	33278.2	40.3	Cone
	3	35275.8	42.7	Cone
GRNT-E	1	29464.6	35.7	Cone
	2	29827.8	36.1	Cone
	3	29464.6	35.7	Cone
LMST-D	1	31099.0	37.6	Cone
	3	29964.0	36.3	Columnar
QRTZ-A	1	27013.0	32.7	Cone
	2	30145.6	36.5	Cone
	3	33823.0	40.9	Cone
LMST-E	1	35412.0	42.9	Cone
	2	38590.0	46.7	Cone
	3	30735.8	37.2	Cone

CURICULUM VITAE

Name: Kiran Lamichhane

Place of Birth: Kathmandu, Nepal

Education:

MS in Civil Engineering (Emphasis in Structural Engineering) (GPA: 3.8/4.0)
South Dakota State University (SDSU), Brookings, South Dakota, Dec 1999

Bachelor of Engineering (BE) in Civil Engineering
Tribhuvan University (TU), Kathmandu, Nepal, Aug 1995

Dissertation Title:

The Effect of Aggregate Porosity on the Chloride Penetrability of High Performance Concretes

Teaching/Research Experiences:

Primary Instructor (Teaching Assistant), University of Wisconsin-Milwaukee
- Fall 2005: Full-time instructor for *Design of Masonry Structures*, a graduate level course
- Fall 2004: Full-time instructor for *Design of Wood Structures*, a graduate level course

Graduate Assistant, University of Wisconsin-Milwaukee
- Project Assistant, Aug 2003 – Dec 2003
- Research Assistant, Aug 2001 – Dec 2002

Graduate Teaching/Research Assistant, South Dakota State University, Jan 1998 – Dec 1999

Licenses/Memberships/Awards:

Fundamentals of Engineering (FE) licensee (Certificate No.: E-8448, South Dakota)

Student member of American Society of Civil Engineers (ASCE) since 2001

Recipient of the Chancellor's Graduate Student Award from the UWM in each of the semesters from Spring 2003 to Fall 2005

Recipient of the Student Satellite Balloon Award in 2003 from the Wisconsin Space Grant Consortium (WSGC)
(http://www.uwgb.edu/wsgc/programs/awards/ssb_awards.asp)

Publications:

Titi, H. H., Tabatabai, H., Ghorbanpoor, A., Lamichhane, K., and Elias, M. (2004). "The Effect of Minnesota Aggregates on Rapid Chloride Permeability Tests," *Final Report*, Minnesota Department of Transportation, Research Services Section, St. Paul, Minnesota, Sep.

Major Professor Date